Role of ATM (ataxia telangiectasia mutated) and Artemis proteins for the repair of DNA double-strand breaks by homologous recombination in mammalian cells
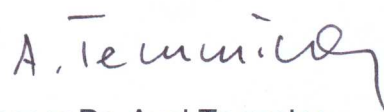
DISSERTATION

zur Erlangung des akademischen Grades eines Doktors
der Naturwissenschaften (Dr. rer. nat.)
des Fachbereichs Biologie,
der Fakultät für Mathematik, Informatik und Naturwissenschaften
der Universität Hamburg

vorgelegt von
Sabrina Köcher
aus
Hamburg

Hamburg, Mai 2011

Genehmigt vom Fachbereich Biologie
der Fakultät für Mathematik, Informatik und Naturwissenschaften
an der Universität Hamburg
auf Antrag von Prof. Dr. J. DAHM-DAPHI
Weiterer Gutachter der Dissertation:
Prof. Dr. T. DOBNER
Tag der Disputation: 08. Juli 2011

Hamburg, den 14. Juni 2011

Professor Dr. Axel Temming
Leiter des Fachbereichs Biologie

Meinen Eltern & Malte

Table of contents

1.   Summary

DNA double-strand breaks (DSB) represent the most dangerous type of DNA damage which, if unrepaired, can lead to cell death. Mis-repaired damage can result in genomic instability, deletions, translocations and mutations, and further to the inactivation of tumor suppressor or activation of proto-oncogenes, all of which can drive carcinogenesis.

DSBs can not only arise exogenously by mutagenic chemicals or ionizing irradiation (IR), they can also occur endogenously as by-products of normal oxidative metabolism (reactive oxygen species). Well conserved repair mechanisms for DSBs are present in all living organisms. In mammalian cells, DSBs are mostly repaired by two fundamentally different processes, non-homologous end-joining (NHEJ), which can act throughout the cell cycle, or homologous recombination (HR), which relies on the presence of a homologous sequence (e.g. sister chromatid) and is therefore restricted to the late S- or G2-phase. Inherited or somatic mutations in any of the key proteins involved in DSB repair generally predispose to malignancy. Understanding the involvement and actions of DNA repair proteins and processes can identify new or improve existing strategies in cancer therapy.

This work focuses on two proteins, namely ATM (ataxia telangiectasia mutated) and Artemis. Defects in either the ATM or the Artemis gene lead to pronounced sensitivity to IR, which has previously been ascribed to a common defect in NHEJ. However, it is not known whether depletion of the two proteins affects HR in the same way, since cell cycle progression is markedly different in both deficient cells. The aim of this thesis was to understand the functions of the ATM and Artemis proteins in DNA DSB repair. Three main questions were addressed: (1) How does cell cycle progression influence DNA repair? (2) Are ATM and Artemis involved in HR during the G2- and S-phase? (3) Do they function epistatically for HR during the G2- and also the S-phase?

Human fibroblast lines defective in either ATM (*AT*) or Artemis were studied in addition to a wild-type (WT) line. DNA damage was monitored by immunohistochemistry, detecting nuclear focus formation of either γH2AX as a general marker for DSBs or Rad51 as a marker for recombination activity using immunofluorecent microscopy. Cell cycle distribution by flow cytometry analysis and differential staining of S- (5-ethynyl-2'-deoxyuridine, EdU) and G2-phase cells (CenpF) revealed a robust IR-induced G1 block in *Artemis* cells, while *AT* cells migrated through the S-phase and accumulated in the G2-phase before mitosis. In these G2-phase *AT* cells, all DSBs were additionally decorated with the Rad51 protein, indicating recombination activity. By contrast, in *Artemis* cells, only 60% of γH2AX foci were also Rad51-positive, hinting at differences in HR. Using a chromosomal reporter construct designed to specifically monitor HR, both Artemis depletion (siRNA) and ATM-inhibition (KU55933) lead to substantial HR defects (ATM>Artemis) hinting again at differences in HR. Corresponding protein expression and phosphorylation was controlled using Western blot

analysis. Immunohistochemistry analysis of recombination activity specifically in G2- and S-phase cells showed similar defects in Rad51 focus formation in the G2-phase and no evidence of repair by HR in either of the deficient strains. Surprisingly, only ATM but not Artemis is required for the HR of radiation-induced DSBs during the S-phase. In contrast to WT and *Artemis* fibroblasts, numerous Rad51 foci form continuously in *AT* cells after irradiation, indicating a recruitment process that is independent of ATM-mediated functions such as the resection of DSB ends. The Rad51 recruitment to DSBs, however, needs functional ATR/Chk1. ATR activation may occur when a progressing replication fork encounters radiation-induced single-strand damage. Despite successful initiation of recombination (recruitment of Rad51 recombinase), HR repair cannot be completed without ATM. Abrogation of ATM function in *Artemis* cells further reduced their survival, but only in those cells that actively replicated in the S-phase.

In conclusion, we describe important differences in HR between *AT* and *Artemis* cells during the S-phase, but a common recombination defect in the G2-phase. We have identified ATM as a core component in the HR of directly and indirectly-induced DSBs downstream of DNA end resection and Rad51 filament formation processes, thus introducing new possibilities for cancer therapies in tumors with compromised expression of the ATM protein.

2.   Introduction

Cellular DNA is permanently exposed to a variety of insults that cause its damage. Both endogenous activities such as meiosis, V(D)J recombination, and oxidative metabolism with its byproducts (reactive oxygen species, ROS) as well as environmental factors such as UV light, numerous genotoxic chemicals, and ionizing irradiation can cause a variety of DNA lesions, including DNA double-strand breaks (DSBs). DNA DSBs are considered to be the most toxic of all DNA lesions. Induced DSBs are potentially lethal to the cell, but can also lead to genomic instability, thereby increasing the risk of cancer. "Cancer is a disease of our genes" (Hoeijmakers, 2001). Over the course of a lifetime, somatic changes such as mutations or translocations accumulate that could activate proto-oncogenes or inactivate tumor suppressor genes (Hoeijmakers, 2001). In radiotherapy, on the other hand, DNA lesions are induced in order to inactivate tumor cells. One concern in radiobiology is understanding the involvement and actions of proteins in DNA repair in the hope of optimizing the applicability of ionizing irradiation (IR) and identifying new strategies for cancer therapies. The current study focuses on two proteins, namely ATM and Artemis. A defect in these proteins leads to pronounced sensitivity of cells and also of whole organisms to ionizing irradiation. This study was designed to improve our understanding of their functions in DNA DSB repair and especially in homologous recombination (HR).

2.1.   Carcinogenesis and cancer therapies

The formation of a tumor is a complex process that usually extends over decades. During tumor progression, normal cells evolve into cells with increasingly neoplastic phenotypes. Tumorigenesis is a multi-step process which requires several mutations in genes responsible for cell growth (i.e. Ras), chromosomal integrity (i.e. telomerase), cell cycle control or apoptosis (i.e. p53). First, initiating mutations cause pre-cancerous alterations, followed by secondary mutations promoting cell transformation and resulting in cancer cells. In contrast to normal tissues, cancer cells constantly proliferate, can be invasive and have the potential to form metastases (Weinberg, 2007).

Cancer therapy targets the DNA by introducing lethal damage in proliferating cells using for example chemotherapeutic drugs or ionizing irradiation. Chemotherapeutic drugs can be divided into different classes, most of which do not directly damage the DNA by DSB induction, but rather affect cell division or DNA synthesis: Alkylating agents (i.e. cyclophosphamide, ifosamide, busulfan), platinum-containing anti-cancer drugs (i.e. cis-platinum, carbo-platinum), and antibiotics (i.e. bleomycin, mitomycin C (MMC)) cause DNA cross-links, which are covalent bonds formed between adjacent bases on the same DNA strand (intrastrand) or between both strands (interstrand) (ICL). Anti-metabolites (i.e. 5-

fluoro-uracil (5-FU) 6-thioguanin) are incorporated into the DNA as pyrimidines or purines, thus interfering with DNA and RNA synthesis. Anti-mitotic drugs such as vinorelbine and also texanes (i.e. docetaxel) bind to tubulin, thereby inhibiting the formation of microtubuli during mitosis (Schoeffler et al., 2005).

Additional chemotherapeutics can also target topoisomerases. Topoisomerases introduce programmed single-strand breaks (SSB) (topoisomerase I) or DSBs (topoisomerase II) into the DNA, which relaxes the torsional stress generated due to normal DNA metabolism during replication or transcription. Topoisomerase inhibitors such as camptothecin and topotecan (topoisomerase I inhibitors) or etoposide and teniposide (topoisomerase II inhibitors) stabilize intermediate complexes that include either a SSB or DSB, respectively (Schoeffler et al., 2005).

Ionizing irradiation (IR) plays a very eminent role in cancer therapy, causing a plethora of types of DNA damage such as DNA-protein cross-links, abasic sites, oxidized bases (i.e. 8-oxoguanine), SSBs, and -mostly toxic- DSBs.

2.2. Responses to DNA damage

In response to DNA damage, the cell has to rapidly recognize and eliminate this damage to prevent deletions, translocations, chromosomal rearrangements, and loss of heterozygozity (LOH). The DNA damage response (DDR) not only results in the initiation of the repair machinery, but also in the activation of cell cycle checkpoints and therefore the delay of cell cycle progression in order to address DNA damage.

2.2.1. Cell cycle checkpoints

The cell cycle is regulated by cyclins and cyclin-dependent serine/threonine kinases (CDKs). The cyclins associated with the CDKs stimulate the catalytic activity of the CDKs. The cellular levels of the CDKs stay basically the same during the cell cycle, while the cyclin levels fluctuate, as controlled by mitotic growth factors. Additionally, CDK-inhibitors (i.e. p21, p27) can inhibit or stimulate cyclin-CDK complexes depending on the cell cycle stage (Weinberg, 2007).

Decisions about the growth or quiescence of the cells are made during the G1 phase of the cell cycle, a period in which they are especially responsive to growth factors, resulting in a rapid accumulation of cyclin D in the early and middle G1 phase. With increasing concentration, the cyclin D CDK4/6 complex abstract most of the p21 and p27 molecules away from the cyclin E-CDK2 complex. This finally enables the cyclin E-CDK2 complex to hyper-phosphorylate the retinoblastoma (Rb) protein at the so-called restriction point, from which the cells continue to progress through the rest of the cell cycle (Weinberg, 2007).

Cell cycle checkpoints are control mechanisms that ensure the fidelity in cell division. These checkpoints control whether the processes in each cell cycle phase have been completed accurately before progression into the next phase of the cell cycle. At cell cycle checkpoints, the cells can arrest and assess DNA damage, which is then either repaired or marks the cells for destruction via apoptosis, thus preventing DNA damage from being propagated in following generations. Multiple checkpoints have been identified.

2.2.1.1. G1 checkpoint

The protein p53 has been identified as the key protein responsible for inducing the G1 checkpoint. In normal unperturbed cells, p53 is bound in the nucleus by murine double minute gene 2 (MDM2), which triggers its ubiquitinylation and sequestration into the cytoplasm and hence blocks p53 in its function (Figure 1, green). In normal unstressed cells, the half-life of p53 is 20 minutes (Bartek et al., 2001; Rotman et al., 1999).

p53 is activated through phosphorylation at Ser15 by ATM, which enhances p53's function as a transcription factor. Activated p53 then induces a series of downstream processes such as the induction of p21 (also known as WAF1 and CIP1), which functions as an inhibitor of the cyclin E-CDK2 complex and therefore inhibits progression from the G1 to the S-phase (Brugarolas et al., 1995). Beside its activation, p53 is also stabilized by ATM function in two ways: Phosphorylation of the checkpoint kinase Chk2 on Thr68 leads to the further phosphorylation of p53 on Ser20. This phosphorylation of p53 alters the domain that is normally recognized and bound by MDM2. In addition, ATM phosphorylates MDM2 on Ser395, which is then unable to ubiquitinylate p53 (Figure 1, green) (Bartek et al., 2001; Rotman et al., 1999).

2.2.1.2. Intra-S-phase checkpoint

The initiation of DNA synthesis requires the dephosphorylation of CDK2 on Tyr15 and Thr14 by the dual specific phosphatase CDC25A. The activation of the cyclin E-CDK2 complex is important for the phosphorylation of CDC45. CDC45 in turn is bound to the replication complex and recruits the enzyme polymerase α/primase, which initiates the replication fork (Figure 1, red). In response to DNA DSBs, ATM phosphorylates and activates Chk2 on Thr68 (Bartek et al., 2001; Rotman et al., 1999). Chk2 then phosphorylates CDC25A, marking it for proteosomal degradation and preventing it from dephosphorylating CDK2 (Figure 1, red). DNA replication cannot be initiated after the inactivation of cyclin E-CDK2 in the early S-Phase (Bartek et al., 2001; Rotman et al., 1999). This CDC25A-mediated checkpoint arrest represents the second major pathway to block cells from progression into

and through the S-phase. It is very rapid and independent of gene activation and protein synthesis.

Another separate pathway is the regulation of the intra-S-phase checkpoint by an interaction between ATM and Nibrin (NBS1) and the structural maintenance of chromosomes protein (SMC1). NBS1 as part of the MRE11-Rad50-NBS1 complex (MRN) acts as a DSB sensor leading to the activation of ATM, which in turn phosphorylates NBS1 on Ser343 and Ser278 (Falck et al., 2005; Lim et al., 2000), among other substrates, in response to DNA DSBs. NBS1 then functions as an adaptor protein for the ATM-dependent phosphorylation of SMC1 on Ser957 and Ser966 (Yazdi et al., 2002). The ATM-dependent phosphorylation of breast cancer 1 (BRCA1) on Ser1387 was also shown to be necessary to activate BRCA1 as a regulator of the intra-S-phase checkpoint (Xu et al., 2001). NBS1 and BRCA1 are necessary for ATM to optimally phosphorylate SMC1 and therefore required for this branch of the intra-S-phase checkpoint (Kim et al., 2002). Goldberg *et al.* described a second branch of the intra-S-phase checkpoint, where hyper-phosphorylation of MDC1 by ATM is required independently of the phosphorylation of NBS1, SMC1 and Chk2 or the degradation of CDC25A (Goldberg et al., 2003). The exact mechanisms of ATM's interference with replication are not yet fully understood.

While ATM responds to DSBs, ATR and its downstream effector kinase Chk1 respond to replication inhibitors like hydroxyurea (HU) or aphidicolin (APH), as well as to damage that blocks replication fork progression like UV light-induced intrastrand cross-links (ICL).

In normal unstressed cells, ATR controls the initiation and progression of DNA synthesis through processes that function similarly during the activation of the ATR-dependent intra-S-phase checkpoint after damage (Petermann et al., 2006; Shechter et al., 2004).

In human cells, ATR exists in a stable complex with the ATR-interacting protein (ATRIP) (Zou et al., 2003a). During replication or after damage induction, ssDNA is found as an intermediate structure which is bound and coated by the ssDNA-binding protein replication protein A (RPA). This ssDNA-RPA structure is recognized and bound by ATRIP, thereby localizing the ATR-ATRIP complex to the site of the ssDNA. In order to efficiently phosphorylate and activate Chk1, the effector kinase of ATR, several other proteins are required. Rad17 and the Rad9-Rad1-Hus1 (9-1-1) complex are recruited to the site of damage. The Rad17 complex is a replication factor C-like (RFC) protein complex; the 9-1-1 is a ring shaped protein complex that resembles proliferating cell nuclear antigen (PCNA). During normal replication, RFC specifically recognizes the 3'-primer/template junction and enables PCNA, the sliding clamp of DNA polymerases, to encircle the DNA. Analogously, Rad17 is required in a damage situation for the recruitment of the 9-1-1 complex to the site of the lesion (Zou et al., 2003b). Zou *et al.* found that RPA stimulates the loading of Rad17 onto ssDNA *in vitro*, which in turn stimulates the ability of Rad17 to recruit the 9-1-1 complex to

the 5' or 3' DNA end (Zou et al., 2003b). Other proteins that are also relocated to the replication fork in response to replication blocking agents are TopBP1 and Claspin. Both proteins interact with ATR and therefore stimulate Chk1 phosphorylation (Zou et al., 2003b). Chk1 is phosphorylated by ATR on Ser317 and Ser345, promoting Chk1's dissociation from the chromatin and its rapid spreading throughout the nucleus (Bekker-Jensen et al., 2006). Like Chk2 in the ATM/Chk2 signalling cascade, Chk1 now phosphorylates CDC25A, which in turn inactivates cyclin E-CDK2 and therefore prevents it from promoting DNA-replication. In addition to Chk1, ATR phosphorylates various other repair or checkpoint proteins in response to replication stress such as γH2AX, BRCA1, p53.
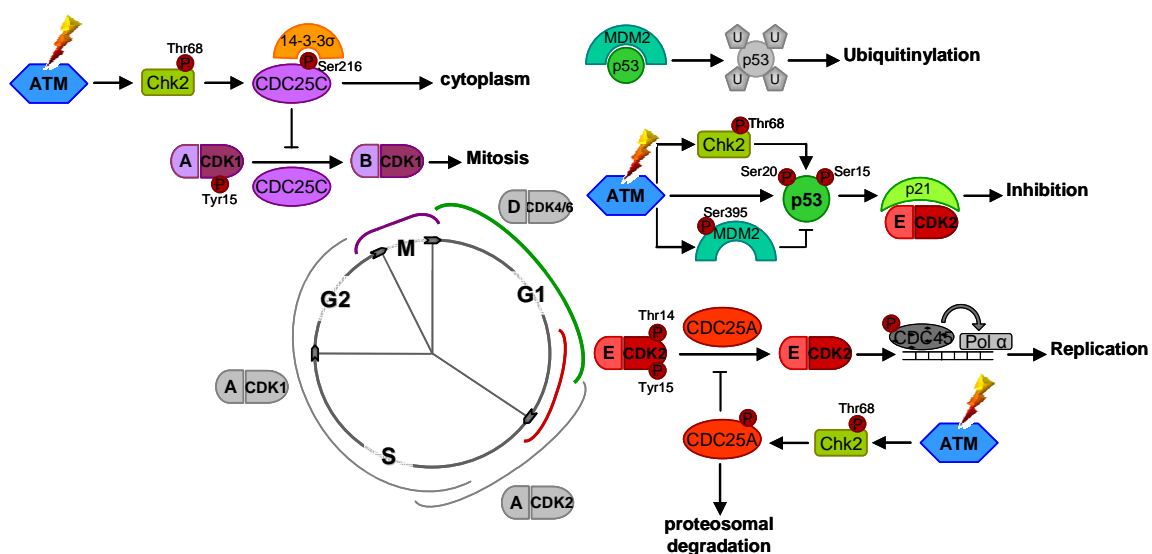
Figure 1. Major ATM-mediated cell cycle checkpoints
The G1 checkpoint (green) is p53 dependent. In damaged cells, activated ATM phosphorylates Chk2 on Thr68, which in turn phosphorylates p53 on Ser20. Additionally, ATM phosphorylates p53 directly on Ser15 and MDM2 on Ser395, blocking it from ubiquitinylating p53 for degradation (like in untreated cells). p53 then induces p21, which inhibits the G1 kinase complex cyclin E-CDK2 and stops the cell cycle from progression into S-phase. Entrance into S-phase (red) requires activation of the cyclin E-CDK2 complex by dephosphorylation, which in turn phosphorylates CDC45. CDC45 binds to the replication complex and recruits polymerase α, which initiates replication. Dephosphorylation of cyclin E-CDK2 is done by CDC25A. In damaged cells in the early S-Phase, activated ATM phosphorylates Chk2 (Thr68), which in turn phosphorylates CDC25A and marks it for proteosomal degradation. Replication cannot be initiated. Entrance into mitosis (purple) requires dephosphorylation of the cyclin B-CDK1 complex by CDC25C. After the generation of DNA damage, activated ATM phosphorylates Chk2 (Thr68), which in turn phosphorylates CDC25C, inhibits its enzymatic activity and marks it for 14-3-3σ binding to relocate it to the cytoplasm.
Indicated in grey are cyclin kinase complexes that are not involved in ATM-dependent cell cycle control.

2.2.1.3. G2/M checkpoint

The third major checkpoint is the G2/M checkpoint (Figure 1, purple). Mitotic entry requires the dephosphorylation of CDK1 at Tyr15 in order to bind to cyclin B, a process executed by the protein phosphatase CDC25C. After DNA damage, Chk2, phosphorylated and activated by ATM on Thr68, phosphorylates CDC25C on Ser216 and inhibits its enzymatic activity. In addition, phosphorylated CDC25C binds to the 14-3-3σ protein to promote its sequestration in the cytoplasm (Rotman et al., 1999). ATM also phosphorylates BRCA1 at S1423, thus regulating the level of 14-3-3σ protein and also activating the Chk1 kinase. Phosphorylation of BRCA1 is not only involved in the intra-S-phase checkpoint, but also in the G2/M checkpoint (Xu et al., 2002).

An early and transient G2 arrest is dependent on ATM and blocks cells that were in G2 at the time of irradiation (Kim et al., 2002).

2.2.2.   DNA repair mechanisms

Having interrupted cell cycle progression, it is now of great importance for the cell to repair the damage in order to avoid cell death or mutations.

Depending on the type of damage, a variety of repair mechanisms have evolved, namely (1) direct damage reversal, (2) base excision repair (BER), (3) single-strand break repair (SSBR), (4) nucleotide excision repair (NER), (5) mismatch repair (MMR), and (6) double-strand break repair (DSBR), some of which are interwoven.

Direct damage reversal refers to the chemical elimination of base alterations without removing the base itself. The main component of this pathway is the alkyltransferase, a protein that transfers non-native alkyl groups from the DNA to its internal cysteine residue, in turn irreversibly inactivating the protein itself.

One example for direct reversal is the repair of O6-methyl-guanine (O6-meG) by methyl-guanine methyltransferase (MGMT). If not repaired, this highly mutagenic lesion would permit the mis-pairing of O6-meG adducts with thymidine during replication, resulting in G:C to A:T transitions (Hoeijmakers, 2001).

<u>B</u>ase <u>E</u>xcision <u>R</u>epair (BER) targets damage which mostly arises due to cellular metabolism (reactive oxygen species), resulting in small chemical alterations to bases, modifications, i.e. methylations, oxidations, and deamination, or base loss.

In the first step of BER, glycosylases remove the suspected base, leaving an abasic site. These sites are then recognized by the APE1 endonuclease, which incises the sugar phosphate bond on the 3' or 5' side of the AP site, generating a SSB. This situation can also

arise directly when a radical attack opens the ring structure of a sugar residue. The initial cleavage step in BER results in the recruitment and activation of poly-(ADP-ribose) polymerase 1 (PARP-1), which synthesizes a poly-(ADP-ribose) (PAR) chain as a signal for other repair proteins to accumulate. The following steps are thus identical for BER and **single-strand break repair (SSBR)**. Two pathways exist to repair SSBs. The dominant one is called short patch repair. DNA polymerase β fills the gap with one nucleotide and removes the 5' abasic sugar residue. The XRCC1-ligase 3 complex seals the nick. In long patch repair, polymerase δ, polymerase ε and PCNA synthesize a stretch of 2-10 bases including the lost base, which results in a displaced DNA flap. FEN1 endonuclease removes this displaced DNA flap and ligase I seals the nick (Hoeijmakers, 2001).

Nucleotide Excision Repair (NER) is a repair mechanism that deals with a variety of helix-destroying lesions (bulky lesions), i.e. pyrimidine-pyrimidine dimers, bulky chemical adducts, and DNA-DNA cross-links that mostly arise from exogeneous sources. Two NER pathways exist with partly distinct substrate specificities: global genome NER (GG-NER) examines the entire genome, while transcription-coupled repair (TCR) repairs damage that blocks elongating RNA-polymerases at sites of active transcription. In GG-NER, a large multi-enzyme complex first screens the DNA for a distorting injury in the double helix. The first stage of the TCR pathway might be its only difference compared to GG-NER, as here a stalled polymerase has to be displaced in order to make the damage accessible for repair. This requires two TCR-specific factors: CSB and CSA. In the subsequent stages of both subpathways, the XPB and XPD helicases unwind the double helix in the vicinity of the lesion (~30 base pairs). The single-strand binding protein RPA binds to the undamaged strand and therefore stabilizes the open intermediate. Endonucleases (XPG and XRCC1/XPF) cleave 3' and 5' of the damage at both ends of the opened stretch (D-loop), leading to the excision of a 24-32 base oligonucleotide containing the lesion. Regular replication factors such as polδ, PCNA and ligase I complete repair by filling the gap (Hoeijmakers, 2001).

Mismatch Repair (MMR) is responsible for the correction of mismatches generated during DNA-replication such as base-base mismatches and insertion-deletion lesion (IDL) mismatches resulting from polymerization errors and template slippage that escaped regular proofreading. If unrepaired, such damage can lead to point mutations, potentially promoting carcinogenesis.

The principal pathway is initiated by the recognition and binding of the mismatch by MutSa and MutSb in interaction with PCNA, with MutSa being primarily responsible for base-base and IDL mismatches, and MutSb for IDL mismatches containing up to 16 extra nucleotides. The process is followed by ATP-dependent endonuclease (EXO1) activation to excise the

patch containing the mispaired base on the newly synthesized strand. In the final step, the strand is corrected by repair synthesis (likely polymerase δ and ε) and ligated (Kunkel et al., 2005).

In addition, cells have evolved DNA damage tolerance processes which enable the cells to bypass lesions that would block replication. Some types of ssDNA damage (i.e. interstrand cross-links (ICLs), lesions after UV irradiation) persist unrepaired until collision with the replication fork. Classical polymerases that mediate undisturbed replication cannot bypass these lesions and therefore block replication. In **t̲rans̲l̲esion s̲ynthesis (TLS)**, post-translational modifications of PCNA recruit special damage tolerant polymerases (e.g. DNA polymerases η and ξ) to bypass the lesions and fill the DNA gaps. PCNA monoubiquitylation is required for the mutagenic translation synthesis, whereas polyubiquitylation is required for an error-free pathway that involves a template switch to the undamaged sister chromatid (Ulrich et al., 2010). The final elimination of damage forms like ICLs also includes the NER and HR pathways (Knipscheer et al., 2009).

Double-strand break repair (DSBR) is the main topic of this thesis and will be discussed in more detail in the next sections.

2.3. Double-strand break signalling

Before DNA DSB repair can be initiated, the damage needs to be recognized and signalled to the cell. ATM is the major kinase that is activated in response to DNA DSBs induced, for instance, by ionizing irradiation, the focus of this thesis. Therefore, the activation of ATM will be described in detail below.

2.3.1. Activation of ATM

The activation of ATM leads to the phosphorylation and activation of many target proteins involved in cell cycle control (see above) and DNA repair (see below), placing ATM's activation in the center of the DNA damage response.

ATM exists predominantly in the nucleus in dividing cells. It responds rapidly to DSB induction by phosphorylating a variety of substrates. After damage occurrence, there is a marked change in ATM activity involving its autophosphorylation.

Bakkenist and Kastan showed in 2003 that ATM is held in its inactive form in untreated cells as a dimmer (Figure 2). In this constitution, the kinase domain of one molecule is bound to a region surrounding Ser1981, located within the FAT domain of the other molecule. Following irradiation, each ATM molecule phosphorylates the other on Ser1981, resulting in dimer

dissociation and fully active monomers. This rapid autophosphorylation of ATM can be detected as early as 30 sec after irradiation with 0.5 Gy, a dose that would induce 15-20 DSBs per cell (Bakkenist et al., 2003).

In contrast to these findings, some *in vitro* studies by Lee and Paull have shown that autophosphorylation is dispensable for ATM monomerization and activation. They showed that S1981A-dimeric ATM (where serine 1981 is replaced by alanine) was fully monomerized and activated *in vitro*. Essential for the activation of the ATM kinase was the presence of DNA and the MRN complex. Furthermore, they found indications that the unwinding of DNA ends by MRN is essential for ATM stimulation (Lee et al., 2005). These findings were also supported by Jazayeri *et al.*, who showed in Xenopus egg extracts that ATM activation is dependent on ssDNA oligonucleotides *in vitro*. The production of these ssDNA oligos depends on MRN independent of functional MRE11 nuclease activity (Buis et al., 2008; Jazayeri et al., 2008). Nussenzweig and co-workers additionally demonstrated normal ATM-dependent phosphorylations of substrates in mice expressing S1987A (analogous to S1981A in human) *in vivo* (Pellegrini et al., 2006). Further, they generated a transgenic mouse model in which all three ATM serine autophosphorylation sites were replaced by alanine and showed that ATM-dependent responses to DNA damage after irradiation remained intact, even in the triple mutant (Daniel et al., 2008).

Parallel to the autophosphorylation of ATM after DSB induction, ATM has been shown to be acetylated by the histone acetyl transferase Tip60 (Figure 2). Sun *et al.* showed that Tip60 forms a complex with the FATC domain of ATM independent of DNA damage. In response to DNA damage, the rapid acetylation of ATM depends on the activity of the Tip60 histone acetyl transferase. Acetylation of ATM plays an important role in the activation of ATM kinase activity. For example, depletion of Tip60 by siRNA inhibited the ATM-dependent phosphorylation of p53 and Chk2 (Sun et al., 2005).

Furthermore, phosphatases might be involved in the damage-induced regulation and activation of ATM. The interaction between ATM and protein phosphatase 2A (PP2A) in untreated cells and the dissociation of PP2A from ATM coupled with the loss of its associated phosphatase activity suggests that PP2A dephosphorylates ATM and therefore inhibits ATM activity in untreated cells (Goodarzi et al., 2004).

The ATM activation process is currently only partially understood and the list of proteins involved is far from being complete.

2.3.2. Response to DNA double-strand breaks

Responses to DNA DSBs can be visualised by the rapid formation of foci, which are huge conglomerates of recruited damage response proteins. Using live cell imaging techniques,

Bekker-Jensen demonstrated the formation of foci and the organisation of protein compartments. Initial factors recruited to the sites of damage are the MRN complex, mediator of DNA-damage checkpoint protein 1 (MDC1), ATM, 53BP1 (p53-binding protein-1) and also BRCA1 (Bekker-Jensen et al., 2006). The MRN complex is the first to bind to the sites of damage, MDC1 follows. Its binding to the DNA requires the phosphorylation of histone H2AX, a member of the histone superfamily H2A, on Ser139 to produce γH2AX in an ATM-dependent manner (Lukas et al., 2004; Stucki et al., 2005) (Figure 2). The phosphorylation of H2AX is delayed in the absence of ATM, but can eventually be induced by the DNA-dependent protein kinase catalytic subunit (DNA-PKcs) or ATR, which are also members of the phosphoinositide 3-kinase-like protein kinase (PIKK) family (Kuhne et al., 2004; Stiff et al., 2004).

MDC1 binds specifically to the C-terminus of γH2AX (Stucki et al., 2005) and acts as a platform to ensure the retention of DNA-damage proteins such as the MRN complex. Retention of the MRN complex at the DSB sites requires direct binding of NBS1 to MDC1 (Lukas et al., 2004). ATM, also bound by MDC1, then phosphorylates additional H2AX molecules in the vicinity of the binding site, causing more MDC1 molecules to bind. This cycling process is probably the reason why H2AX phosphorylation stretches over megabases of DNA flanking the DSB (Lavin et al., 2007).

Additionally, it has been shown that ATM is recruited to the DSB by NBS1. NBS1ΔC-complemented NBS cells (mutation in the C-terminal end of NBS1) did not form phospho-Ser1981-ATM foci, although they were able to form γH2AX foci. Instead, they only showed an increased pan-nuclear signal for phospho-Ser1981-ATM (Falck et al., 2005). Thus, NBS1 not only binds MDC1, it also binds ATM via its evolutionarily conserved C-terminus (Falck et al., 2005). Therefore, the recruitment of ATM to the DSB requires the ATM interaction motif at the NBS1 C-terminus and MRN binding to the DNA ends, which stabilizes the NBS1-ATM interaction (Figure 2).

A third factor recruited to the DSB is 53BP1. 53BP1 was originally identified as a p53 binding partner that can enhance the transcriptional activity of p53 (Iwabuchi et al., 1994). 53BP1 was found to rapidly translocate to nuclear foci after damage induction and is therefore part of the DNA damage response machinery. The RING-finger ubiquitin ligase RNF8 assembles at the break through interaction with phosphorylated MDC1 (Figure 2). The RNF8 FHA domain specifically recognizes ATM-mediated phosphorylations at the N-terminus of MDC1 ("TQXF" motifs). RNF8 ubiquitinylates H2AX (K63-linked ubiquitin conjugates), acting as a regulatory ubiquitinylation signal and therefore facilitating the accumulation of 53BP1 and also BRCA1 at the sites of damage (Figure 2) (Panier et al., 2009). Although 53BP1 does not have an ubiquitin binding motif and detailed interactions are therefore unclear, it has been shown that γH2AX ubiquitinylation is essential for 53BP1 binding to the DSB site (Panier et

al., 2009). Both of these proteins, 53BP1 and BRCA1, are also substrates of ATM in response to DSBs. Their functions in early DNA damage response are not well characterized.

The major process in DDR is the stabilization and enhancement of protein-protein-interactions and therefore the recruitment of additional molecules to the DSB site. In repetitive activation and stabilization loops, ATM has a central role upstream as well as downstream of other DNA damage response proteins.
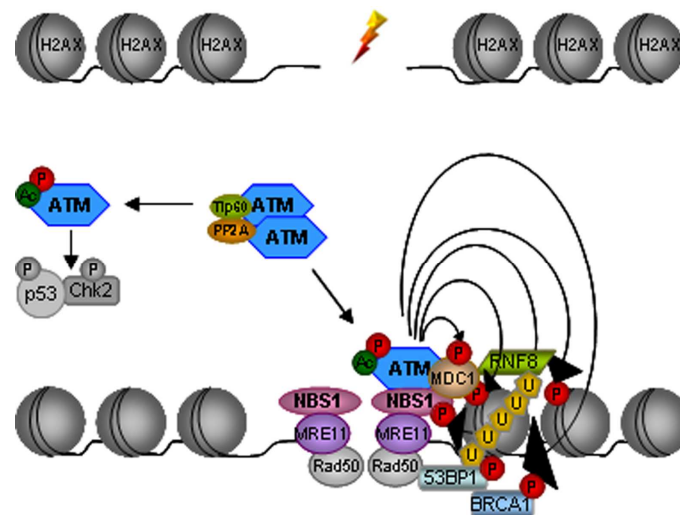
Figure 2. Assembly of DNA damage response (DDR) proteins
Induction of DNA damage activates ATM via monomerization, acetylation (Tip60) and phosphatase (PP2A) dissociation. ATM monomers activate p53 and Chk2 and also translocate to the DSB where the MRN complex has already bound. MRE11 binds to the DNA ends together with Rad50, which brings the two ends together. ATM associates with NBS1 (C-terminus). ATM phosphorylates H2AX molecules in addition to NBS1. MDC1 binds to γH2AX (C-terminus), ATM, and NBS1, and therefore ensures the retention of these proteins. ATM phosphorylates additional H2AX molecules in the vicinity, ensuring that more MDC1 molecules bind. In addition, RNF8 interacts with MDC1 and ubiquitinylates H2AX, causing 53BP1 and BRCA1 to accumulate at the DSB site, both of which are phosphorylated by ATM. 53BP1 interacts with the MRN complex through Rad50, contributing to the activation and stabilization of ATM. Cycling protein-protein interactions constitute the major processes in DDR.

2.4.   Double-strand break repair pathways

In mammalian cells, DSBs are mostly repaired by two fundamentally different processes, non-homologous end-joining (NHEJ) or homology directed repair (HDR). The latter can be either error free, namely in the form of gene conversion (GC), or error-prone, as with single-strand annealing (SSA). The DSB repair pathways differ in the requirement of a homologous template and fidelity of the repair, but share the requirement of the nucleolytic removal of damaged DNA by nucleases.

2.4.1.   Non-homologous end-joining

NHEJ is a simple ligation-based mechanism that functions throughout the cell cycle, which is why it is probably the major pathway for the repair of DNA DSBs in eukaryotes (Sargent et al., 1997a). Regardless of the sequences, it directly rejoins the two DNA ends of the DSB, a process that is only precise for simple "clean" breaks with blunt ends or small 5' or 3' complementary overhangs. Such breaks require just the core components of NHEJ: Ku70, Ku80, DNA-PKcs, XRCC4, XLF, and ligase IV (LigIV) (Figure 3) (Lieber, 2008; Weterings et al., 2004).

The Ku70/Ku80 heterodimer forms a ring that can specifically bind to double-stranded DNA and occupies approximately 16-18 bp at both DNA ends (Walker et al., 2001). This DNA-Ku70/80 complex then recruits other components including DNA-PKcs, XRCC4 and ligase IV, forming a repair synapse. As structural studies with crystallography have indicated, DNA-PKcs also has an open channel that can accommodate double-stranded DNA (~ 12bp) (Chiu et al., 1998). Upon recruitment, DNA-PKcs occupies the broken termini, causing the Ku70/80 heterodimer to translocate to 10bp away from the free ends (Yoo et al., 1999). Once the catalytic subunit binds to Ku, the kinase activity is activated, leading to autophosphorylation. This in turn results in a conformational change which may make the DNA ends available for further processing, if necessary. Otherwise direct ligation can occur, the final step in NHEJ. Compatible "clean" DNA ends can be joined directly without previous processing, a process which is mediated by the XRCC4/LigIV complex, which also contains XLF (XRCC4-like protein/Cernunnos) as a cofactor. XRCC4 is definitively required for the stabilization of DNA-ligase IV (Wyman et al., 2006). Cells lacking XRCC4 do not display any ligase IV (Bryant et al., 2006). Interactions between Ku and XRCC4 as well as DNA-PKcs and XRCC4 stabilize the XRCC4/LigIV complex. Final ligation seals the nick (Lieber, 2008).

Cells defective in any of the components involved at the core NHEJ are not only radiosensitive and DSB repair deficient, but also impaired in V(D)J and CS recombination, essential processes in the maturation of the immune system. DSBs being part of such normal genetic activities require NHEJ for repair (Ma et al., 2005a).
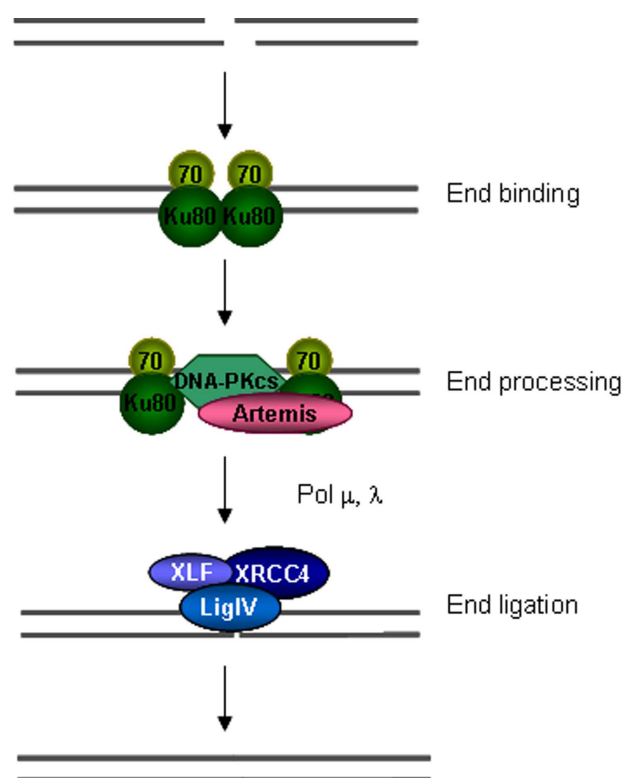
Figure 3. Model of the key steps in non-homologous end-joining (NHEJ)
In the first step, the Ku70/80 heterodimer binds to both ends which then recruits DNA-PKcs, forming a repair synapse. Most DSB ends are not ligatable and require processing, which can be done by the Artemis nuclease. Polymerases μ and λ can synthesize bases before ligation by XRCC4/Lig IV and cofactor XLF.

DNA DSBs mostly differ in the chemical composition of their DNA ends. For example, DSB ends resulting from ionizing irradiation-induced damage are not directly ligatable. They are not proper substrates for ligases, which require 3' hydroxyl and 5' phosphate groups. Not only damage in the phosphodiester backbone but also base and sugar damage is caused by ionizing irradiation (i.e. through hydroxyl radicals). These "dirty" DSB ends require nucleolytic processing and DNA synthesis to remove and replace non-ligatable nucleotide residues and incompatible single-stranded DNA overhangs before proper joining can proceed.

In the case of DNA ends carrying 3' phosphate or 5' hydroxyl groups, the polynucleotide kinase is recruited to the DNA ends through interaction with XRCC4 and removes these 3' phosphate or 5' hydroxyl groups (Helleday et al., 2007).

Another subclass of secondary DNA end structures can be processed by structure-specific nucleases such as Werner syndrome protein (WRN) or Artemis. The Artemis nuclease is part of this thesis and will be discussed later (Ma et al., 2005b; Weterings et al., 2004).

Some DSB ends require the synthesis of a limited number of nucleotides before ligation, a process which is presumably performed by polymerases pol μ and λ, enzymes which share partially overlapping features. Both polymerases are bypass polymerases and therefore have

great flexibility in the use of nucleotides and templates. Pol λ is almost exclusively template-dependent, whereas pol μ can carry out both template-dependent and template-independent synthesis (Lieber, 2008; Wyman et al., 2006).

The processing of the DNA termini often causes small deletions or insertions (1-3 nts), which is why NHEJ mostly appears to be an imprecise, error-prone pathway.

2.4.2. Homology directed repair

While NHEJ functions independently of cell cycle stage and sequence homology, the major requirement for HDR is a homologous sequence elsewhere in the genome. Depending on where these sequences are found, two major homologous recombination pathways are possible. The error-free pathway, called gene conversion (GC), finds the homologous sequence for recombination repair elsewhere in the genome (e.g. sister chromatids). When adjacent repeat sequences flank the DSB, repair can occur via a non-conservative, error-prone pathway, namely single-strand annealing (SSA), which is always accompanied by sequence loss between the two repeats.

2.4.2.1. Gene Conversion

GC is active in the late S- or G2-phase of the cell cycle due to its requirement of a homologous sequence on the sister chromatid, the preferred source of a repair template. The basic mechanism of GC is the invasion of a 3' end into the sister chromatid so that repair synthesis can operate across the breakpoint (Cao et al., 1990).

As illustrated in Figure 4, GC is a process of multiple steps, initiated by a 5' to 3' resection at the DNA DSB end, yielding a 3'-ssDNA overhang. This resection step involves the MRN complex. The nucleolytic component of the MRN complex, MRE11, has been identified to have a 3' to 5' but not 5' to 3' exonuclease activity (Paull et al., 1998). Therefore, other components must be involved in resection. Exonuclease 1 (EXO1) (Nimonkar et al., 2008) and C-terminal binding protein interaction protein (CtiP) are believed to be the additional players in this resection step (Huertas et al., 2008; Mimitou et al., 2008; Sartori et al., 2007; Takeda et al., 2007). However, the generation of long single-stranded overhangs and the nucleases involved in this process are subject of current investigation and still need to be more exactly defined.

After generation of long single-stranded 3' overhangs, these are coated with and stabilized by ssDNA-binding protein RPA. The key step in GC is the subsequent invasion of the 3'-ssDNA overhang into the homologous duplex DNA. The central player that guides this strand invasion is Rad51 (Haber, 2000; Raderschall et al., 1999). Rad51 is functional as a long

helical polymer that winds around the ssDNA to form a nucleoprotein filament (Ogawa et al., 1993). In order to load Rad51 onto the DNA overhang, RPA has to be displaced, which is done with the help of a series of associated proteins such as BRCA2, Rad52, Rad54, Rad54B, and likely also the Rad51 paralogs (Rad51B, Rad51C, Rad51D, XRCC2, XRCC3) (Sigurdsson et al., 2001). BRCA2 interacts with Rad51 and RPA at the DSB site and is required for the nuclear localization and loading of Rad51 (Pellegrini et al., 2006). It has been shown that BRCA2 binds Rad51 through the conserved BRC repeats in the center of the protein. These motifs promote the accumulation of Rad51 onto single-stranded DNA, but prevent filament formation on double-stranded DNA (Carreira et al., 2009a; Carreira et al., 2009b; Wong et al., 1997). Rad52 also directly interacts with Rad51 and RPA, which enhances the ssDNA binding specificity and stimulates Rad51-mediated strand invasion. How Rad54 promotes joint-molecule formation is not clear. It might mediate topological changes in the duplex DNA, thus promoting strand invasion.

Next, the Rad51-ssDNA invades the sister chromatid, forming a heteroduplex wherever base pairs are formed, displacing a DNA-strand and resulting in a so-called D-loop (Helleday et al., 2007).

The very end of the invaded strand functions as a primer for DNA synthesis across the original break to restore the missing sequence information at the break site. DNA synthesis is probably performed by DNA polymerase η, well in line with the observation that cells lacking pol η show a defect in HR (Kawamoto et al., 2005).

On the other side of the D-loop, an X-shaped structure is formed at the transition between hetero- and homoduplex (Helleday et al., 2007). This structure is called a Holliday junction (HJ). Sliding of the HJ can release the newly synthesised strand. The 3' end of this strand can then anneal to the 5' end of the DSB. Many proteins have been shown to bind, modulate, or resolve the HJ *in vitro* (e.g. WRN, Bloom syndrome protein (BLM), p53, Rad54, PLAP75, hMSH2, hMSH6), but the exact mechanisms remain unclear (Bugreev et al., 2006; Mohaghegh et al., 2001; Raynard et al., 2006; Subramanian et al., 2002; Yang et al., 2002). For example, Rad54, WRN and BLM support the migration of HJs, though it is not clear how the direction of this migration is controlled (Helleday et al., 2007). It has been shown that Rad54 mediates the removal of Rad51 from the double-stranded DNA, allowing access of the DNA polymerases to the 3'-OH end (Li et al., 2009).

The final step of this pathway consists of the removal of flaps that might have formed during the annealing step through structure-specific endonucleases such as XPF/ERCC1; such proteins fill in gaps and ligate remaining nicks in processes that involve many proteins such as polymerase η and ε, PCNA, and ligase I (Batty et al., 2000).

This model has been called synthesis-dependent strand annealing (SDSA), where only one strand invades the template DNA.
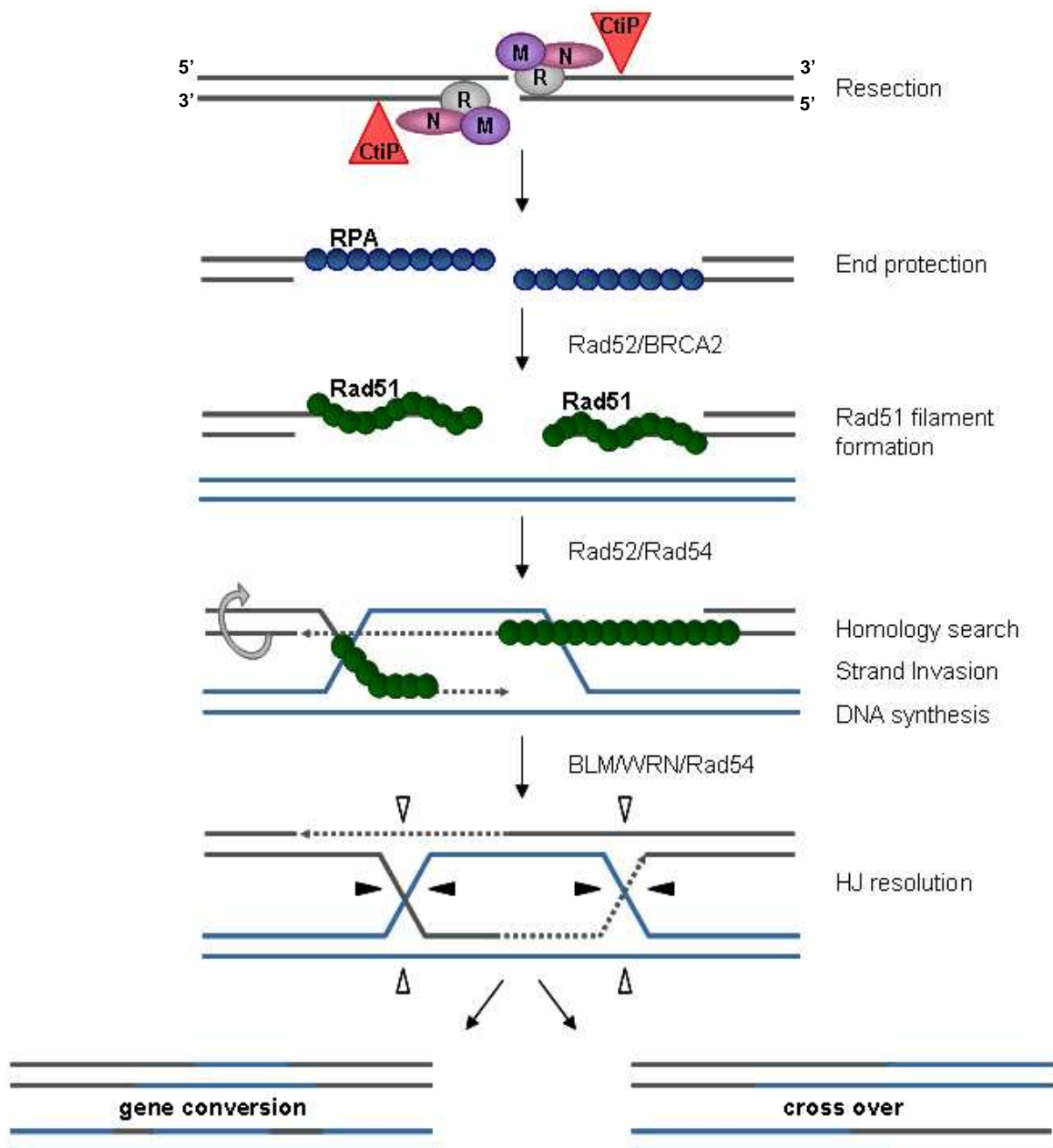
Figure 4. Model of the key steps in gene conversion (GC)
This pathway is initiated by a 5'-3' resection step to create 3'-ssDNA overhangs, which are then coated and stabilized by RPA. Rad51 with the help of Rad52 and BRCA2 replaces RPA, forming a Rad51 nucleofilament which invades the homologous chromatid, resulting in the formation of a double Holliday junction (HJ). If the two junctions are resolved in the same "plane" (both horizontal or both vertical), no crossover will be generated, whereas when the two junctions are resolved in opposite planes (one horizontal, one vertical), a crossover is produced.

According to the classical but more complex double Holliday junction model, both Rad51 nucleofilaments invade the homologous DNA template, forming a double Holliday junction. Double HJs can be resolved in two ways: either in the same "plane" (both vertical or both horizontal), which results in a non-crossover event where the flanking sequence continuity is

preserved, or in the opposite way (one vertical, one horizontal), which would result in a crossover event (Johnson et al., 2000). However, it has been observed that BLM, topoisomerase III and RMI1 resolve double HJs in a way that prevents crossover products, well in line with the observation that crossovers in mammals are rare after the induction of DNA DSBs (Raynard et al., 2006; Wu et al., 2003).

As in NHEJ, non-ligatable DNA end structures also need to be processed.

The question thus arises as to how the cell might regulate these repair pathways. Several studies indicate that the initiation of GC is tightly linked to cyclin-dependent kinases (CDKs) that are specifically active during the S and G2 phase. It has been shown that CDK1 activity is required for the efficient 5' to 3' resection of the DSB ends and the loading of Rad51 by regulating BRCA2 phosphorylation (Aylon et al., 2004; Esashi et al., 2005; Ira et al., 2004).

2.4.2.2. Single-Strand Annealing

When a DSB occurs between two flanking repetitive sequences oriented in the same direction, it could be repaired by single-strand annealing (SSA).

Similar to GC, the SSA pathway is initiated by a 5' to 3' resection step which is likely also mediated by the same nucleolytic components also involved in GC (e.g. MRN, EXO1, CtiP). Resection expands until homologous regions flanking the break are freely exposed on long single-stranded 3' overhangs. The stretch of ssDNA exposure and the length of the homology can range from just a few to hundreds of bases. In SSA, the generated overhangs are also covered with RPA for stabilization. In contrast to the GC pathway, SSA is Rad51-independent, though it does fully depend on Rad52 (Symington, 2002).

Rad52 binds to the resected DNA termini and promotes the alignment and annealing of the two complementary strands (Mortensen et al., 1996; Reddy et al., 1997). However, once the homologies are annealed, the sequences between the homologies are flapped out. These flaps are trimmed by the ERCC1/XPF endonuclease. It has been shown that ERCC1/XPF forms a complex with Rad52, stimulating the DNA structure-specific endonuclease activity of ERCC1/XPF (Motycka et al., 2004; Sargent et al., 1997b).

The final step in SSA is the ligation of the remaining nicks, possibly by ligase III. It is noteworthy that SSA is always associated with the loss of one of the repetitive sequences and the sequence between the repeats. Therefore, SSA leads to large deletions and is always error-prone. Although approximately 10% of the human genome consists of repetitive sequences, SSA is believed to play a fairly limited role in DSB repair, probably due to the fact that such repeats exhibit great sequence diversity and because of the error-proneness of the pathway itself (Helleday et al., 2007).

2.4.2.3. One-ended DSBs

Of increasing interest in recent research on DNA DSB repair is the repair of the so-called "one-ended DSBs", which are generated during replication. One-ended DSBs arise when DNA replication breaks down, i.e. encounters a SSB on the template DNA. Only one arm of the replication fork is ruptured and contains the DSB, the processing of which results in a 3' single-strand overhang. This serves as a substrate for the Rad51-mediated strand invasion of the sister chromatid, creating a D-loop. Cleavage of the resulting Holliday junction allows the resumption of the DNA replication, just as in the SDSA model in the GC repair pathway described above (Arnaudeau et al., 2001; Michel et al., 2001).

Importantly, cells have to ensure that one-ended DSBs are repaired solely in an accurate manner by GC. NHEJ of this type of damage would be disadvantageous, since NHEJ could promote the misjoining of the one-ended DSB and another DSB at a different locus, thus resulting in asymmetric translocations (Helleday et al., 2007).

One possibility of controlling NHEJ in the S-phase is through DNA-PKcs activity, which is essential for NHEJ. However, it has been shown that the phosphorylation and activation of DNA-PKcs is reduced in irradiated S-phase cells (Chen et al., 2005a).

Another possibility for the dominance of GC in the S-phase is the fact that replication and GC share some proteins (i.e. RPA, polymerases). Therefore, the access of some GC factors to the damage site might simply be faster.

2.5.   Double-strand break repair and cancer

One of the hallmarks of tumor cells is their highly rearranged karyotypes in both chromosome number and also structural integrity of each homologous pair (Thompson et al., 2002). In most cases, chromosomal aberrations include loss or gain of chromosomes or chromosome fragments and the amplification of chromosome segments (Lengauer et al., 1998). These rearrangements have conferred growth advantages during the evolution of the tumor (Thompson et al., 2002). Loss of fragments or whole chromosomes can lead to the inactivation of tumour suppressor genes, whereas the amplification of certain regions could activate proto-oncogenes and therefore promote carcinogenesis. Chromosomal aberrations are a consequence of the loss of fidelity in DSB repair (Thompson et al., 2002).

Concerning the DSB repair pathways described, it is likely that only the GC mechanism is capable of restoring the original sequence at the break site. NHEJ and SSA have high mutagenic potential, since they produce point mutations or insertions (NHEJ) and more or less extensive deletions (NHEJ, SSA).

Although GC is supposed to be error-free, it can also be mutagenic. For example, when the broken wild type allele is replaced by a mutant non-functional allele, this results in LOH (i.e.

inactivation of tumour suppressor genes) (Pfeiffer et al., 2000). Additionally, if GC was initiated in G1, this would also carry a high risk of chromosomal rearrangements, as the homologous template (homologous chromosome, pseudogene) could only be found on a distant chromosomal locus.

It is noteworthy that all DSB repair pathways have the potential to induce chromosomal aberrations and therefore may foster carcinogenesis.

Chromosomal aberrations have been observed, for example, in lymphomas. In many cases, chromosomal translocations have been found with one of the breakpoints in either an Ig or a T-cell receptor (Tcr) locus. These localizations indicate that there might be a link between chromosomal aberrations and V(D)J or class switch recombinations. In this way, DSBs are implicated in the generation of translocations in lymphoid tumours (at least in chromosomes 2, 7, 14 or 22 that carry the Ig and Tcr loci) (Vanasse et al., 1999). Other evidence for the involvement of DSBs in chromosomal aberrations comes from studies in which cells or animals were exposed to ionizing irradiation, causing DSBs among other forms of damage. At relatively low doses, IR does not cause extensive cell death but does lead to chromosomal instability. Experiments using the introduction of site-specific DSBs (I-SceI recognition site) confirmed an increase in the number of chromosomal aberrations after the generation of the DSB by the I-SceI Endonuclease (Richardson et al., 2000). Therefore, the correct repair of DSBs is critical for maintaining genomic stability.

Loss of or defects in any of the components of DBS repair may increase the rate of incorrect repair and therefore the risk to develop cancer, particularly in combination with the loss of the tumour suppressor gene p53. Some human tumors manifest defects in certain repair pathways. For example, it has been shown that high-grade bladder tumors are unable to perform accurate NHEJ, instead use a highly mutagenic end-joining pathway which may contribute to further genomic instability (Bentley et al., 2004).

Concerning GC, heightened expression of Rad51 promotes aneuploidy and increases the level of crossover events, resulting in chromosomal translocations (Richardson et al., 2004). The protein Rad54 provides another link between defects in GC and cancer development, mutations of which have been observed in lymphomas, colon cancer, and breast cancer (Matsuda et al., 1999).

Additionally, somatic mutations of ATM, involved in DDR, cell cycle responses and DSB repair, occur in significant frequencies in lung adenocarcinomas (Ding et al., 2008).

2.6. Inherited syndromes with defects in DNA repair genes

Inherited defects in any of the DNA repair pathways generally predispose to malignancy. Some of these genetic disorders and their particular cancer predispositions are listed below (Table 1).

At least three defects are associated with inherent defects in NER: Xeroderma pigmentosum (mutations in one of the genes XPA – XPG), Cockayne syndrome (mutations in CSA or CSB genes), and trichothiodystrophy (TTD), all characterized by exquisite sensitivity to sunlight.

There is no known syndrome associated with defects in BER core proteins due to the fact that defective/no-repair of endogenous lesions caused by the by-products of the normal cellular metabolism induce embryonic lethality (Hoeijmakers, 2001).

Furthermore, some of the key proteins that recognize DSBs are mutated in genetic disorders, known as "genomic instability syndromes".

In addition to ataxia telangiectasia (which is discussed in detail below), the phenotypes of the ataxia telangiectasia-like disorder (ATLD) and the Nijmegen breakage syndrome (NBS) resemble one another. All three conditions display immunodeficiency, extreme radiosensitivity, cancer predisposition (in particular lymphomas), and chromosomal instability. ATLD results from mutations in the Mre11 gene; in NBS the NBS1 (Nibrin) protein is mutated. Both Mre11 and NBS1 are part of the MRN complex and therefore the syndromes associated with the loss or mutation of those proteins share overlapping phenotypes such as microphaly and growth retardation. Since both the MRN complex as well as ATM are involved in DDR and DSB, repair-deficient cell lines are defective in both processes (Hoeijmakers, 2001; Thompson et al., 2002).

Werner (WRN), Bloom (BLM) and Rothmund Thompson syndromes (RTS) display defects in the associated proteins WRN, BLM and RecQL4, respectively, which are all members of the RecQ DNA helicase family and involved in homologous recombination. Mutations in the WRN protein predominantly cause premature aging and various cancers. BLM and RTS syndromes, on the other hand, cause leukemia and osteosarcomas, respectively, in addition to serious physiological defects. All three cellular phenotypes are characterized by protracted replication. Further, inherited defects in BRCA1 and BRCA2 strongly predispose to breast cancer (Hoeijmakers, 2001). Half of the known genetic BRCA1 and BRCA2 defects lead to cancers of the breast and ovary (Carreira et al., 2009b).

The syndromes ataxia telangiectasia (AT) and radiosensitive severe combined immunodeficiency (RS-SCID) will be described in detail below.

Table1. Human syndromes with defective genome maintenance (adapted from Hoeijmakers, 2001)

Syndrome	Affected Maintenance Mechanism	Main type of genome instability	Major cancer predisposition
Xeroderma pigmentosum	NER (±TCR)	Point mutations	UV-induced skin cancer
Cockayne syndrome	TCR	Point mutations	None*
Trichothiodystrophy	NER / TCR	Point mutations	None*
Ataxia telangiectasia (AT)	DSB response / repair	Chromosome aberrations	Lymphomas
AT-like disorder	DSB response / repair	Chromosome aberrations	Lymphomas
Nijmegen breakage syndrome	DSB response / repair	Chromosome aberrations	Lymphomas
BRCA1 / BRCA2	HR	Chromosome aberrations	Breast (ovarian) cancer
Werner syndrome	HR? / TLS?	Chromosome aberrations	Various cancers
Bloom syndrome	HR?	Chromosome aberrations (SCE↑)	Leukemia, Lymphomas, others
Rothmund-Thomson syndrome	HR?	Chromosome aberrations	Osteosarcoma

*Defect in transcription-coupled repair triggers apoptosis, which may protect against UV-induced cancer.
Abbreviations: BER, base excision repair; DSB, double-strand break; HR, homologous recombination; MMR, mismatch repair; NER, nucleotide excision repair, SCE, sister chromatid exchange; TCR, transcription-coupled repair; TLS, translesion synthesis

2.6.1. Ataxia telangiectasia

The ATM protein was identified to be mutated (lost or inactivated) in the genetic disorder ataxia telangiectasia (*AT*). *AT*, also called Louis-Bar Syndrome, is an autosomal recessive genetic disorder characterized by progressive cerebellar ataxia, progressive apraxia of eye movements, insulin-resistant diabetes, oculocutaneous telangiectasia, and high incidence of lymphoid tumors (30%), as well as immunodeficiency, clinical and cellular radiosensitivity, cell cycle checkpoint defects and chromosomal instability (Lavin, 2008).

The responsible gene, ataxia telangiectasia mutated (ATM), was discovered and cloned in 1995 by Yosef Shiloh and colleagues.

ATM is localized on chromosome 11q22-23. Its 66 exons (3056 amino acids) encode for a large 370 kDa protein that is a member of the phosphoinositide 3-kinase-like protein kinase (PIKK) family (Savitsky et al., 1995). PIKKs also include ATR (ataxia telangiectasia and

Rad3-related), DNA-PKcs (catalytic subunit of the DNA-dependent protein kinase) and the protein kinase SMG1, also involved in the DNA damage response.

ATM is a serine/threonine protein kinase and targets "SQ/TQ" motifs. Its kinase domain is located on the C-terminus and has multiple substrates (the ATM/ATR network might have as many as 700 substrates), of which p53 was the first to be discovered {Lavin, 2008 #3; Matsuoka, 2007 #50}. Phosphorylation of p53 and its resulting G1-S checkpoint activation were discovered to be defective in all *AT* cell lines (Kastan et al., 1992).

Besides the kinase domain, PIKK family members contain a FAT domain, a FATC domain and a substrate-binding site (SBS) near the N-terminus. The FATC domain is located at the extreme C-terminus (Figure 5). The FAT and FATC domains only occur in combination and encompass the kinase domain, suggesting mutual interaction probably by protein folding to ensure proper kinase function. Furthermore, three autophosphorylation sites have been identified in ATM (Ser367, Ser1893, and Ser1981) (Bosotti et al., 2000; Kozlov et al., 2006).

ATM is involved in the recognition of DNA DSBs, the activation of cell cycle checkpoints and also in the repair of DSBs. ATM-dependent phosphorylation enhances or suppresses the activity of targets, many of which have proved to be protective against genomic instability. Being the key player in these processes, an understanding of ATM delivers insight into the DNA damage response, cell cycle checkpoint activation, signalling pathways in DNA repair, and cancer development.
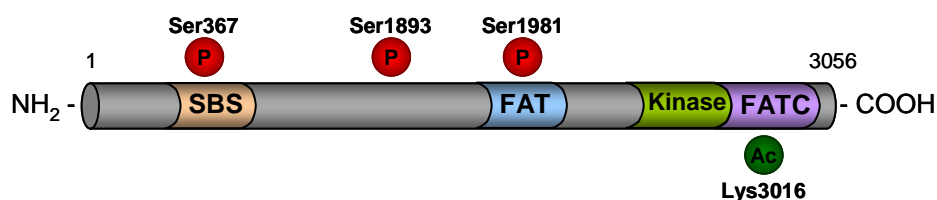
Figure 5. Schematic illustration of ATM
ATM contains a substrate-binding site (SBS), a FAT domain, a FATC domain (extreme C-terminus) and a kinase domain located in between the FAT and FATC domains. Additionally, three autophosphorylation sites have been identified (Ser367, Ser1893, Ser1981) as well as an acetylation site (Lys3016) located within the FATC domain.

2.6.2. Radiosensitive severe combined immunodeficiency and the Artemis protein

The human severe combined immune deficiency (SCID) is characterized by a completely defective T-cell development. In about 20% of SCID patients, the phenotype is characterized by a virtually complete absence of both T and B-lymphocytes, while natural killer (NK) cells are normally present and functional (T⁻B⁻NK⁺SCID). SCID is lethal within the first year of life because of the occurrence of multiple protracted infections. Allogeneic stem cell transplantation can cure this immunodeficiency. SCID is associated with mutations in one of

the two lymphoid-specific recombination-activating gene proteins 1 or 2 (RAG1 or RAG2) in V(D)J recombination. The V(D)J recombination process ensures the somatic diversification of immunoglobulin and anti-T-cell receptor encoding genes. The highly polymorphic antigen recognition regions of these receptors are composed of variable (V), diversity (D), and joining (J) gene segments that undergo somatic rearrangement (V(D)J recombination) prior to their expression. Each V, D and J segment is flanked by recombination signal sequences (RSSs). In the initiating step of V(D)J recombination, the RAG proteins specifically recognize the RSS and introduce a nick into the DNA double-strand. After the generation of this nick, the resulting free 3'-OH attacks the phosphodiester bond of the opposite strand, resulting in two hairpin-sealed coding ends. Thereafter, the corresponding coding end hairpins are opened and joined by the ubiquitously expressed factors of the NHEJ pathway. The subsequent step consists of the recognition and signalling of the DNA damage to the repair machinery, which provides the link between V(D)J recombination and DNA repair. Therefore, in the final phase of V(D)J recombination, factors of the NHEJ pathway (Ku70, Ku80, DNA-PKcs, XRCC4, LigIV) ensure the religation of the two broken chromosomal ends. V(D)J recombination represents a critical checkpoint in the development of the immune system.

Any defect in one of the known components of the V(D)J recombination/DNA repair machinery leads to the abortion of the V(D)J rearrangement process, an early block in both T- and B-cell maturation, and ultimately to severe combined immunodeficiency (SCID).

In some patients, the defect is accompanied by an increased sensitivity to ionizing radiation (radiosensitive severe combined immunodeficiency, RS-SCID). A role for the genes known at the time to be involved in V(D)J recombination/DNA repair was ruled out as responsible for the RS-SCID condition. Artemis was then identified as the gene responsible, a founder mutation which causes RS-SCID in Navajo and Apache Native Americans (1:2000 cases) (Li et al., 2002). Artemis was identified and cloned in 2000 by Moshous and colleagues (Moshous et al., 2000).

Artemis is located on the short arm of chromosome 10. Human Artemis consists of 692 amino acids that encode for a 97 kDa protein (Moshous et al., 2001), which exhibits an intrinsic ssDNA-specific 5' to 3' exonuclease activity and acquires endonuclease activity when complexed with DNA-PKcs. Artemis, as with its homologs PSO2 in yeast and muSNM1 in mouse, is a member of the large metallo-ß-lactamase superfamily with a metallo-ß-lactamase domain at the N-terminal region (Figure 6) (Callebaut et al., 2002; de Villartay et al., 2009; Pannicke et al., 2004). The N-terminus itself is divided into two further domains important for the enzymatic activity. Amino acids 1-155 of human Artemis comprise the metallo-ß-lactamase domain. Five sequence motifs (Asp37, His33, His35, His38, His115) in the metallo-ß-lactamases are highly conserved and possibly participate in metal coordination, substrate binding and enzymatic activities. Like all members of the metallo-ß-

lactamase superfamily, Artemis needs divalent conditions to be catalytically active (Callebaut et al., 2002; de Villartay et al., 2009; Pannicke et al., 2004).

Amino acids 156-385 of human Artemis build the ß-CASP domain (metallo-ß-lactamases-associated CPSF Artemis, SNM1 PSO2) named after its representative members. This domain is highly conserved and acts specifically on nucleic acids. Recently, de Villartay *et al.* reported that a histidine residue within the ß-CASP domain (His254) plays a key role in Artemis activity (de Villartay et al., 2009).
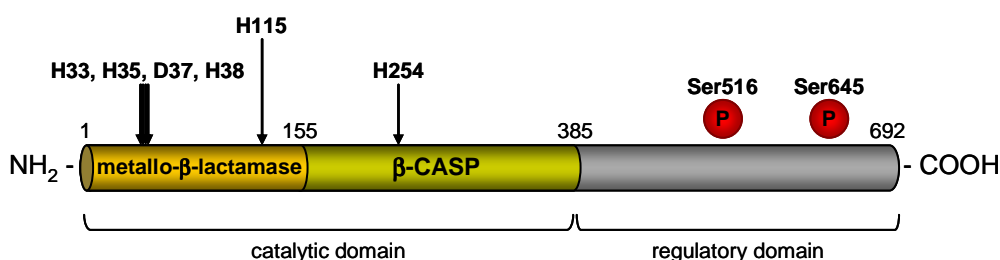
Figure 6. Schematic illustration of Artemis
Artemis contains a metallo-ß-lactamase/ß-CASP domain at the N-terminus which is the catalytic domain of the enzyme. The C-terminus is the regulatory domain. The positions of the amino acid residues involved in metal ion binding (Asp37, His33, His35, His38, His115) are indicated. The His254 within the ß-CASP domain plays a key role in Artemis activity. Artemis is phosphorylated in response to DNA damage at Ser516 and Ser645.

While the N-terminus of Artemis is important for its enzymatic role, the C-terminus appears to be a regulatory domain involved in its interaction with DNA-PKcs. Artemis is phosphorylated by DNA-PKcs, one of the key players of NHEJ, in the C-terminal domain at the two basal sites Ser516 and Ser645 (Chen et al., 2005b; Ma et al., 2005b). Ma *et al.* showed that DNA-PKcs regulates Artemis by both phosphorylation and complex formation (Ma et al., 2005b). The phosphorylation and binding of DNA-PKcs may cause a conformational change in Artemis, resulting in an activated form of Artemis with endonuclease activity (Niewolik et al., 2006). The C-terminus is believed to auto-inhibit Artemis' endonucleolytic activities, which can be reversed by phosphorylation of this tail by DNA-PKcs. In support of this data, it has been shown that C-terminally truncated Artemis derivates imitate *DNA*-PKcs activated wild-type Artemis protein and exhibit intrinsic endonuclease activity (Niewolik et al., 2006). On the other hand, Goodarzi *et al.* reported that auto-phosphorylated DNA-PKcs recruits Artemis to the sites of DNA damage (Goodarzi et al., 2006).

The Artemis endonuclease can cleave DNA hairpin ends that are generated particularly during V(D)J recombination and can also occur at DNA DSB sites after damage. Therefore, the interaction between DNA-PKcs and Artemis provides a link in the RS-SCID phenotype between the radiosensitivity and the SCID.

As mentioned above, genetic analyses indicate the involvement of Artemis not only in V(D)J recombination but also in NHEJ. It has been shown that Artemis reveals its endonuclease activity when complexed with DNA-PKcs. *In vitro* studies have demonstrated that this Artemis/DNA-PKcs complex can process hairpins and 5' or 3' overhangs to generate either blunt ends or 3' overhangs of 2-4 bases (Figure 7) (Lu et al., 2007; Ma et al., 2002; Povirk et al., 2007). Therefore, Artemis is believed to be involved in the opening of hairpin-sealed coding ends during V(D)J recombination as well as in the end processing step of NHEJ after DNA damage (Ma et al., 2002). In NHEJ, Artemis may have a role only when end trimming is necessary prior to ligation. For example, the Artemis/DNA-PKcs complex may remove chemically modified termini, often induced by IR (3'-phosphate or 3'-phosphoglycolate termini) or radiomimetic agents (5'-aldehyde termini). The Artemis/DNA-PKcs complex can convert such chemically modified ends to a form suitable for ligation with minimal loss of terminal sequence.
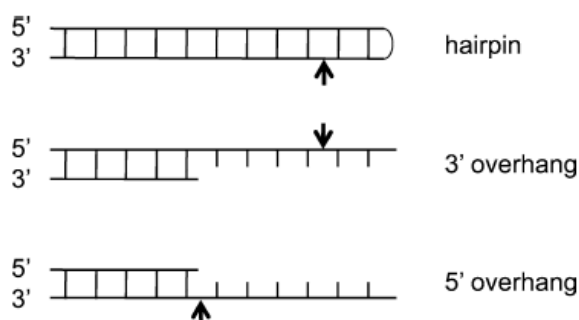
Figure 7. Endonucleolytic properties of the Artemis/DNA-PKcs complex. Shown are schematic structures of a hairpin DNA end and DNA ends with 3' or 5' overhangs. Arrows mark the major cleavage sites. (adapted from Kurosawa et al., 2010)

Although other nucleases also presumably participate in the processing reaction, Artemis is likely to be a central enzyme in the end processing step of NHEJ in higher eukaryotes.

In contrast to ATM, Artemis appears not to be implicated in checkpoint activation (Deckbar et al., 2007). However, it was suggested that Artemis rather facilitates the recovery from the G2- or inta-S-phase checkpoints (Geng et al., 2007; Wang et al., 2009).

2.6.3. ATM and Artemis in double-strand break repair

One of the characteristics of the *AT* phenotype is extreme radiosensitivity (one of the highest degrees of radiosensitivity known in humans). Additionally, it became clear early on that *AT* cells are not susceptible to apoptosis (Duchaud et al., 1996; Takagi et al., 1998). Taken together, it is therefore likely that ATM is not only involved in cell cycle checkpoint activation and DNA damage response, but also in DNA DSB repair itself.

However, pulsed-field gel electrophoresis and enumeration of γH2AX foci have indicated a repair defect only for a small fraction of DSBs (10-15%) (Beucher et al., 2009; Deckbar et al., 2007; Riballo et al., 2004). Since this fraction of unrepaired DSBs is similar for G1 and G2 phases, it has been suggested that an ATM defect does not display a defect in a certain pathway but rather a defect in the repair of a subset of DSBs that need processing in an ATM-dependent manner. Artemis, the nuclease involved in resolving hairpin intermediates during V(D)J recombination, has been described as an additional component of NHEJ (Ma et al., 2002). Even though DNA-PK rather than ATM activates Artemis during V(D)J recombination, it has been shown that Artemis can be phosphorylated by ATM and subsequently process DNA ends as part of the NHEJ DSB repair pathway (Chen et al., 2005b; Riballo et al., 2004). Furthermore, Artemis-deficient cells display the same fraction of 10-15% unrepaired DSBs in the G1- and G2-phases as *AT* cells, indicating the same repair defect, while simultaneously showing proficient checkpoint responses (Deckbar et al., 2007; Riballo et al., 2004).

So far, the direct involvement of ATM in DSB repair pathways has only been shown in conjunction with the activation of Artemis and has yet to be further defined. Most recent approaches have shown ATM's involvement in chromatin relaxation in response to DNA double-strand breaks. Ziv *et al.* characterized an ATM-dependent phosphorylation of KRAB associated protein 1 (Kap-1) on Ser824 with rapid kinetics peaking 30 min after irradiation and disappearing after several hours (Ziv et al., 2006). Kap-1 normally promotes heterochromatin formation via interactions with proteins like heterochromatin protein 1 (HP1), histone deacetylases (HDACs), and ATP-dependent chromatin remodelers. ATM interactions with Kap-1 transiently loosen interactions between Kap-1 and heterochromatic structures to enable repair in compact regions. Down-regulation of Kap-1 nullifies the requirement for ATM (Beucher et al., 2009; Goodarzi et al., 2008).

The defect in DSB repair in *AT* and *Artemis* cells, in contrast to wild type cells, is only observed at later time points (>2 h) after DSB induction in the G1- or G2- phase. Recent theories describe the fraction of unrepaired breaks as representing the slow component of DSB repair, DSBs that are located within or close to heterochromatic regions (Goodarzi et al., 2009). Furthermore, the slow component of DSB repair and therefore breaks located in heterochromatic regions involve NHEJ in G1 and specifically HR in G2, both requiring ATM and Artemis (Beucher et al., 2009).

Elucidation of the proteins and their functions in HR is one of the hot topics in radiobiology. These proteins execute a number of distinct steps, namely sensing the DSB, recruiting the appropriate resection and/or repair proteins and finally repairing the DSB itself. Control of these processes is in addition cell cycle dependent. Accurate repair by HR is particularly

important during the S-phase, where a significant portion of DSBs arises not from direct fracture of the DNA, but rather as a consequence of replication.

The pronounced IR sensitivity of human fibroblasts that have an inherited defect in either the ATM or the Artemis gene has been ascribed to a common defect in NHEJ. However, it is not known whether HR is also affected in the same way, since cell cycle progression is markedly different in both deficient cells. Analyses concerning the involvement of the ATM kinase and Artemis nuclease in DSB repair have thus far only been performed separately in the G1 and G2-phase.

In the current study, we have addressed the dependence of HR on ATM and Artemis throughout the cell cycle. In this context, we wished to elucidate how cell cycle progression can influence DNA repair. Further, we sought to identify whether ATM and Artemis-deficient strains are able to initiate and complete HR during the replicative S-phase. Moreover, we questioned whether ATM and Artemis function epistatically for HR during the S-phase.

3. Materials and Methods

3.1. Materials

3.1.1. Laboratory Equipments

➢ General:

Bio-photometer	Eppendorf, Hamburg, Germany
Centrifuge function line	Heraeus, Hanau, Germany
Freezer -20°C	Kryotech, Hamburg, Germany
Freezer -80 °C	Fryka, Esslingen, Germany
Hot-plate thermostat 5320	Eppendorf, Hamburg, Germany
Magnetic stirrer, RH Basis	IKA Labortechnik, Staufen, Germany
Minispin plus centrifuge	Eppendorf, Hamburg, Germany
Pair of scales AE160 / P1200	Mettler, Giessen, Germany
pH meter 300	Beckmann Instruments GmbH, Munich, Germany
Pipetboy	Eppendorf, Hamburg, Germany
Pipettes	Eppendorf, Hamburg, Germany
Refrigerated centrifuge 5804R	Eppendorf, Hamburg, Germany
Refrigerated centrifuge, Megafuge 1.0R	Heraeus, Hanau, Germany
Refrigerated microcentrifuge R	Beckmann Instruments GmbH, Munich, Germany
Refrigerator	Bosch, Stuttgart, Germany
Water bath	Lauda, Lauda-Königshofen, Germany

➢ Cell culture:

Axiovert 40CFL	Carl Zeiss, Göttingen, Germany
Cell incubator Hera cell 240	Kendro, Hanau, Germany
Cell incubator inCu safe	Sanyo, Leicestershire, UK
Coulter Counter model Z1	Beckman Coulter, Krefeld, Germany
Mr. Frosty	Nalgene, NY, USA
Olympus CK2	Olympus Optical Co., LTD, Japan
Sterile work benches, Herasafe	Kendro, Hanau, Germany

➢ Western blot:

Bag sealer	Severin, Sundern, Germany
Criterion Precast Gel System (Criterion electrophoresis cell and Citerion Blotter)	Bio-Rad Laboratories, Hercules, CA, USA
Developer, curix 60	agfa, Mortsel, Belgium
Light sensitive CCD camera system (NightOWL)	Berthold Technologies GmbH&Co. KG Bad Wildbad, Germany
Power Supply Consort E455 / E802	Labortechnik Fröbel GmbH, Lindau/ Bodensee Germany
Tilting table / shaker platform	neoLab, Heidelberg, Germany
Western blot development cassette	Amersham Pharmacia, Buckinghamshire, UK

➢ Others:

7900HT Fast Real-Time PCR System	Applied Biosystems, CA, USA
Flow Cytometer FACSan	Beckmann Instruments GmbH, Munich, Germany
Fluorescence microscope, Axioplan 2 System for confocal pictures: Apotome, AxioCam MRn	Carls Zeiss, Göttingen, Germany
Primus Thermal cycler	MWG Biotech, Ebersberg, Germany
X-ray generator type RS225 research	Gulmay Medical LTD, Oxford, UK

3.1.2. Laboratory Material

➢ General:

Gloves, latex	Hartmann, Heidenheim, Germany
Gloves, nitrile	Ansell, Staffordshire, UK
Parafilm	Pechiney Plastic, Chicago, USA
Pasteur pipettes, plastic	Falkon, NJ, USA
Pipette tips	Eppendorf, Hamburg, Germany
Pipette tips, stuffed	Eppendorf, Hamburg, Germany
Pipettes, plastic (1-50ml)	Falkon, NJ, USA
Tubes 1.5ml, 2ml	Eppendorf, Hamburg, Germany
Tubes 15ml, 50ml	Falkon, NJ, USA
Wipes	Wepa, Arnsberg, Germany

➢ Cell culture:

6 well plates	Falkon, NJ, USA
Cell culture flasks T25, T75	Sarstedt, Nümbrecht, Germany
Cryo-tubes	Sarstedt, Nümbrecht, Germany
Pasteur pipettes, glass	Carl Roth GmbH, Karlsruhe, Germany
Sterile filter (Rotilabo 0,22 µm)	Millipore, MA, USA

➢ Western Blot:

Filter paper, Whatman	Bio-Rad Laboratories, Hercules, CA, USA
PVDF membrane	GE Healthcare, Buckinghamshire, UK
X-ray film	Amersham Pharmacia Biotech, Freiburg, Germany

➢ Others:

Cover slips	Karl Hecht, Sondheim, Germany
MicroAmp® Fast Optical 96-well Reaction Plate (0.1ml)	Applied Biosystems, CA, USA
Microscope slides	Karl Hecht, Sondheim, Germany
Optical Adhesive Covers	Applied Biosystems, CA, USA
Round-bottom tube (FACS)	Sarstedt, Nümbrecht, Germany

3.1.3.   Chemicals, reagents and kits

➢ Reagents:

ß-mercaptoethanol	Sigma-Aldrich, Deisenhofen, Germany
2-propanol	Merck, Bad Soden, Germany
Antifade mounting medium, Vectashield	Vector Laboratories, Ca, USA
ATM inhibitor KU55933	Tocris Bioscience, Missouri, USA
Bovine serum albumin (BSA)	PAA, Pasching, Austria
Bromphenol blue	Sigma-Aldrich, Deisenhofen, Germany
Caffeine	Sigma-Aldrich, Deisenhofen, Germany
Coomassie Brilliant Blue G250	Sigma-Aldrich, Deisenhofen, Germany
Coomassie Brilliant Blue R250	Sigma-Aldrich, Deisenhofen, Germany
Crystal violet stain	Sigma-Aldrich, Deisenhofen, Germany
Dimethyl sulfoxide (DMSO)	Sigma-Aldrich, Deisenhofen, Germany
Disodium hydrogen phospate (Na_2HPO_4)	Merck, Bad Soden, Germany
Ditheotheratol (DTT)	Sigma-Aldrich, Deisenhofen, Germany

DNA-PK inhibitor NU7026	Calbiochem/Merck Bad Soden, Germany
Ethanol	Th. Geyer, Hamburg, Germany
Formaldehyde 37%	Merck, Bad Soden, Germany
Glucose	Sigma-Aldrich, Deisenhofen, Germany
Glycerin	Sigma-Aldrich, Deisenhofen, Germany
Hydrochloric acid (HCl)	Merck, Bad Soden, Germany
Magnesium chloride (MgCl$_2$)	Sigma-Aldrich, Deisenhofen, Germany
Methanol	J.T. Baker, NJ, USA
Potassium chloride (KCl)	Merck, Bad Soden, Germany
Potassium dihydrogen phosphate (KH$_2$PO$_4$)	Merck, Bad Soden, Germany
RNase	Serva, Heidelberg, Germany
Sodium chloride (NaCl)	J.T. Baker, NJ, USA
Sodium dodecyl sulfate (SDS)	Sigma-Aldrich, Deisenhofen, Germany
Sodium hydrogen phosphate (NaH$_2$PO$_4$)	Merck, Bad Soden, Germany
Sucrose	Merck, Bad Soden, Germany
Tris-HCl	Sigma-Aldrich, Deisenhofen, Germany
Triton X	Serva, Heidelberg, Germany
Trizma base	Sigma-Aldrich, Deisenhofen, Germany
Tween 20 (polyoxyethylene (20) sorbitan monolaurate)	Sigma-Aldrich, Deisenhofen, Germany
UCN-01	Sigma-Aldrich, Deisenhofen, Germany

> ➢ Kits:

BCA Protein Assay	Pierce Biotechnology, IL, USA
EdU Click-iT ™ Assay Kit	Invitrogen, Karlsruhe, Germany
Enhanced chemiluminescence (ECL)	Amersham Pharmacia Biotech, Freiburg, Germany
Mycoplasma PCR Elisa Kit	Roche Diagnoistics, Mannheim, Germany
RNeasy Mini Kit	Qiagen, Hilden, Germany
Transcriptor 1st Strand cDNA Synthesis Kit	Roche Diagnoistics, Mannheim, Germany

3.1.4. Cell lines and media for cell culture

All cell lines used in this study were regularly tested for mycoplasma infection.

1BR.3 hTert	primary human skin fibroblasts generated from a healthy donor, immortalized with an hTert-expressing (*human telomerase reverse transcriptase*) retrovirus, kindly provided by Dr. P. A. Jeggo (University of Sussex, Brighton, UK); cultivation in alpha-Medium supplemented with 10% fetal calf serum, 100 U/ml penicillin and 100 µg/ml streptomycin.
AT1BR hTert	primary human skin fibroblasts generated from a donor with ataxia telangiectasia carrying a homozygous mutation in the ATM gene, immortalized with an hTert-expressing (*human telomerase reverse transcriptase*) retrovirus, kindly provided by Dr. P. A. Jeggo (University of Sussex, Brighton, UK); cultivation in alpha-Medium supplemented with 10% fetal calf serum, 100 U/ml penicillin and 100 µg/ml streptomycin.
FO2-385 hTert	primary human skin fibroblasts generated from a donor with RS-SCID carrying a homozygous mutation in the Artemis gene, immortalized with an hTert-expressing (*human telomerase reverse transcriptase*) retrovirus, kindly provided by Dr. P. A. Jeggo (University of Sussex, Brighton, UK); cultivation in alpha-Medium supplemented with 10% fetal calf serum, 100 U/ml penicillin and 100 µg/ml streptomycin.
CJ179 hTert	primary human skin fibroblasts generated from a donor with RS-SCID carrying a homozygous mutation in the Artemis gene, immortalized with an hTert-expressing (*human telomerase reverse transcriptase*) retrovirus, kindly provided by Dr. P. A. Jeggo (University of Sussex, Brighton, UK); cultivation in alpha-Medium supplemented with 10% fetal calf serum, 100 U/ml penicillin and 100 µg/ml streptomycin.
HeLa	human epithelial cervical cancer cell line, derived from a patient named Henrietta Lacks in 1951, one of the oldest and most commonly used human cell lines; cultivation in DMEM supplemented with 10% fetal calf serum, w/o 100 U/ml penicillin or 100 µg/ml streptomycin.

HeLa pGC HeLa cell line containing a single stably integrated copy of the reporter construct for gene conversion, generated by Mansour et al; cultivation in DMEM supplemented with 10% fetal calf serum, w/o G418.

All media and reagents for cell culture were obtained from Invitrogen GmbH Karlsruhe, Germany.

DMEM
α-Medium MEM-α-powder, 0.22% (w/v) NaHCO$_3$ to 1l with ddH$_2$O
Opti-MEM
Penicillin 10,000 U/ml Penicillin
Streptomycin 10,000 µg/ml Streptomycin
Trypsin-EDTA
G418 Sulphate Geneticin, selective antibiotic
Fetal calf serum (FCS)
Cryopreservation solution 10% DMSO in FCS

3.1.5. Buffers and solutions

Deionized water was used for all buffer preparations. Ultrapure RNase-free water (Invitrogen, Karlsruhe, Germany) was used for RNA-interference experiments.

PBS (phosphate buffered saline)
140 mM NaCl
3 mM KCl
8 mM Na2HPO4

Crystal violet staining solution
0.1 % (w/v) Crystal violet/ddH2O

➢ **Solutions for Western blot:**
Ponceau red
3 % Trichloroacetic acid
2 % (w/v) Ponceau S/ddH2O

Protein extraction buffer (5x)
Protease inhibitor cocktail in PBS or TBS (Sigma-Aldrich, Deisenhofen, Germany)

Protein loading buffer, pH 6.8 (5x)

50 mM	Tris-HCl
100 mM	DTT
2% (w/v)	SDS
0.1% (w/v)	Bromophenol blue
10%	Glycerol

10x Tris-glycine buffer (TG buffer)

1.92 M	Glycine
0.25 M	Trizma base

Electrophoresis buffer (1x)

100 ml/l	10x TG buffer
10 ml/l	10% SDS

Transfer buffer

200 ml	10x TG buffer
400 ml	Methanol
1.4 l	cold ddH$_2$O

TBS, pH 7.5 (10x)

100 mM	Tris-HCl
1 M	NaCl

TBST (0.2% Tween 20)

2 ml	Tween 20
998 ml	TBS

Blocking Solution (10% BSA or non-fat milk)

10 % (w/v)	BSA / PBS
10 % (w/v)	non-fat milk / PBS

Coomassie blue staining solution

2 mM	Coomassie brillant blue R250
0.6 mM	Coomassie brillant blue G250
42.5%	Ethanol
10%	Acetic acid

Destaining solution

13%	Methanol
10%	Acetic acid

Stripping buffer, pH 2.5

200 mM	Glycine
1% (w/v)	SDS

➤ **Solutions for Immunofluorescence:**

Fixing solution

2%	Formaldehyde 37% / PBS

Permeabilization solution

0.2%	Triton-X
1%	BSA / PBS

Blocking solution

3%	BSA / PBS

PBST (0.5% Tween 20)

0.5 ml	Tween 20
995 ml	PBS

3.1.6. Antibodies

Primary antibodies

➤ Polyclonal

Rabbit anti-Artemis	Novus Biologicals, Cambridge, UK
Rabbit anti-ATM	Epitomics, CA, USA
Rabbit anti-Rad51	Abcam, Cambridge, UK
Rabbit anti-pChk2 Thr68	Cell Signaling, MA, USA
Rabbit anti-Chk2	Cell Signaling, MA, USA
Rabbit anti-pChk1 Ser345	Cell Signaling, MA, USA
Rabbit anti-Chk1	Cell Signaling, MA, USA
Rabbit anti-53BP1	Novus Biologicals, Cambridge, UK
Rabbit anti-CenpF	Lifespan Biosciences, WA, USA

➢ Monoclonal

Mouse anti-β–actin   Sigma-Aldrich, Deisenhofen, Germany

Mouse anti-γH2AX Ser139   Cell Signaling, MA, USA

Mouse anti-Rad51   Abcam, Cambridge, UK

Secondary antibodies

➢ Western blot analyses

horseradish peroxidase-linked anti-rabbit IgG   Amersham Pharmacia Biotech, Freiburg, Germany

horseradish peroxidase-linked anti-mouse IgG   Amersham Pharmacia Biotech, Freiburg, Germany

➢ Immunofluorescent microscopy

anti-mouse Alexafluor594 IgG   Invitrogen, Karlsruhe, Germany

anti-rabbit fluorescein IgG   Amersham Pharmacia Biotech, Freiburg, Germany

3.1.7. Oligonucleotides (sense and antisense siRNAs)

➢ **Molecular probes for TaqMan® Gene Expression Assay**

The TaqMan® Gene Expression Assay was obtained from Applied Biosystems, CA, USA.

hArtemis (FAM-labelled)	`CTTTGATGATCCTCTGCCAATACCT`	(F)
	`TGCTTTTCTGATACTGCAGTCATTGA`	(R)
GAPDH (FAM-labelled)	`TTGGGCGCCTGGTCACCAGGGCTGC`	(F)
	`GTTGTCATGGATGACCTTGGCCAGG`	(R)

➢ **siRNA sequences:**

All siGENOME ON-TARGETplus SMART pool duplexes were obtained from Dharmacon, CO, USA.

hArtemis:

(1) sense sequence   `GUACGGAGCCAAAGUAUAA`

    antisense sequence   `5'-P UUAUACUUUGGCUCCGUACUU`

(2) sense sequence   `GCACAACUAUGGAUAAAGU`

    antisense sequence   `5'-P ACUUUAUCCAUAGUUGUGCUU`

(3) sense sequence   `UGAAUAAGCUAGACAUGUU`

    antisense sequence   `5'-P AACAUGUCUAGCUUAUUCAUU`

(4) sense sequence   `CACCAAAGCUUUUCAGUGA`

    antisense sequence   `5'-P UCACUGAAAAGCUUUGGUGUU`

hATM:

(1) sense sequence		GCAAAGCCCUAGUAACAUA
antisense sequence	5'-P	UAUGUUACUAGGGCUUUGCUU
(2) sense sequence		GGUGUGAUCUUCAGUAUAU
antisense sequence	5'-P	AUAUACUGAAGAUCACACCUU
(3) sense sequence		GAGAGGAGACAGCUUGUUA
antisense sequence	5'-P	UAACAAGCUGUCUCCUCUCUU
(4) sense sequence		GAUGGGAGGCCUAGGAUUU
antisense sequence	5'-P	AAAUCCUAGGCCUCCCAUCUU

hRad51:

(1) sense sequence		UAUCAUCGCCCAUGCAUCA
antisense sequence	5'-P	UGAUGCAUGGGCGAUGAUAUU
(2) sense sequence		CUAAUCAGGUGGUAGCUCA
antisense sequence	5'-P	UGAGCUACCACCUGAUUAGUU
(3) sense sequence		GCAGUGAUGUCCUGGAUAA
antisense sequence	5'-P	UUAUCCAGGACAUCACUGCUU
(4) sense sequence		CCAACGAUGUGAAGAAAUU
antisense sequence	5'-P	AAUUUCUUCACAUCGUUGGUU

controls:

ON-TARGETplus Cyclophilin B Control siRNA (Human), ON-TARGETplus GAPD Control Pool (Human), ON-TARGETplus Non-targeting Pool #1

Control siRNA conjugated with a Cy3 fluorescent dye was obtained from Qiagen.

3.1.8.   Plasmids

pCMV3xnls-I-SceI	A kind gift from M. Jasin
pEGFP-N1	Clontech, BD Bioscience, Heidelberg, Germany
pGC	Previously constructed by our group

3.1.9.   Transfection

Two different chemical transfection methods were used:

➢ HiPerFect transfection reagent for siRNA	Qiagen, Hilden, Germany
➢ LipoFectamin2000 transfection agent for plasmid DNA	Invitrogen, Karlsruhe, Germany

3.1.10. DNA staining solutions

DAPI (4′,6-Diamidin-2-phenylindol)   1mg/ml

Propidum iodine   10µg/ml

3.1.11. Molecular weight markers

Protein markers: Bench Mark pre-stained protein ladder (Invitrogen, Karlsruhe, Germany)

Magic Mark Western standard (Invitrogen, Karlsruhe, Germany)

SeeBlue® Plus2 pre-stained standard (Invitrogen, Karlsruhe, Germany)

3.2.   Methods

3.2.1.   Cell manipulation

All cell culture work was conducted in a sterile laminal flow hood. Cell growth was examined regularly using an inverted-phase microscope. For cell passaging, the medium was removed from the flasks, leaving the cells adhered to the growth surface of the flask. The cells were washed with 5-10 ml pre-warmed sterile PBS. After removing the PBS, pre-warmed trypsin-EDTA was added (1 ml per T25 flask, 2 ml per T75 flask) and the cells were subsequently incubated at 37℃ until they detached from the surf ace. To help dislodge the remaining adherent cells, the bottom of the flask was tapped sharply with the palm of the hand. After all cells had detached, medium containing serum was added to inactivate the trypsin. For resuspension, the cells were gently pipetted up and down. The cells were then counted using the cell counter and the appropriate number of cells was distributed to fresh flasks for subculturing.

For cell preparation, resuspended cells were collected by centrifugation at 1,200 rpm for 5 min. The cell pellet was washed by adding 5 ml pre-warmed sterile PBS. The cell suspension was centrifuged at 1,200 rpm for 5 min. After centrifugation, the supernatant was removed and the cell pellet was used for experiments.

Sub-confluent cells were used for preservation. Trypsinized and resuspended cells were centrifuged at 1,200 rpm for 5 min. Thereafter, the supernatant was removed and the cell pellet was gently suspended in cell preservation solution, aliquotted in cryo-tubes (3-5x10^6 cells/tube) and incubated at -80℃ overnight using a Mr. Frosty before finally being stored in liquid nitrogen (-196℃).

For re-culturing of the stored cells, the cells were quickly thawed at 37℃ and gently pipetted into a T75 cell culture flask containing 15 ml pre-warmed medium/10% FCS. Shortly after the

cells had attached to the growth surface of the flask, the medium containing the cell preservation solution was removed and 15 ml fresh pre-warmed medium/10% FCS was added.

3.2.2. Colony formation assay

Colony formation assays were developed (Puck et al., 1956) to study the effect of specific treatments (i.e. ionizing radiation) on the cells' ability to form colonies (i.e. to continuously produce offspring). Cells were seeded with an appropriate number of cells and allowed to adhere at 37°C (3-4 h) prior to drug treatment or irradiation. After X-irradiation, cells were incubated for three weeks to allow for colony formation. The cells were then washed with PBS, fixed with 70% ethanol, and stained with crystal violet. Colonies were subsequently counted by eye. Colonies containing fifty or more cells (> 5 cell divisions) were considered to be "survivors". The plating efficiency (PE) was determined as the number of colonies formed divided by the number of seeded cells. Survival curves were derived from triplicates of at least three independent experiments. As a control, DMSO was used instead of the inhibitor at the same concentration.

3.2.3. Immunofluorescence

Immunofluorescence is a technique that allows for the visualization of a specific protein or antigen in cells or tissues through the binding of a specific secondary antibody chemically conjugated to a fluorescent dye responsible for emitting the signal. Stained samples are examined using a fluorescence microscope providing monochromatic light at the desired wavelength. We applied this technique to visualize the local enrichment of proteins involved in DDR or DSB repair at the sites of DNA damage, forming so-called "foci", and/or to visualize different stages of the cell cycle through differential staining of pan-nuclear proteins specifically expressed in certain cell cycle phases (i.e. CenpF in G2). All experiments for immunofluorecent microscopy were performed using cover slips. To this end, cells were grown in 6-well plates containing 1-3 cover slips each, followed by drug treatment and irradiation. After certain time points, the cells were fixed in 2% formaldehyde in PBS for 10 minutes and washed (3x) with PBS. The fixed cells were then permeabilized for 5 min. on ice. The permeabilization step is needed to ensure free access of the antibody to its antigen. Afterwards, blocking solution was added to the cover slips (the side containing the fixed cells) for at least 1h in order to block nonspecific sites where the antibody might bind. Cells were subsequently incubated with primary antibody in washing solution containing 1% BSA for 1 h. After washing with PBS three times for 10 min to remove excess unbound antibody, cells were incubated with either anti-mouse conjugated with Alexafluor594 or anti-rabbit

conjugated with fluorescein antibodies (in washing solution/1% BSA). Finally, the DNA was stained using DAPI (1:1000). This step and the following must be performed in the dark. After washing the cells again three times for 10 min each, the cells were mounted using antifade mounting medium. The cover slips - with the cells facing down - were placed on microscope slides with some mounting medium. The cover slips were pressed gently onto the microscope slide and sealed with nail polish to preserve the samples. The slides were then examined and photographed under the Zeiss Axioplan 2 (fluorescent microscope, by which the fluorescent tags are excited with the respective wavelength, resulting in emission of a fluorescent signal).

3.2.4.   Western blot

The expression levels of proteins of interest were examined by western blot analysis. Total proteins were extracted from the whole cells. The same amount of protein was electrophorized on a 4-15% gradient SDS-PAGE gel and then transferred onto a PVDF membrane. Protein expression was monitored by chemo-luminescence detection.

➢   Protein extraction and quantification

The extraction of the total proteins was achieved according to Finnie *et al.* (Finnie et al., 1995). Cells were collected by trypsinization and the cell suspension centrifuged. The pellet was resuspended in the same volume of protein extraction buffer and alternatingly shock-frozen in liquid N_2 and thawed at 37℃ (3x). The lysed mixture was cen trifuged at 12,000 rpm/4℃ for 15 min. The supernatant containi ng the total soluble protein was then transferred to a new tube and optionally stored in -80℃.

The BCA-method was used to determine total protein concentration (Smith et al., 1985) based on the use of the Biuret-reaction. The Biuret-reaction is a chemical indicator of peptide bonds. The Biuret reagent (copper sulphate dissolved in a strong base) changes from green-blue to violet in the presence of proteins. The BCA protein assay reagent was prepared by mixing reagent A and reagent B of the Pierce BCA reaction kit in a ratio of 50:1. 2 µl protein extract was added to 48 µl ddH2O. 50 µl ddH2O was used as a blank control. 1 ml of the BCA reagent (A+B) was added to the blank as well as to the diluted samples. Following vortexing, the samples were incubated at 37℃ for 3 0 min. The colour intensity was determined using a spectrophotometer at a wave length of 562 nm.

> ➢ Sodium dodecyl sulfate-polyacrylamide gel electrophoresis (SDS-PAGE) and transfer to PVDF membrane

For the electrophoresis, the same concentration of total protein and 5x loading buffer was added to ddH$_2$O up to a final volume of 20 µl. The samples were vortexed and denatured at 100°C for 5 min., spun down, placed on ice or optio nally stored at 4°C. The samples were then loaded onto SDS-polyacrylamide gels. For molecular weight determination, Magic Mark, Bench Mark, or See Blue Plus2 Protein Standards were run in parallel lanes on the gel. The electrophoresis was performed at 100 V for 10 min to collect the proteins through the stacking gel and at 200 V for 60 min for separation. The electrophorized proteins were transferred onto PDVF membranes with 0.2 µm pores. The membranes were activated by submersion in methanol for 5 min. and then washed for 5 min. in ddH2O. Both gel and membrane were equilibrated in transfer buffer for 5 min. Transfer was performed by electro-blotting for 4 h at 50 V and 4°C. After blotting, t he gel was stained in Coomassie Blue staining solution for 30 min and the membrane in Ponceau red to confirm the completeness of the transfer.

> ➢ Detection of proteins

After blotting, the membrane was blocked for 1 h in blocking solution (10% non-fat milk or 10% BSA) at RT to prevent any unspecific protein binding to the PVDF material that would lead to a strong background. All of the following incubations were performed on a shaker platform to achieve optimal contact between solutions and membrane. The membrane was incubated for 5 min in TBST solution at RT, followed by overnight incubation at 4°C with the primary antibody in 5% non-fat milk or 5% BSA in TBST. The membrane was then washed three times for 10 min in TBST solution at RT. Thereafter, the secondary antibody (ECL anti-rabbit/anti-mouse IgG) was added in 5% non-fat milk or 5% BSA (1:3000/1:1000 respectively) and incubated for 1 h at RT. The membrane was washed again three times with TBST solution in order to remove unbound secondary antibodies from the membrane. For signal detection, the membrane was incubated for 30 sec. with the ECL solution (consisting of equal volumes of solution 1 and 2 from the Amersham ECL kit). An X-ray film was exposed to the membrane and the chemo-luminescence signal was detected after the film had developed (curix 60 developer). Alternatively, the chemo-luminescent signals were detected using a sensitive CCD-camera (NightOWL). After detection of the respective protein signal on the membrane, the signal of the housekeeping protein β-actin was analogously measured as a control to verify equal loading of the samples.

3.2.5.   Double-strand break reporter assay for gene conversion

In this study, we used a reporter assay to quantify the repair pathway of gene conversion (GC). This assay is based on a repair substrate that relies on the restitution of a GFP gene upon completed recombination repair of an induced DSB. The pGC substrate consists of two inactive GFP genes (Figure 8). The first copy is inactivated by the insertion of an 18-bp I-SceI recognition site into the unique BcgI site of the GFP-coding sequence. The second copy is a truncated fragment of GFP (inactive) located 2.2 kb downstream of the mutated GFP fragment sequence and placed in the same orientation (Figure 8). The homology shared by both fragments is 520 bp long, with 219 bp upstream and 301 bp downstream of the I-SceI recognition site. After induction of the DSB by I-SceI endonuclease, the cell can repair this DSB by GC using the truncated copy, thus resulting in GFP expression.

I-SceI

CMV Promotor | GFP | ΔGFP

Figure 8. Reporter construct for gene conversion
The pGC reporter has two non-functional GFP copies that share 520 bp of homology. DSB repair conducted by gene conversion results in functional GFP. The construct is not drawn to scale.

We used HeLa pGC cells containing a single stably integrated copy of the reporter construct for gene conversion (Mansour et al., 2008) for transfection with the I-SceI expression vector pCMV3xnls-I-SceI to induce the DSB. The cells were assessed 72 h post-transfection for green fluorescence by flow cytometry. 48 h prior to induction of the DSB by I-SceI, HeLa pGC cells (3×10^5) were seeded in 6-well plates and siRNAs (25 nM) were transfected (HiPerFect transfection reagent, Qiagen) to down-regulate specific proteins in order to study their impact on gene conversion. The transfection of the I-SceI expression plasmid (2 µg) and the second round of siRNA (50 nM) were performed using LipoFectamin2000 (Invitrogen). KU55933 inhibitor or DMSO controls were given shortly before the co-transfection. Experiments were done in duplicates and repeated three times.

3.2.6.   Transfection techniques

➢   Plasmid transfection:

In order to quantify repair using the DSB reporter assay, a DSB had to be induced in the HeLa-pGC clones. We transiently transfected the I-SceI-expressing vector pCMV3xnls-I-SceI by using LipoFectamin2000 transfection agent for plasmid DNA according to the manufacturer's instructions. For transfection in 6-well plates, we used 2 µg of the I-SceI

expression vector and 5 µl LipoFectamin2000 transfection agent per well. Plasmid-DNA and transfection agent were incubated in Opti-MEM medium and then added to the cells containing normal medium/10% FCS without antibiotics. 24 h later, the medium was replaced by fresh medium/10% FCS and further incubated to allow for DNA repair.

Transfection efficiency is dependent on cell type. To monitor the efficiency of the transfection in HeLa cells, we used the pEGFP-N1 plasmid that encodes for the GFP protein. The percentage of green fluorescent cells was assessed by flow cytometry at various time points up to 48 h post-transfection. HeLa cells reached a maximum of 40.7 ± 6.7% GFP-positive cells between 24 and 48 h post-transfection (Figure 9).
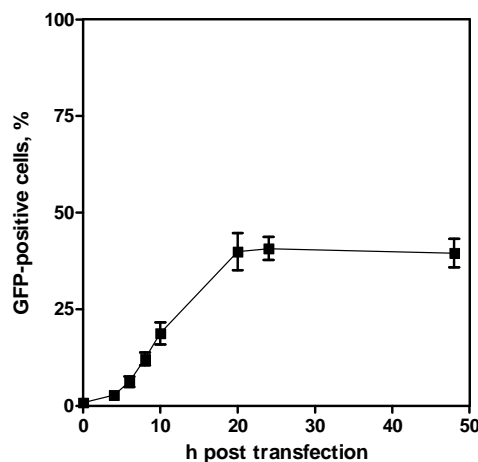
Figure 9. Transfection efficiency in HeLa cells
HeLa cells were transfected with the GFP-expressing plasmid pEGFP-N1. Cells were harvested after the indicated time points and assessed for expression of GFP by flow cytometry. GFP expression reached a maximum at 24 h post-transfection, with 40.7 ± 6.7 % GFP-positive cells. This expression level was consistent for up to 48h post-transfection.
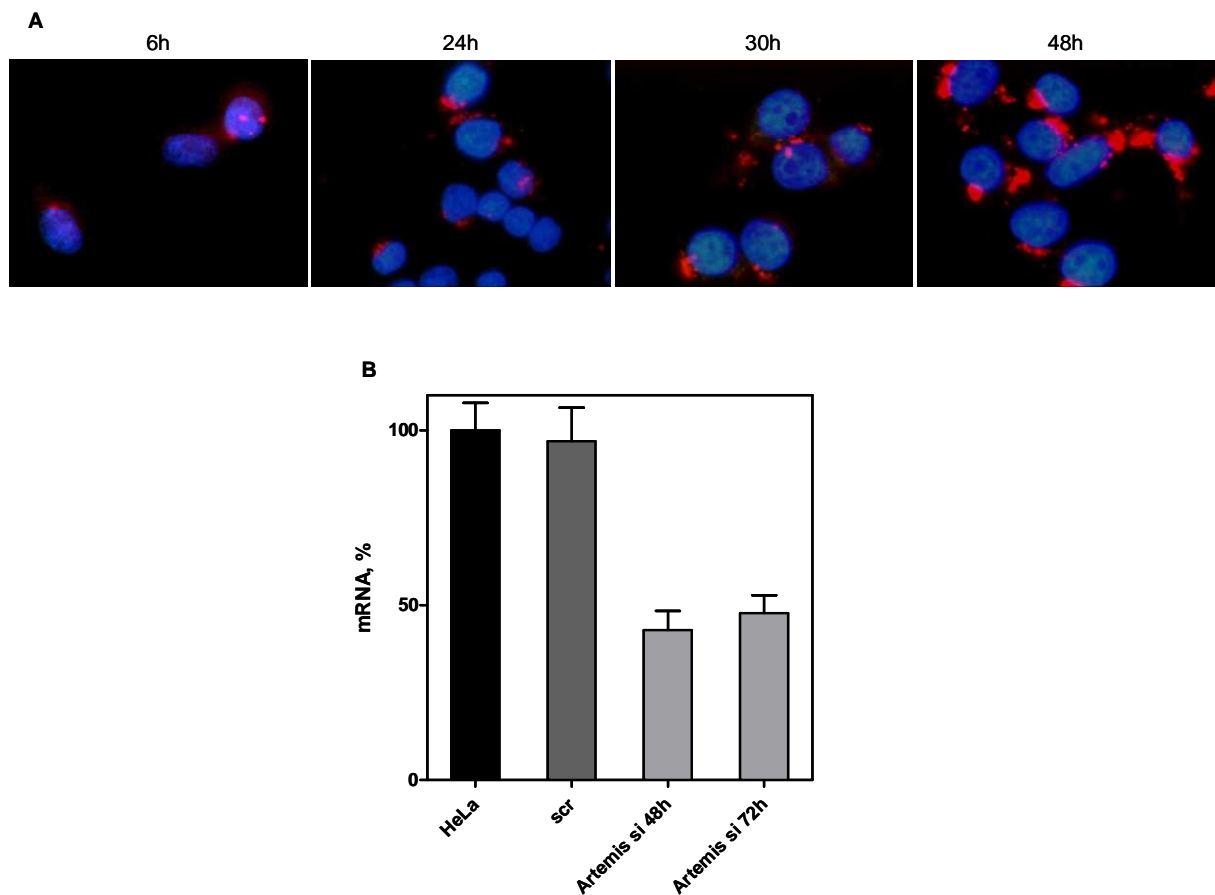
➤ siRNA transfection:

RNA interference (RNAi) is a mechanism that inhibits gene expression at the level of translation. The RNAi pathway is initiated by the enzyme dicer, which cleaves long double-stranded RNA molecules into short fragments of approximately 20 base pairs. These fragments are called small interfering RNA (siRNA). The siRNA is recognized by a multi-protein complex called the RNA-induced silencing complex (RISC), which incorporates one strand of the siRNA and uses it to target complementary mRNA molecules for degradation. The RNAi pathway is found in many eukaryotes and participates in controlling gene activity.

In cell culture, synthetic siRNA introduced into the cells can similarly be used to drastically decrease the expression of a gene of interest through the degradation of its mRNA. The RNAi technique may not totally abolish the expression of the protein and is therefore referred to as "knockdown" to distinguish it from "knockout" procedures.

To prevent the destruction of siRNA molecules added to regular medium by traces of RNAse, experiments using siRNA were performed in RNAse-free medium. In this study Rad51, Artemis, ATM and control (scrambled, Cyclophilin B, GAPDH) siRNA oligonucleotides were obtained from Dharmacon. We used smartpool siRNA, which is composed of four different oligonucleotides targeting the same mRNA, to enhance the knockdown effect. We transiently transfected siRNAs by using HiPerFect transfection reagent (Qiagen) according to the manufacturer's instructions. 3×10^5 cells (HeLa with or without reporter construct for GC) were seeded in 6-well plates in 1.4 ml medium/10% FCS (no antibiotics). For the transfection of 6-well plates, 25 nM siRNA and 8 µl HiPerFect transfection reagent were added to 100 µl Opti-MEM. This solution was distributed onto the plates before the cells had attached ("fast forward protocol"). We used three methods to control for siRNA transfection efficiency: (1) by monitoring general efficiency though the distribution of the siRNAs within the transfected cell population by using a special siRNA chemically conjugated with a fluorescent dye, (2) by monitoring the amount of target mRNA through real-time PCR, and (3) by frequently monitoring the expression of particular proteins in western blot analysis.

(1) Cells were grown on cover slips and transfected with Cy3 conjugated siRNA. The cover slips were fixed using 2% formaldehyde in PBS for 10 min, washed (3x) with PBS and permeabilized for 5 min. on ice. To identify the nuclei, the DNA was stained with DAPI for 10 min, washed (3x) with PBS and mounted onto a microscope slide, which were then sealed with nail polish to preserve the samples. The slides were examined under the fluorescent microscope (Zeiss Axioplan 2), by which the fluorescent tags of the siRNAs are excited with the respective wavelength, resulting in the emission of a fluorescent signal. In this way, the siRNAs could be localized within the cell population (Figure 10A). With time, we found an increasing localization of the siRNA in the cytoplasm of the cells, reaching maximal intensity at 48 h post-transfection (Figure 10A). (2) HeLa cells were grown in 6-well plates as indicated above, transfected with control siRNA (scrambled) or anti-Artemis siRNA, and cell pellets were harvested 48 and 72 h post-transfection. To monitor the amount of target mRNA, we isolated RNA using the RNeasy Mini Kit (Qiagen) according to the manufacturer's instructions. We used 50 ng RNA to synthesize cDNA using the 1st Strand Synthesis-Applied Two Step Protocol (Roche) according to the manufacturer's instructions. cDNA synthesis consists of two steps: (i) the template RNA – primer mixture is denatured for 5 min. at 70°C, (ii) buffer, RNAse inhibitor, dNTPs, DTT, and reverse transcriptase are added for the cDNA reaction (47°C 50 min., 75°C 10 min. in the Pr imus Thermalcycler). The generated cDNA can be used for amplification without further purification. We used molecular probes for human Artemis (target) or GAPDH (control) labelled with FAM for amplification and prepared the PCR reaction mix using the TaqMan® Gene Expression Assay (Applied Biosystems). The real time reaction was performed and monitored in a 7900HT Fast Real-

Time PCR system (Applied Biosystems) with 40 cycles of 15 sec at 95℃ and 1 min at 60℃. GAPDH was used as a housekeeping gene, with samples being normalized to this internal standard. With this approach, we detected a maximal reduction of Artemis mRNA at 48 h post-transfection, to 47.2% ±5% (Figure 10B). (3) The most essential method to monitor knockdown efficiency is the expression of the particular protein for which we used western blot analysis. Extensive control experiments in addition to RT-PCR indicated that a second transfection with siRNA could significantly improve knock-down efficiency. We therefore transfected the cells for a second time after 48 h as described in detail in part 2.2 of the results.

Figure 10. siRNA transfection and knockdown efficiency
(A) HeLa cells were grown on cover slips and transfected with Cy3 conjugated siRNA. Cover slips were fixed at the time points indicated, stained with DAPI and examined under a fluorescent microscope. Cy3 conjugated siRNA (red) can be detected in the cytoplasm of the cells at 6 h post-transfection. Accumulation in the cytoplasm was maximal at 48 h post-transfection.
(B) Quantification of the mRNA level by RT-PCR. mRNA from HeLa cells was isolated post-transfection with either anti-Artemis or scrambled siRNA. After generation of cDNA, RT-PCR was performed using molecular probes for human Artemis or GAPDH as a housekeeping gene, and normalized to the GAPDH standard. Maximal reduction of Artemis mRNA was detected 48 h post-transfection.

3.2.7. Cell cycle analysis

➢ Flow cytometry

To monitor cell cycle distribution by flow cytometry (FACScan, BD Bioscience), the cells were harvested, fixed and permeabilized in 80% ethanol (-20℃) and optionally stored at -20℃. The fixed cells were spun down at 1200 rpm for 5 min, washed with PBS, centrifuged again, and the DNA was quantitatively stained with PI solution (containing RNAse A) for 30 min at RT in the dark. The fluorescence intensity of the cells therefore correlates with the amount of DNA. As the DNA content of the cells duplicates during S-phase, the relative number of cells in each cell cycle phase (G1/G0 vs S vs G2/M) can be determined.

➢ Differential staining for immunofluorescent microscopy

To monitor cell cycle distribution in fluorescent microscopy, cells were incubated with 5-ethynyl-2'-deoxyuridine (EdU, 1:2000, Click-iT^{TM} Assay Kit, Invitrogen) for 24 h. EdU is a thymidin nucleoside analog and is incorporated into the DNA in actively replicating cells during the incubation interval. The detection of EdU is based on a copper-catalyzed covalent reaction between an azide (contained by a fluorescent dye) and an alkyne (contained by EdU) and functions with standard formaldehyde fixation and detergent permeabilization. With differential staining for EdU (following the manufacturer's protocol) and additionally for CenpF, we were able to discriminate between cell cycle phases in addition to non-cycling G1/G0 cells (CenpF and EdU negative) (see Results 4.1.4.). The differentially stained fractions were counted by eye.

3.2.8. Isolation of lymphocytes

We used human lymphocytes as an internal standard in flow cytometry analyses. Fresh heparinized blood samples were mixed well in a 1:1 ratio with NaCl. 4 ml of the solution was gently layered onto 4 ml pre-warmed Ficoll gradient (Pharmacia) in a 15 ml tube. We centrifuged the sample for 30 min. at 1500 rpm at RT (without bracket) to separate serum, lymphocytes, and erythrocytes. The lymphocytes are subsequently located in a thin white layer between the Ficoll and the serum. We carefully transferred this layer into a new tube, washed it with PBS and fixed it in ethanol (-20℃) before further use in flow cytometry.

3.2.9. Irradiation

Irradiation was performed at RT using the X-ray generator (Gulmay) with 200 keV, 15 mA, and an additional Cu-filter at a dose rate of 0.8 Gy/min.

3.2.10. Graphics and statistics

All experiments were independently repeated at least three times. Data points represent the mean (± SEM) of all individual experiments.

Statistical analysis, data fitting and graphic production were performed with the GraphPad Prism 5.0 program.

4. Results

4.1. Radiosensitivity, cell cycle regulation and residual damage in *AT* and *Artemis* cells

4.1.1. Radiosensitivity

One of the characteristics of the two "genomic instability syndromes" ataxia telangiectasia (AT) and RS-SCID (Artemis) is the exquisite sensitivity to ionizing irradiation. To verify this hypersensitivity, we cultivated ATM and Artemis-deficient human fibroblasts and used the clonogenic colony formation assay to study cell survival after ionizing irradiation. The dose at which 10% of the cells survived (D10) was found to be 4 Gy in WT cells, while both deficient strains required only 2 Gy to reduce survival to the same level (Figure 11). Hence, the radiosensitivity in *AT* and *Artemis* cells is two-fold higher than that of wild-type fibroblasts, confirming previous findings (Kuhne et al., 2004; Kurosawa et al., 2010; Wang et al., 2005).
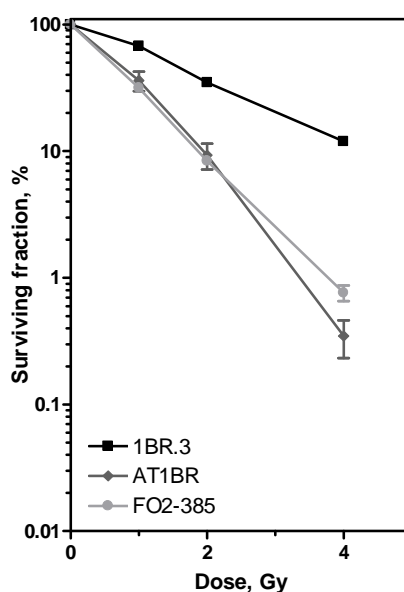
Figure 11. Similarly enhanced radiosensitivity in *AT* and *Artemis* fibroblasts
Radiosensitivity of exponentially growing immortalized human fibroblasts was measured by clonogenic survival assay after X-irradiation. Shown are 1BR.3 (WT, black), AT1BR (*AT*, grey), and FO2-385 (*Artemis*, light grey) survival curves.

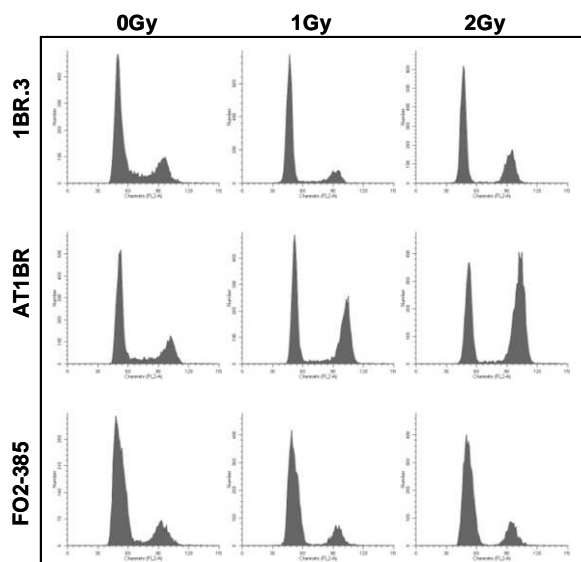### 4.1.2. Cell cycle distribution

This hypersensitivity has been ascribed to a common defect in DNA DSB repair that has been observed in both the G1- and G2-phase of the cell cycle (Deckbar et al., 2007; Riballo et al., 2004). Experiments have thus far been performed in a way that disconnects the repair process from cell cycle progression. However, ATM has major impact on the activation of all

cell cycle checkpoints. In contrast, Artemis is not known to be involved in triggering any checkpoints, but rather plays a minor role in recovery from cell cycle arrest (cell cycle adaption). We thus sought to integrate repair and cell cycle progression into the same set of experiments.

4.1.3.   Cell cycle distribution assessed by flow cytometry analysis

We irradiated cells in exponential growth with 1 and 2 Gy of X-ray and monitored their cell cycle distributions 24 h later by propidium iodine (PI) staining and flow cytometry (FACS) analysis. After irradiation, all three strains displayed virtually no S-phase. WT cells showed an accumulation in G1 after 1 Gy and additionally in G2 after 2 Gy (Figure 12). *Artemis* cells accumulated predominantly in the G1-phase. In contrast, *AT* cells displayed an enormous fraction of cells in the G2-phase 24 h after irradiation (Figure 12).

This observation was unexpected, as cells irradiated in G2 are known to need ATM for the activation and maintenance of a G2/M block (Rotman et al., 1999). However, the increasing number of G2 cells in *AT* cannot simply be explained by the arrest of the fraction of cells that were in G2 at the time of irradiation, implying that some cells were proliferating in other phases before being arrested in G2.

**Figure 12.   Different cell cycle distributions in *AT* and *Artemis* cells after IR**
Cell cycle distributions in untreated cells and 24 h after X-irradiation with 1 or 2 Gy. Cells were fixed and stained with propidium iodide (PI) and analysed for their DNA content by flow cytometry. Depicted are the cell cycle profiles of 1BR.3 (WT), AT1BR (*AT*), and FO2-385 (*Artemis*) fibroblasts w/o irradiation.

4.1.4.   Cell cycle distribution assessed by immunofluorescent microscopy

To characterize the fractions of proliferating and arrested cells in more detail, we established a nuclear staining technique that allowed us to follow cell cycle progress and to determine the amount of residual DNA damage separately in the G1-, S- and G2-phase (see below).

We first used CenpF staining as a G2 marker to distinguish between G1- and G2-phase cells. Centromere protein F (CenpF) is increasingly expressed and bound to the nuclear

matrix as cells progress through the S- and G2-phase, reaching maximum expression in the G2-phase (Beucher et al., 2009; Landberg et al., 1996; Rattner et al., 1993). To verify the staining for CenpF as a potential G2 marker, we fixed exponentially growing WT fibroblasts on a cover slip and in parallel detached the remaining cells from the petri dish. We were therefore able to stain the same cell population for both fluorescence microscopy with anti-CenpF antibody and DAPI as well as for flow cytometry with anti-CenpF antibody and PI. Microscopic enumeration of CenpF-positive cells by eye revealed 19.5% positive cells. Comparison with the flow cytometry results showed that this fraction of 19.5% corresponded mainly with G2 cells, while most S-phase cells remained below the visible threshold (Figure 13).
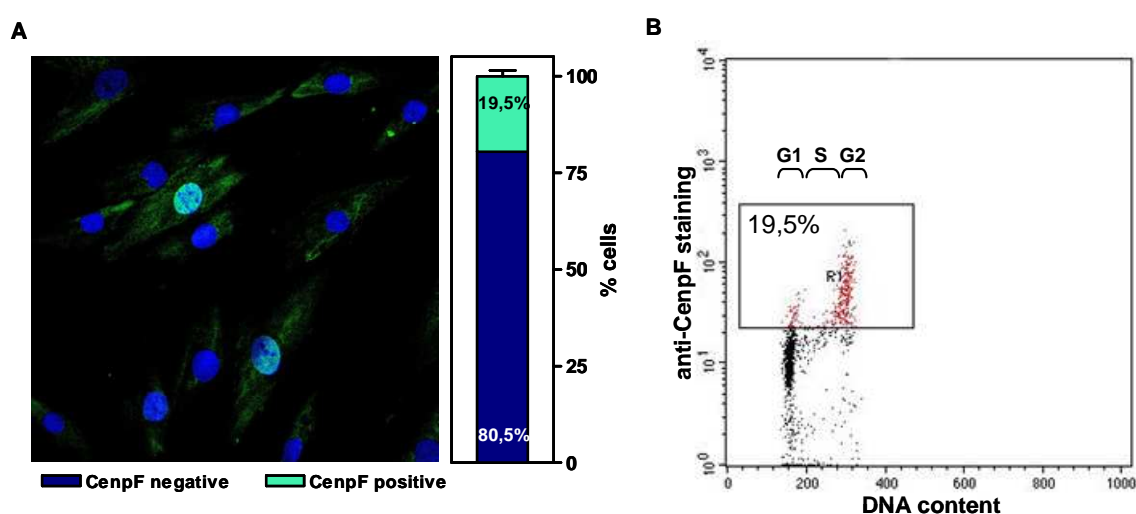
Figure 13. anti-CenpF stained cells mainly represent G2-phase cells
Exponentially growing 1BR.3 (WT) fibroblasts were stained for centromere protein F (CenpF). (A) Microscopic enumeration of CenpF-positive cells by eye revealed 19.5% positive cells. (B) Comparison with flow cytometry showed that this fraction of 19.5% mainly corresponds to G2 cells, while most S-phase cells remained below the visible threshold.

Having established that CenpF staining is a reliable marker to detect G2-phase cells, we additionally made use of the incorporation of the thymidine analogue EdU (5-ethynyl-2'-deoxyuridine) to distinguish between cycling cells that had travelled through the S-phase and hence incorporated EdU during the 24 h repair interval (EdU-positive) and those having arrested in distinct cell cycle phases without passing through the S-phase (EdU-negative). Exponentially growing fibroblasts were irradiated with 1 or 2 Gy before being supplemented continuously with the thymidine analogue EdU to identify proliferating cells and fixed after 24 h.

Detection of the S-phase passage by EdU-staining, nuclear staining with anti-CenpF antibody and counterstaining with DAPI results in differentially stained subfractions (Figure 14):

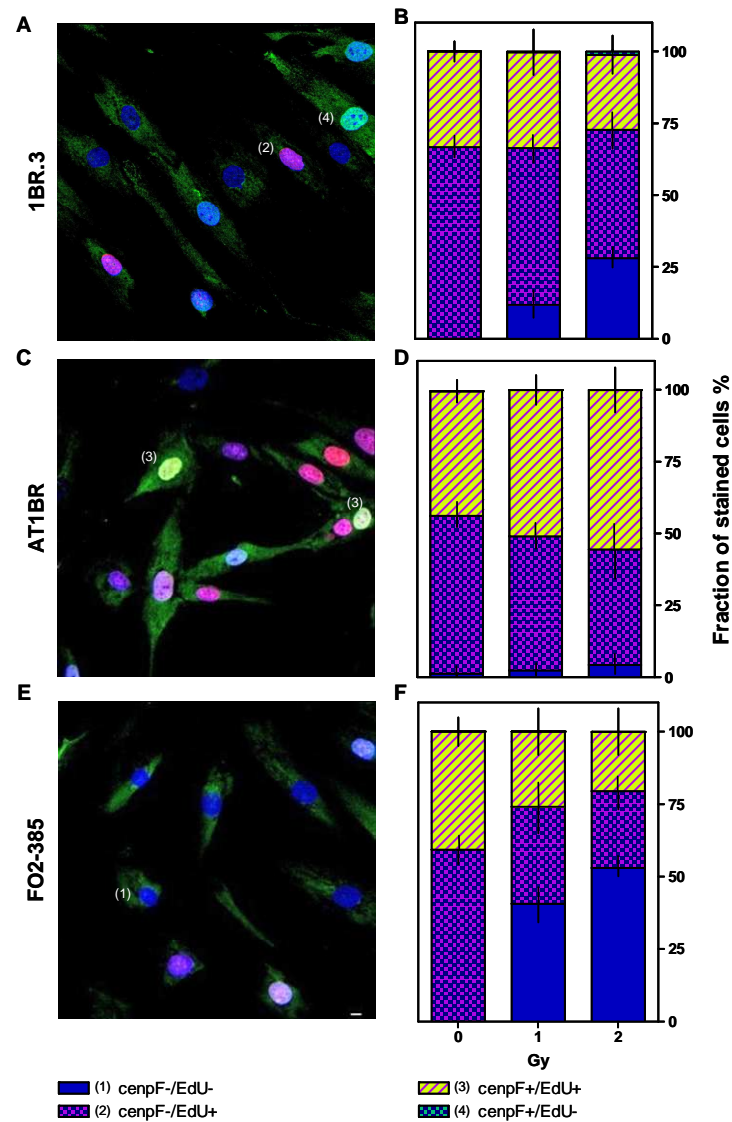Example 1 (blue, CenpF-/EdU-): non-cycling cells in G1

Example 2 (purple, CenpF-/EdU+): cycling cells in the G1 or S-phase

Example 3 (yellow and pink, CenpF+/EdU+): G2 cells after transit through the S-phase

Example 4 (blue-green, CenpF+/EdU-): G2 cells arrested directly in G2

Untreated controls of all three strains included a certain fraction of non-cycling cells (7.1 ±2.7%, 23.5 ±1.2% and 19.6 ± 2.1 in WT, *AT* and *Artemis* cells, respectively, were both EdU- and CenpF-negative). In the following, these numbers were subtracted from the entire population, which was then set to 100%. Only those additional cells that were arrested in G1 after IR are depicted (Figuer 14, blue bars). After IR, WT and in particular *Artemis* (up to 50% after 2 Gy) but not *AT* cells accumulated in G1 without incorporating EdU. *AT* cells, in contrast, showed an increased G2-fraction after transit through the S-phase (Figure 14, example (3), yellow and pink). Remarkably, a small fraction of WT cells irradiated in G2 did not proceed through mitosis during the following 24 h (Figure 14, example (4) blue-green). Confirming previous observations, 25% and 50% of irradiated WT and in particular *Artemi*s cells, respectively, failed to incorporate EdU during the 24 h observation period and stained positive only for DAPI, thus displaying a sustained G1-arrest (Figure 4, example (1) blue bars). A small but reproducible fraction of WT cells (1.6% after 2 Gy, which increased to 10% after 6 Gy, (data not shown)) stained positive only for CenpF (Figure 14, example (4) green bars), indicating their instant arrest in G2. In contrast, all CenpF-positive *AT* cells were also EdU-positive (Figure 14, example (3) yellow bars), confirming that all G2-arrested cells had previously passed through S.

Together, these results confirm the considerable impact of ATM on the activation of primary G1 and G2/M checkpoints, though *AT* cells do display a strong secondary G2/M block activated independently of ATM. *Artemis* cells, on the other hand, exhibit a noticeable G1 block after irradiation which may result from a defect in DSB repair.

Figure 14. Cell cycle analysis by differential staining with EdU and CenpF
Cell cycle distribution in untreated cells and 24 h after X-irradiation with 1 or 2 Gy. Exponentially growing fibroblasts were irradiated with 1 or 2 Gy, supplemented with the thymidine analog EdU to identify proliferating cells, and fixed after 24 h. Detection of S-phase passage by EdU, nuclear staining with CenpF to detect G2-phase cells and counterstaining with DAPI results in different subfractions. (A, C, E) These differently stained patterns can been seen:
Example 1 (blue, cenpF-/EdU-): non-cycling cells in G1
Example 2 (purple, cenpF-/EdU+): cycling cells in the G1 or S-phase
Example 3 (yellow and pink, cenpF+/EdU+): G2 cells after transit through the S-phase
Example 4 (blue-green, cenpF+/EdU-): G2 cells arrested directly in G2
(B, D, F) Quantification of differentially stained subfractions. Untreated controls of all three strains included a certain fraction of non-cycling cells (7.1 ±2.7%, 23.5 ±1.2% and 19.6 ± 2.1 of WT, *AT* and *Artemis* cells, respectively, were both EdU- and CenpF-negative), subtracted in the following. Only cells that were arrested additionally in G1 after IR are depicted (blue bars). After IR, WT (B) and in particular *Artemis* ((F) up to 50% after 2 Gy) but not *AT* (D) cells accumulated in G1 without incorporating EdU. *AT* cells, in contrast, showed an increased G2 fraction after transit through the S-phase ((C,D) example (3), yellow and pink). A small fraction of WT cells irradiated in G2 did not proceed through mitosis during the following 24h ((A,B) example (4) blue-green).

4.1.5. Focus formation and residual damage

The defects in *AT* and *Artemis* cells have been recently described to similarly affect DSB repair in the G1- and G2-phase (Beucher et al., 2009; Deckbar et al., 2007; Riballo et al., 2004). In vivo, DSB induction and repair can be monitored by determining the number of focal clusters of phosphorylated H2AX histones by immunofluorescence, the so-called "γH2AX foci". Radiation damage is the energy deposit per unit mass, meaning that the amount of visible damage (i.e. γH2AX foci) depends on the radiation dose and the amount of nuclear DNA. Therefore, we first assessed the DNA content of all three cell lines by PI-staining and flow cytometry analysis using human lymphocytes (L) as an internal standard. Human peripheral lymphocytes consist only of G1-phase cells and thus show a PI profile with a single peak (Figure 15, leftmost graph). We then mixed the lymphocytes with separate PI-stained cell suspensions from each of the fibroblast strains. In this way, the DNA profiles of the fibroblast lines could be compared through the use of this internal standard. Both WT and *Artemis* cells showed G1 peaks in close proximity to the lymphocyte standard peak, exhibiting comparable cell cycle profiles. *AT* cells, in contrast, showed a more remote G1 peak, indicating a higher DNA content (Figure 15). We observed a DNA content in *AT* cells that was 1.5 times higher compared to both WT and *Artemis* cells. To compare the number of DBSs in different cell lines, all following results obtained for *AT* cells were normalized to a diploid DNA content by dividing the counted foci number by 1.5.
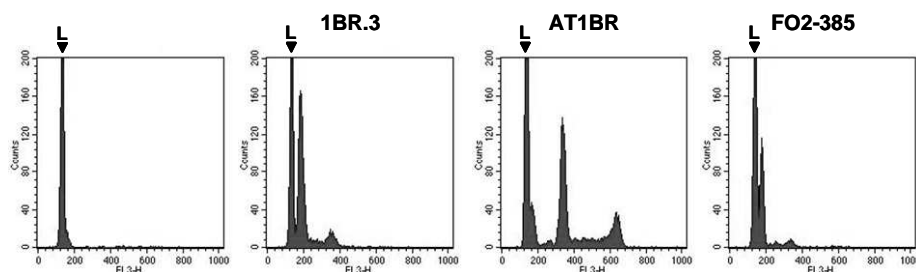
Figure 15. DNA content of fibroblast lines
The DNA content of the fibroblast strains 1BR.3 (WT), AT1BR (*AT*), and FO2-385 (Artemis) was assessed by PI staining and flow cytometry. Human lymphocytes (L), indicated by error ▼, were added to each cell suspension as an internal standard. DNA content was observed to be 1.5 times greater in *AT* cells compared to both WT and *Artemis* cells.
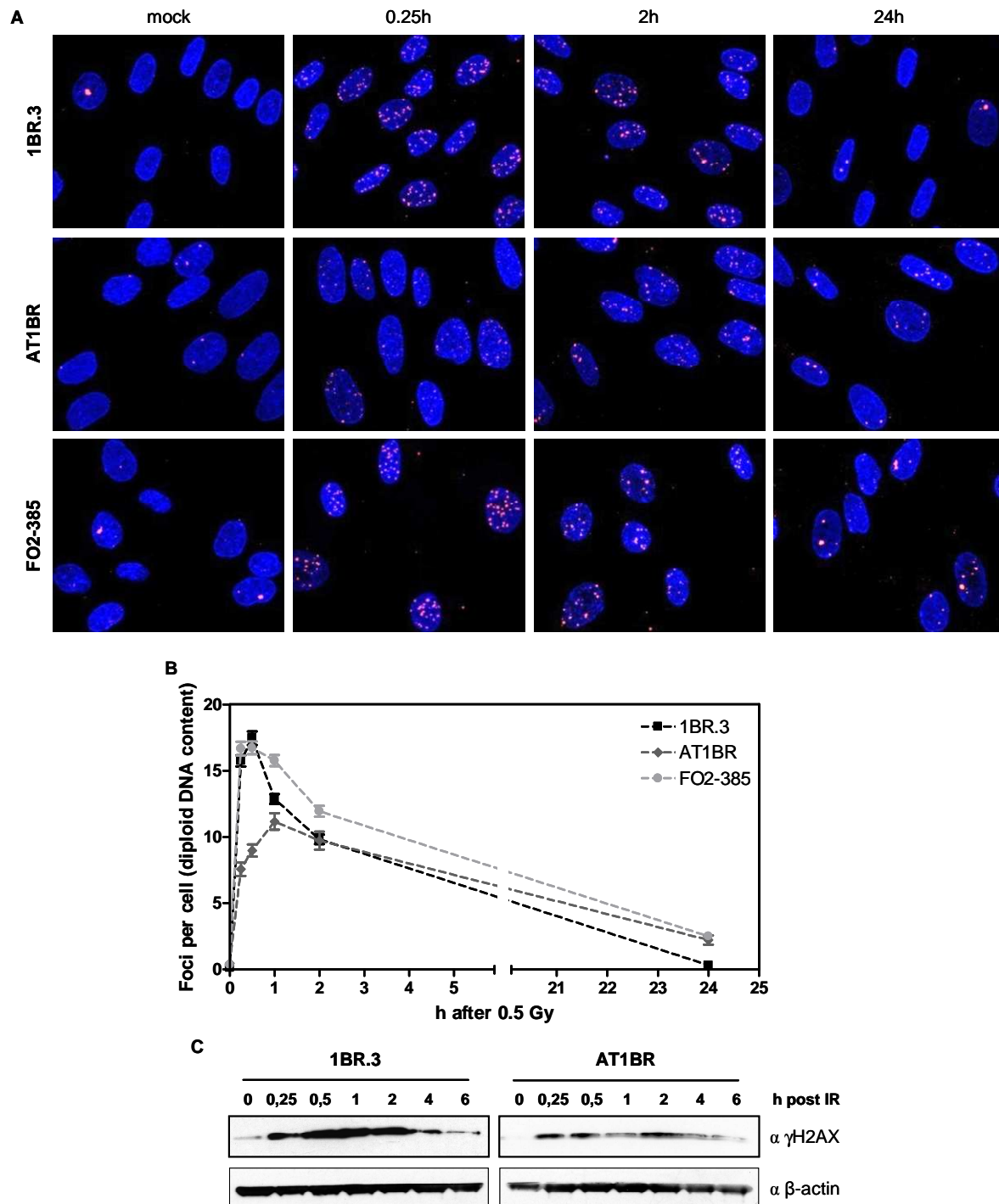
4.1.6. γH2AX foci kinetics

The phosphorylation of the H2AX histone on Ser139 (γH2AX) occurs mainly in an ATM dependent manner, which in turn recruits other DNA damage response proteins (i.e. MDC1, MRN, 53BP1, RNF8, etc.). Together with the latter proteins, ATM ensures the stabilization of the DDR-protein complex at the damage site, resulting in the phosphorylation of additional H2AX molecules in the vicinity of the DSB (see Introduction 2.3.2.). The phosphorylation of

the H2AX histone in the absence of ATM can be executed by other members of the PIKK family such as DNA-PK or ATR (Kuhne et al., 2004; Stiff et al., 2004).

To analyze DNA DSB repair, we monitored γH2AX focus formation in WT, *AT* and *Artemis* cells and followed their focus kinetics over 24 h to monitor repair. We used confluent fibroblasts grown on cover slips, which were then irradiated and fixed at various time points. We sought to count the emerging foci early after irradiation, beginning at 15 min. Cells were irradiated with doses as low as 0.5 Gy, inducing on average 15-20 DSBs, and stained for γH2AX and CenpF in order to exclude G2-phase cells from γH2AX counting.

At the first time point of 15 min, WT and *Artemis* cells showed distinct, bright γH2AX signals (Figure 16) and revealed 15.7 ± 0.4 and 16.6 ± 0.5 residual nuclear foci, respectively. Smaller, fuzzy foci and an average number of 7.5 ± 0.5 were observed in *AT* cells.

The number of γH2AX foci in WT and *Artemis* cells declined after the first 30 min, indicating DSB repair. In contrast, *AT* cells showed increasing foci numbers with a peak of 11.16 ± 0.62 foci at 1 h. However, *AT* cells displayed not only a remarkable delay in focus formation, but also smaller and more subtle γH2AX foci at early time points (Figure 16), suggesting the necessity of ATM in DDR. After 24 h, all three strains had repaired the majority of the breaks. While WT cells almost showed complete DSB repair (0.3 ± 0.1 foci), *AT* and *Artemis* cells exhibited slightly more foci (2.2 ± 0.3 and 2.5 ± 0.3, respectively), indicative of their repair defects (Figure 16). In order to test whether the weaker, fuzzy foci in *AT* cells correspond with a reduced phosphorylation for the entire γH2AX signal per nucleus, we conducted a western blot analysis using whole cell extracts from WT and *AT* cells. 0.25 h after irradiation with 10 Gy, both WT and *AT* cells displayed a γH2AX signal, though the signal was weaker in the *AT* cells. γH2AX expression increased in WT cells (0.5 – 2 h) and subsequently decreased (4 h) to almost background level (6 h), probably as the result of successful repair. In contrast, *AT* cells displayed a moderate and delayed increase in γH2AX expression peaking at 2 h. Compared to the WT cells, the γH2AX expression at the 6 h time point was more intense, hinting at the repair deficiency of these cells. Western blot analysis confirmed a much weaker γH2AX signal in *AT* cells in response to ionizing irradiation compared to the WT (Figure 16).

**Figure 16. γH2AX foci kinetics of WT, *AT*, and *Artemis* fibroblasts**
DDR and repair of DSBs was assessed using the γH2AX foci staining technique and counterstaining with DAPI of WT (1BR.3), *AT* (AT1BR), and *Artemis* (FO2-385) fibroblasts after 0.5 Gy. (A) Distinct γH2AX foci (red) are distinguishable in all strains, though these were less intense in *AT* cells at early time points. (B) Quantification of DSBs by enumeration of γH2AX foci at the time points indicated. Foci numbers/nucleus were normalized to a diploid DNA content. Early after irradiation, focus formation in *AT* cells is delayed with fewer total foci. Residual γH2AX foci after 24 h showed higher numbers in *AT* and Artemis cells compared to the WT. We did not define the time interval between 2 and 24 h. However, it is known that these cell lines show bi-exponential repair kinetics during this time (Riballo et al., 2004). (C) Western blot analysis of WT and *AT* fibroblasts 0.25 – 6 h after 10 Gy confirmed γH2AX appearance in *AT* cells.

4.1.7. Residual damage in the G1- and G2-phase

In order to distinguish between G1- and G2-phase cells, we quantified γH2AX foci 24 h after IR in exponentially growing cells that stained either only DAPI-positive (G1) or showed the additional G2 marker CenpF (Figure 17). S-phase cells displayed a strong pan-nuclear γH2AX signal and were excluded from analysis.

Separate analyses of G1 and G2 cells (Figure 17) 24 h after irradiation revealed larger numbers of residual γH2AX foci in both deficient cell lines in both phases compared to the WT. Among the deficient strains, *Artemis* cells showed 5.0 ±0.2 foci in G1 and 10.8 ±1.0 foci in G2, compatible with the 2-fold higher DNA content and suggesting equally efficient repair in both phases. *AT* cells, in contrast, showed 4.1 ±0.8 foci in G1 and 12.1 ±0.8 in G2, numbers which cannot be explained simply by a two-fold increase in DNA content in G2. These results instead suggest that either less repair occurred in the G2-phase in *AT* cells or – more likely – that additional breaks arose while the cells passed through the S-phase before arresting in G2.
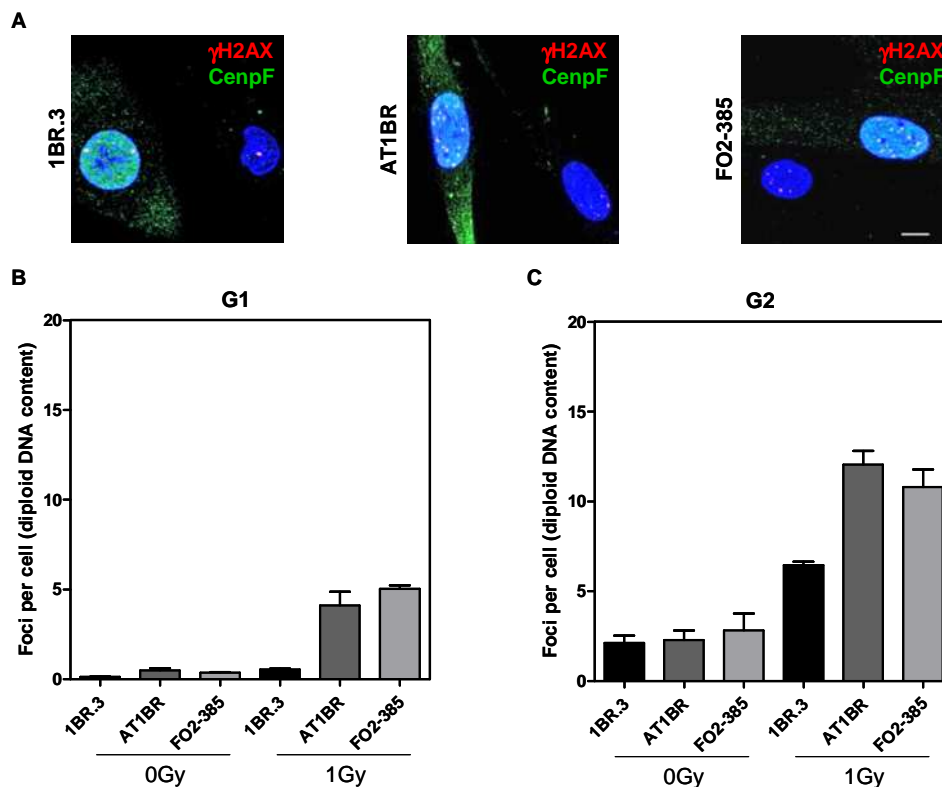

Figure 17. Increased number of residual double-strand breaks in both G1- and G2-phase *AT* and *Artemis* fibroblasts
(A) Differential staining for G2-phase cells (CenpF-positive) 24 h after irradiation with 1 Gy of X-ray in addition to detection of γH2AX foci; counterstaining with DAPI. Each panel shows one CenpF-positive and one CenpF-negative cell. Quantification of residual γH2AX foci 24 h after 1 Gy in CenpF-negative G1- (B) and CenpF-positive G2-phase cells (C). Foci numbers/nuclei are normalized to a diploid DNA content.

4.2. *AT* and *Artemis* cells show distinct homologous recombination defects

4.2.1. Residual Rad51 foci

The similar *AT* and *Artemis* repair phenotypes have been hitherto linked to the deficient repair of a common subset of DSBs (10-15%) in both the G1- and G2-phase (Deckbar et al., 2007; Riballo et al., 2004). We now observed different amounts of residual damage between the two lines. The difference is that the observation period (24 h) included the progress through the S-phase, raising the possibility that repair in *AT* and *Artemis* cells differ specifically in the S-phase. Two explanations for these differences can be considered: (1) the occurrence of replication associated damage, and/or (2) homologous recombination to a yet unknown extent. To address the latter possibility, we monitored Rad51 focus formation 24 h after IR as a marker of recombination activity, i.e. recruitment of the major recombinase and presumably its loading onto single-stranded DNA (Raderschall et al., 1999) (see Introduction). Differential staining for the G2 marker CenpF in addition to Rad51 showed discrete nuclear Rad51 foci only in CenpF-positive G2-phase cells (Figure 18) and/or EdU-positive S-phase cells (see below), but never in G1/G0 cells, confirming that recombination processes are restricted to the S- and G2-phases of the cell cycle.
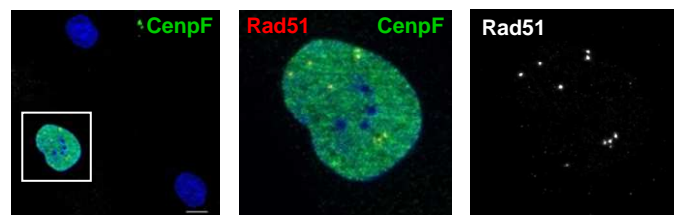
Figure 18. Rad51 foci in CenpF-positive cells
Differential staining for G2-phase cells (CenpF-positive) 24 h after 1 Gy of X-ray in addition to detection of Rad51. Rad51 foci were visible only in CenpF-positive G2-phase cells (left panel). Magnification revealed distinct Rad51 foci (red). The right panel depicts the red channel only.

Enumeration after 1 Gy revealed an average of 11.7 ±1.1 Rad51 foci in *AT* cells but only 5.7 ±0.5 and 6.6 ±0.5 in WT and FO2-385 *Artemis* cells, respectively (Figure 19). Comparing these residual Rad51 foci with the number of residual γH2AX foci in G2-phase cells, Rad51 and γH2AX foci in WT and *AT* cells were found to be widely co-localized. Parallel counting thus yielded identical numbers. In remarkable contrast, only 60% of the residual γH2AX foci in FO2-385 *Artemis* cells were simultaneously decorated with Rad51 (Figure 19). To confirm this unexpected result, we incorporated a second Artemis deficient cell line, CJ179. This clone displayed essentially the same phenotype as the FO2-385 cells, though with generally lower number of foci. Accordingly, enumeration after 1 Gy showed 5.1 ±1.1 Rad51 foci compared to 8.7 ±0.8 residual γH2AX foci (corresponding to 59%) (Figure 19).
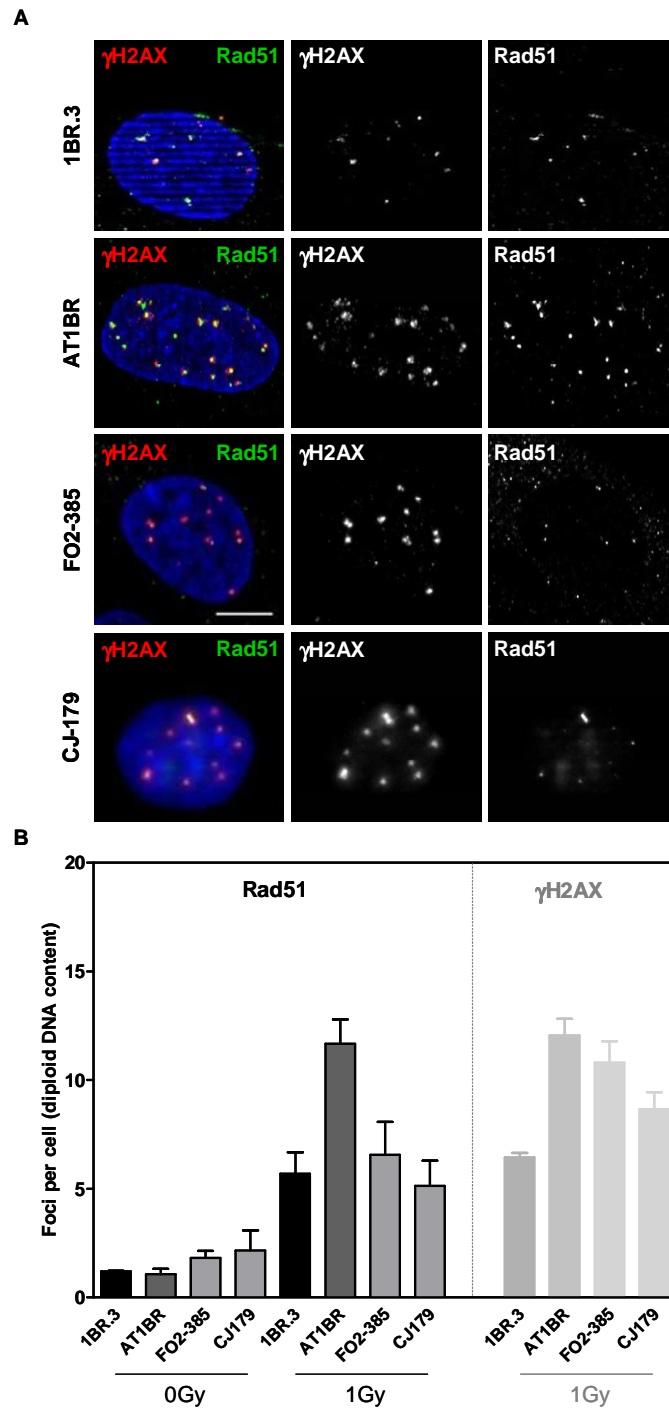
Figure 19. The number of Rad51 foci in G2 is elevated in *AT* but not in *Artemis* cells.
(A) Cells were irradiated with 1 Gy, co-stained 24 h later for γH2AX (red) and Rad51 (green) and counterstained with DAPI. Colocalization of both signals results in a yellow spot. As depicted in (A), analysis revealed that all Rad51 foci colocalize with γH2AX in 1BR.3 (WT) and AT1BR (*AT*) cells, but not in either of the *Artemis* strains. Shown are G2 cells. G1 cells which did not stain for Rad51 (Figure18) and S-phase cells with hyper-intense γH2AX signals were not considered. (B) Quantification of Rad51 foci 24 h after IR with 1 Gy as described before and compared with γH2AX foci (taken from Figure 17) revealed identical numbers of both damage markers in 1BR.3 (WT) and AT1BR (*AT*) cells, but not in either of the *Artemis* strains. Foci numbers/nuclei were normalized to a diploid DNA content.

γH2AX foci are considered to be a general equivalent of un-rejoined DSBs, while Rad51 foci represent an early step in homologous recombination. However, persistent Rad51 foci can also indicate incomplete recombination processes. Thus, our observations of both the lower number of Rad51 foci in *Artemis* (compared to γH2AX foci) as well as the increased amount of Rad51 foci in *AT* cells compared to the other strains may reflect HR defects, with the respect defects perhaps targeting different steps of the process.

### 4.2.2. Quantification of homologous recombination using the pGC reporter system

In order to more directly quantify HR, we used the pGC reporter construct (Mansour et al., 2008) stably integrated into HeLa cells (see Material and Methods 3.2.5.). 72 h after DSB induction through the expression of the I-SceI endonuclease, successful gene conversion led to green fluorescence in 1.9% ±0.25% of the cells, as quantified by flow cytometry (Figure 20).
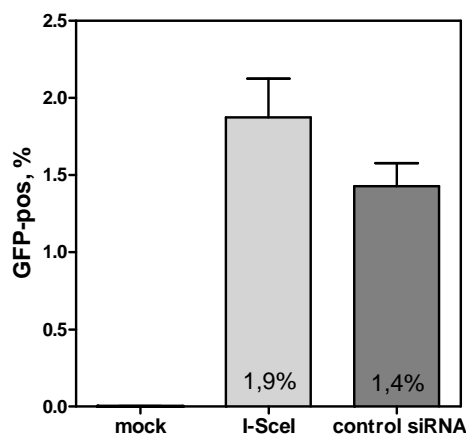
Figure 20. Gene conversion efficiency in the HeLa pGC reporter assay
The expression of GFP represents successful gene conversion at I-SceI-induced DSBs. Pretreatment with control siRNA (scrambled, anti-GAPDH, anti-Cyclophilin B) reduced the efficiency slightly to 1.4% GFP-positive cells compared to 1.9% in cells transfected solely with the I-SceI expression plasmid.

In order to investigate the impact of either Artemis or ATM on HR, we inactivated both proteins by either siRNA or chemical inhibitors. To this end, we treated HeLa cells twice with anti-Artemis or control siRNA in a 48 h interval and monitored the Artemis expression with western blot analysis for a total observation period of 96 h. We were able to detect a moderate knockdown after 24 h, which was more pronounced after 48 h and - after the second transfection - persistent up to 96 h (Figure 21). This reduction in the Artemis protein efficiently reduced overall repair of DSBs, as detected by the increased number of residual γH2AX foci (Figure 21) and increased radiosensitivity monitored by clonogenic cell survival after 2 Gy (Figure 21).
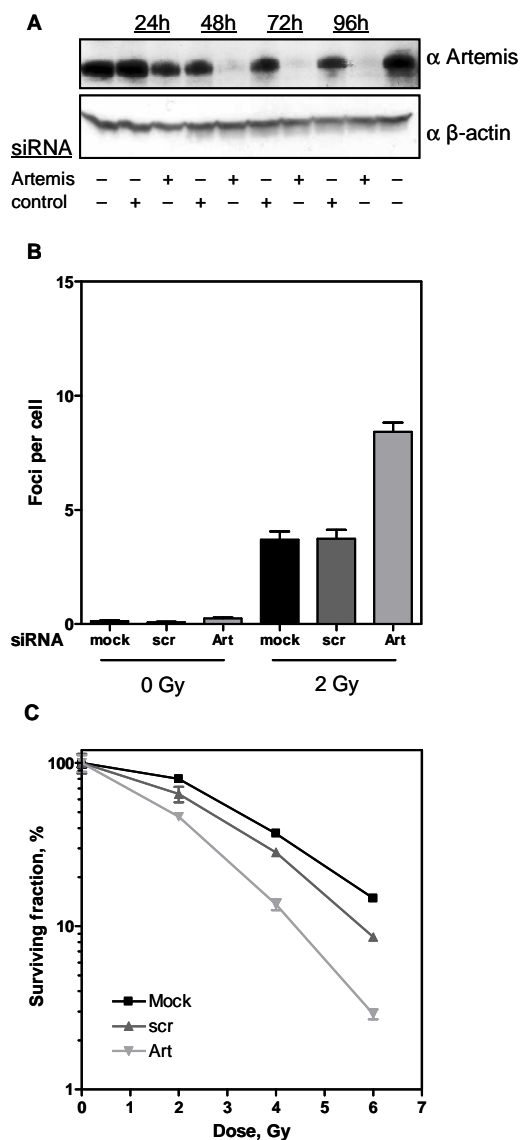
Figure 21. Inactivation of Artemis reduced survival in HeLa cells and increased the number of residual DSBs
(A) HeLa cells were treated twice with anti-Artemis or control siRNA (second time after 48 h). Artemis expression was monitored by western blot analysis for up to 96 h. (B) Artemis knockdown efficiently increased the number of residual γH2AX foci 24 h after 2 Gy and (C) also radiosensitivity.

In addition to the Artemis depletion, a HeLa pGC clone was transfected with the I-SceI expression vector after 48 h, after knock-down was considered to be sufficient. Repair was measured 72 h later. Protein expression was controlled in parallel by western blot (Figure 22, 24). Artemis depletion significantly reduced HR frequency to 51 ± 6% compared to control siRNA (Figure 22). In contrast, ATM depletion by siRNA in the same experimental setting reduced HR frequency to only 67 ± 5% compared to controls. Combining both Artemis and ATM depletion only slightly enhanced the effect compared to Artemis siRNA alone (Figure 22 columns 2-4). It is possible that the siRNA treatment allowed for the retention of residual
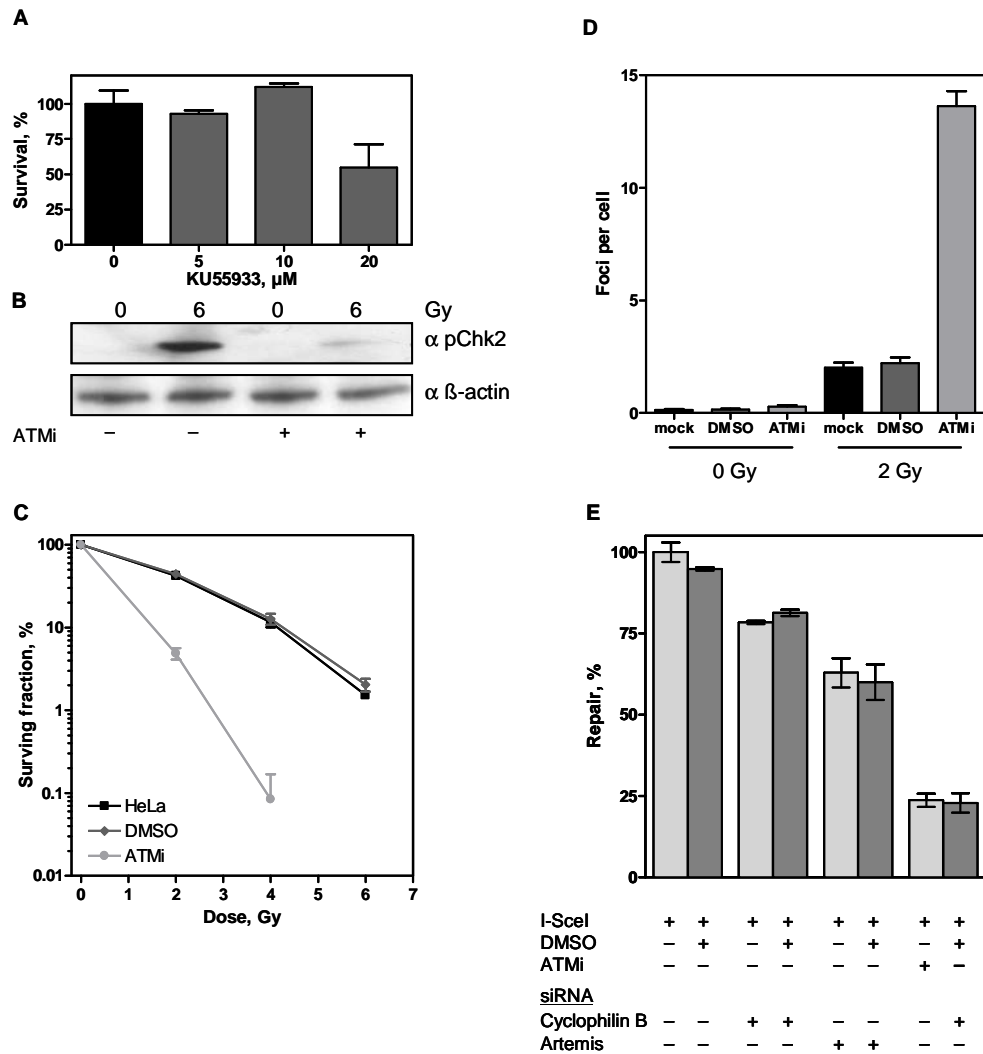
ATM activity, as western blots confirmed an efficient but incomplete depletion of the ATM protein (Figure 22).
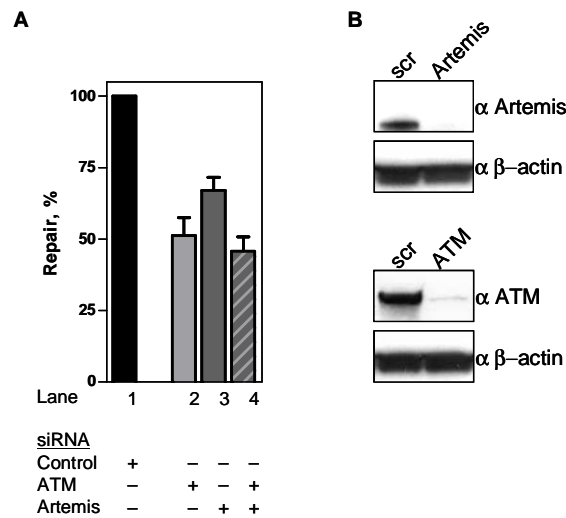
Figure 22. Reduced rate of gene conversion in the absence of Artemis and ATM
(A) Gene conversion was determined after DSB induction using HeLa pGC cells. Cells treated with control siRNA were transfected with the I-SceI expression vector and the fraction of GFP-positive cells was determined 72 h later by flow cytometry (control siRNA reduced gene conversion from 1.9 to 1.4%, Figure 20) and expressed as 100% relative repair efficiency (lane1). Artemis, ATM, and combined siRNA pretreatment all reduced this repair efficiency (lanes 2 -4).
(B) Western blot of HeLa pGC cells treated with control siRNA or siRNA against Artemis or ATM.

To test this possibility, we employed the ATM-specific inhibitor KU55933: We first tested the toxicity of the inhibitor in HeLa cells, for which no effect on cell survival could be seen at concentrations of 5 or 10 µM; survival was reduced by 50%, however, at 20 µM KU55933 (Figure 23). We therefore used 10 µM in the following experiments. We confirmed successful inhibition by monitoring the phosphorylation of the downstream ATM target Chk2 on Thr68 by western blot analysis using a phosphor-specific monoclonal antibody. 30 min after 6 Gy X-irradiation, DSMO-treated controls displayed a pronounced pChk2 signal which was almost completely abrogated in the inhibitor-treated HeLa cells, confirming a sufficient inhibition of ATM (Figure 23). Accordingly, overall DSB repair capacity was reduced (Figure 23D) and the radiosensitivity of HeLa cells increased (Figure 23C) after applying the ATM inhibitor. Having confirmed a sufficient inhibition of ATM using KU55933 (solubilized in DMSO), we had to eliminate the possibility of DMSO itself influencing the transgene pGC repair system. We were able to prove in extensive control experiments that DMSO treatment did not influence repair efficiency in combination with additional control siRNA, Artemis siRNA, or ATMi treatments (Figure 23E).

A

B

C

D

E

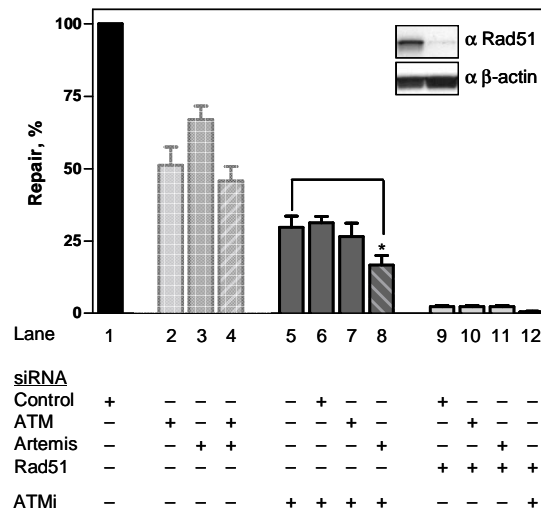| I-SceI	+	+	+	+	+	+	+	+
DMSO	–	+	–	+	–	+	–	+
ATMi	–	–	–	–	–	–	+	–
<u>siRNA</u>								
Cyclophilin B	–	–	+	+	–	–	–	+
Artemis	–	–	–	–	+	+	–	–

Figure 23. Inactivation of ATM reduced survival in HeLa cells and increased the number of residual DSBs
(A) Toxicity of the ATM inhibitor KU55933 in HeLa cells. The cells were incubated with 5, 10, or 20 µM KU55933 for 24 h. The effect on survival was assessed by the colony formation assay and normalized to control treatment with DMSO. (B) HeLa cells were treated with the ATM inhibitor KU55933 (10µM), which efficiently reduced Chk2 phosphorylation 1 h after IR with 6 Gy. (C) The ATM inhibitor drastically increased radiosensitivity and (D) also the number of residual γH2AX foci. (E) The effect of DMSO control treatment on the I-SceI reporter assay for gene conversion was determined. DMSO did not influence repair efficiency in combination with control siRNA (anti-Cyclophilin B), anti-Artemis siRNA or ATMi treatment.

Chemical inhibition of ATM in HeLa pGC reduced HR efficiency to 25% (Figure 24 columns 5-7). To rule out the possibility that ATM inhibitor treatment allowed for residual ATM activity, we combined the inhibitor with anti-ATM siRNA or control siRNA. We were not able to further suppress gene conversion through this double ATM inactivation, supporting previous findings that the KU55933 inhibitor completely abrogates ATM function (Beucher et al., 2009; Hickson et al., 2004). However, combining Artemis depletion with ATM inhibition (Figure 24 column 8) did further compromise HR capacity significantly (p=0.038) to 17 ±3% of controls. This additive effect suggests that both proteins serve essential but partly divergent functions in

HR. For comparison, we depleted Rad51, completely abrogating gene conversion (Figure 24, columns 9-12) and confirming previous observations (Mansour et al., 2008).


Lane	1	2	3	4	5	6	7	8	9	10	11	12
siRNA												
Control	+	–	–	–	–	+	–	–	+	–	–	–
ATM	–	+	–	+	–	–	+	–	–	+	–	–
Artemis	–	–	+	+	–	–	–	+	–	–	+	–
Rad51	–	–	–	–	–	–	–	–	+	+	+	+
ATMi	–	–	–	–	+	+	+	+	–	–	–	+

Figure 24. Reduced rate of gene conversion in the absence of ATM and Artemis
Gene conversion was determined after DSB induction using HeLa pGC cells. The left-hand side of the graph is taken from Figure 22. HeLa pGC cells were treated with 10 µM KU55933 directly prior to transfection of the I-SceI expression vector. Repair was measured 72 h thereafter. The ATM inhibitor further reduced gene conversion efficiency to 25% (lane 5-8). Control siRNA and ATM siRNA in addition to the ATM inhibitor did not affect recombination in controls (lane 6, 7). The combination of Artemis siRNA and ATM inhibition (lane 8) was significantly different from ATM inhibition alone (lane 5) (Mann-Whitney two-tailed T-test, p=0.0381) and further reduced gene conversion to 17%. Rad51 depletion completely abrogated gene conversion (lanes 9-12).

Since only ATM has been shown to be implicated in cell cycle regulations as described in the introduction, we next sought to rule out the possibility of measuring solely cell cycle-related effects after knockdown of ATM (and/or Artemis) in this system. To this end, we monitored the cell cycle distribution parallel to the pGC reporter assay. One set of samples was fixed in the middle of the 72 h repair interval at 36 h post-I-SceI-expression, stained with PI and assessed by FACS. PI staining and FACS during the repair interval at 36 h after I-SceI expression revealed that the DNA profiles of control siRNA, ATM siRNA, Artemis siRNA, Rad51 siRNA, and ATM inhibitor-treated cells all displayed G1, S, and G2/M phases similar to those of the mock-treated controls. Hence, the DNA profiles confirmed that neither knockdown of ATM and/or Artemis nor chemical inhibition of ATM by KU55933 cause cell cycle arrests in the HeLa pGC reporter system (Figure 25).

Together, these results indicate that about 20% of gene conversion activity in this system is independent of ATM and Artemis but it fully relies on Rad51.
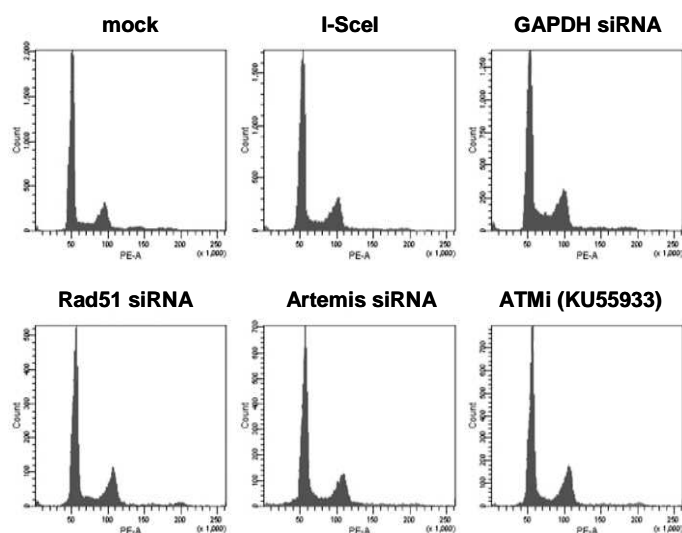
Figure 25. Cell cycle distribution 36 h after I-SceI expression
Within the total repair interval (72 h), the DNA content of mock-treated, I-SceI-transfected, control siRNA (GAPDH), Rad51 siRNA, Artemis siRNA-transfected, and ATM inhibitor-treated cells (10 µM KU55933) was assessed at 36 h by PI staining and FACS. Depicted are the corresponding cell cycle profiles.

4.3. Discrepancies in Rad51 focus formation are due to replication-associated double-strand breaks

In the absence of ATM and Artemis we monitored differences in gene conversion using the I-SceI reporter assay (Figure 25), and also discrepancies in persistent Rad51 foci in CenpF positive G2-phase *AT* and *Artemis* cells (Figure 19). We had only monitored single time points of 72 h and 24 h, respectively, where DSB repair is known to be widely completed, and possibly occurred throughout the cell cycle. We wanted to investigate the development of the Rad51 foci separately in the G2- and S-phases to detect possible kinetic differences that hint more directly at functional discrepancies.

4.3.1. Rad51 focus formation in the G2-phase

To observe Rad51 focus formation during only the G2-phase, we marked S-phase cells and excluded them from analysis. To this end, cells were EdU-labeled for 30 min directly prior to irradiation. The subsequent addition of 5 µM aphidicolin prevented S-phase cells from entering into G2 (Beucher et al., 2009). Aphidicolin is a specific inhibitor of DNA-polymerase alpha and blocks cells during replication in a reversible manner. In control experiments we monitored the successful stoppage of replication through the addition of EdU after aphidicolin treatment and verified the lack of EdU incorporation (data not shown).

Rad51 foci in the G2-phase were monitored in EdU-negative/CenpF-positive cells. WT cells showed a rapid increase in foci numbers and a subsequent decline, likely due to repair by HR (Figure 26). Both *AT* and *Artemis* cells showed only a moderate increase and nearly no decline in Rad51 foci with time, which confirms the reduced capability of HR in both defective strains, as has also been observed previously (Beucher et al., 2009). The increase in focus number was delayed in *AT* cells, well in line with the delayed DNA damage response (see Introduction 2.3.2.) and formation of γH2AX foci (Figure 16). However, cells of either deficient strain still in G2 6 h post-IR displayed identical numbers of Rad51 foci (Figure 26). Repair in G2 appears not to differ substantially between *AT* and *Artemis* cells.
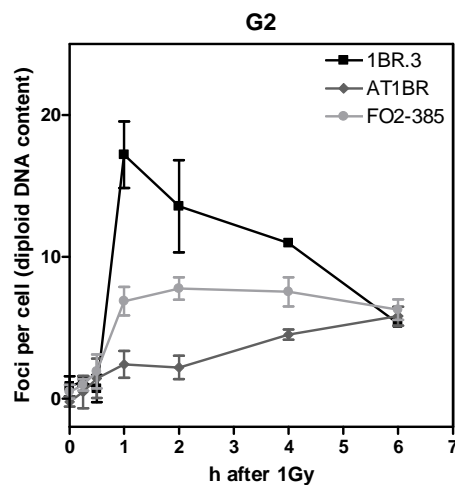
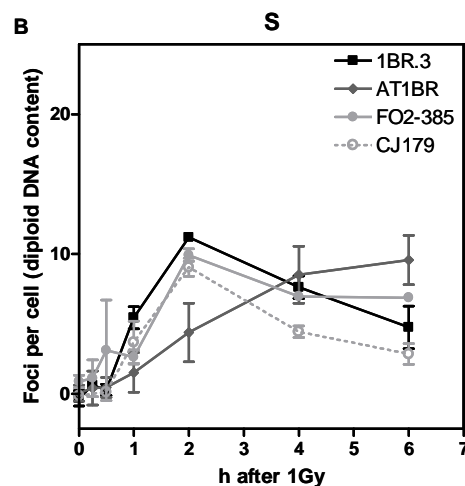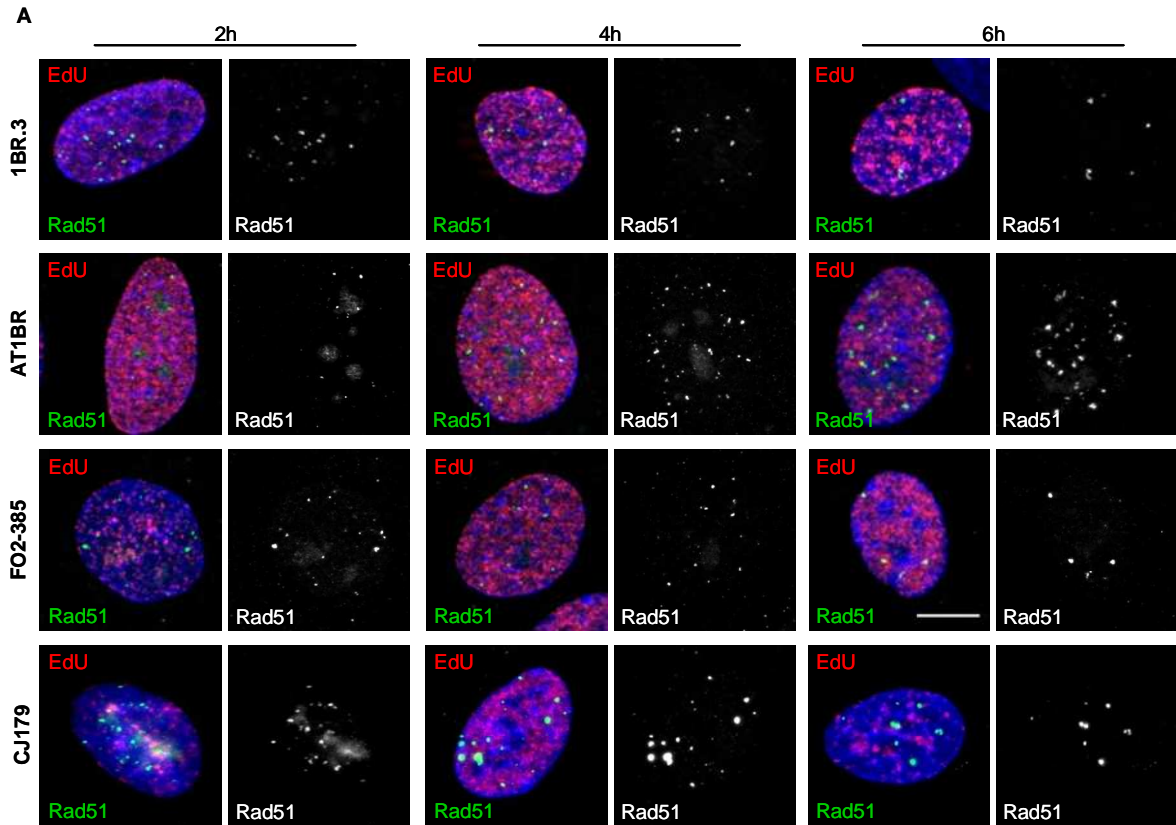**Figure 26. Rad51 foci kinetics in the G2-phase**
Fibroblasts were pulse-labelled with EdU, irradiated with 1 Gy and further incubated with 5 µM aphidicolin to block the transition of S-phase cells into G2. Kinetics of Rad51 foci numbers were monitored in CenpF-positive and EdU-negative G2-phase cells for the time interval indicated.

4.3.2.   Rad51 focus formation in the S-phase

The different numbers of residual Rad51 foci seen before (Figure 19) developed in *AT* and *Artemis* cells only after they had traveled through the S-phase before arresting in G2 (Figure 19). We thus sought to elucidate whether Rad51 foci arise preferably during replication. Cells were EdU-labeled for 30 min directly prior to irradiation and nuclear Rad51 signals subsequently recorded in the S-phase cells (Figure 27), as was done for the G2 cells. Discrete foci were clearly distinguishable after 1 h, reaching a maximum number in *WT* and FO2-385 *Artemis* cells at 2 h (11.1 and 9.9 foci) (Figure 27A and B) and declining thereafter, again presumably due to successful repair. We also studied the Artemis-deficient CJ179 cell line to confirm our results. The second *Artemis* line displayed a virtually identical repair proficiency (maximum number of Rad51 foci at 2 h 9.1 ± 0.7) and also a subsequent decline

(Figure 27). Notably, the concordant Rad51 kinetics of WT and *Artemis* cells strongly suggest that Artemis is not required for HR during the S-phase.

Surprisingly, the number of Rad51 foci in *AT* cells increased continuously over the entire time period, reaching values of 9.6 foci at 6 h (Figure 27).

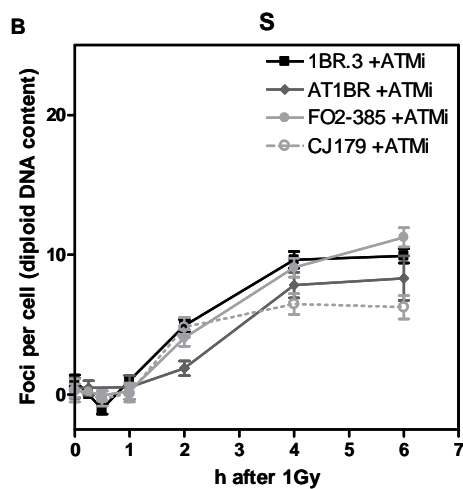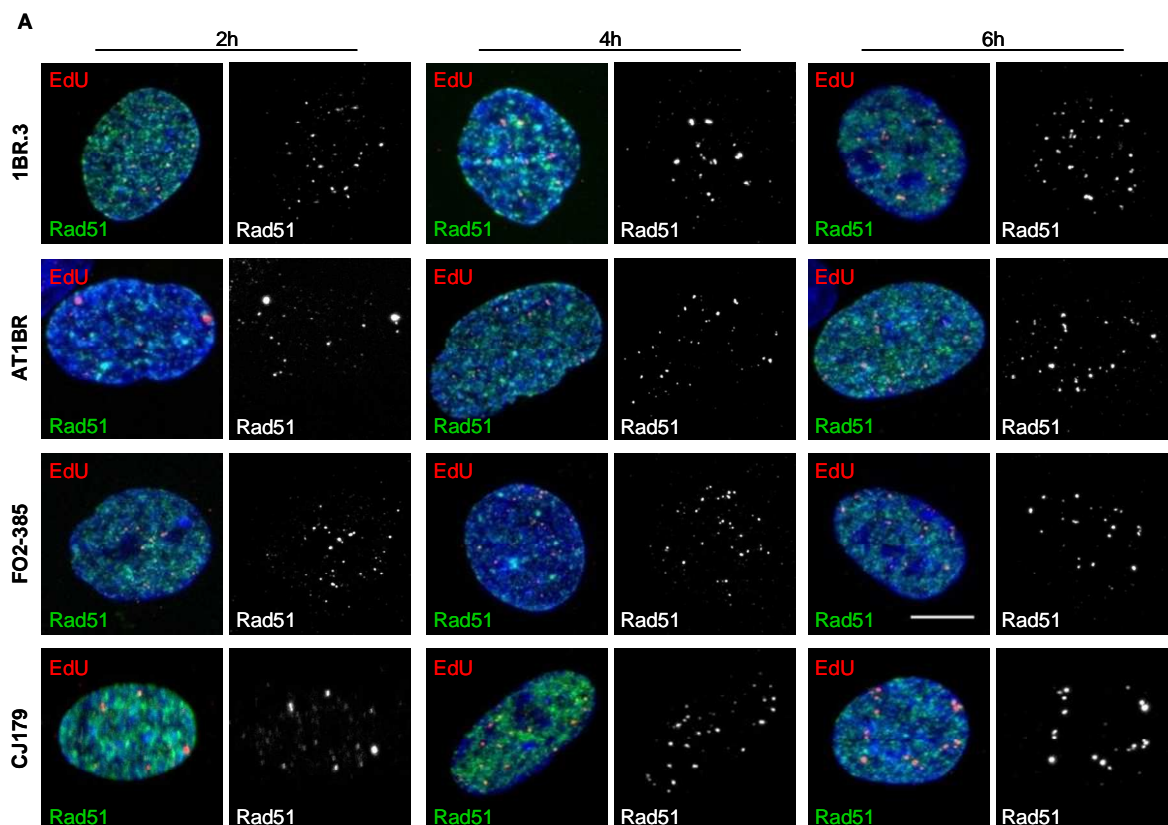**Figure 27. Rad51 foci kinetics in the S-phase**
Cells were pulse-labelled with EdU, irradiated with 1 Gy and the kinetics of Rad51 foci were followed during the S-phase in the EdU-positive population. (A) Distinct Rad51 foci show a larger number at 2 h in WT and both *Artemis* strains (2 h < 6 h) than in *AT* cells. In contrast, *AT* cells show continuously increasing numbers (2 h > 6 h). (B) Quantification of (A)

To confirm this finding, we inhibited ATM function in WT and *Artemis* cells. We first treated WT fibroblasts with the ATM inhibitor for 24 h and monitored cellular radiosensitivity to verify that the ATM inhibition was efficient. X-irradiation of 2 Gy reduced the survival of WT cells to 40%. Addition of the ATM inhibitor but not of DMSO drastically decreased colony formation to 8% (Figure 28, left chart). The number of residual γH2AX foci measured after 24 h roughly doubled when IR was combined with ATM inhibitor treatment (Figure 28, right chart). Together, these results confirm a functional inhibition of ATM. Applying the ATM inhibitor to all fibroblast lines, we found kinetics with delayed but steadily increasing numbers of Rad51 foci in the S-phase for all strains (Figure 29) that closely match those of *AT* cells with or without inhibitor. Conversely, the quick increase and subsequent decline of Rad51 foci were abrogated in WT and *Artemis* cells, indicating that this repair component is Artemis-independent but ATM-dependent, while the delayed formation of Rad51 signals does not require functional ATM.
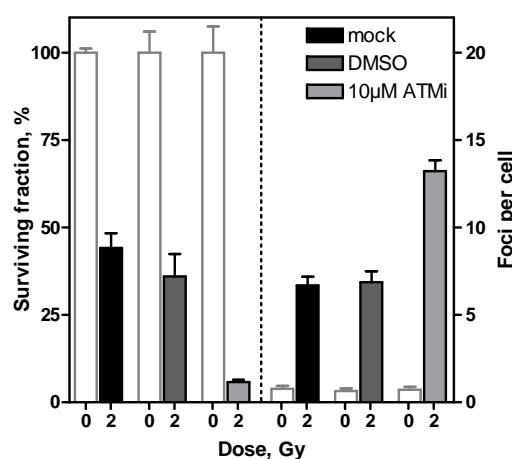
Figure 28. ATMi increases radiosensitivity of WT fibroblasts
WT fibroblasts were irradiated with 2 Gy and treated with the ATM-specific inhibitor KU55933 for a repair interval of 24 h. Depicted on the left-hand side is the decreased survival at 2 Gy (light grey bars) and on the right-hand side the increased number of γH2AX foci (light grey bars) after ATM inhibition.

Figure 29. Rad51 focus kinetics in S-phase fibroblasts after ATMi treatment
(A) Upon ATM inhibition, all strains show similarly increasing numbers of Rad51 foci (2 h < 6 h).
(B) Quantification revealed kinetics like those of *AT* cells alone (Figure 27).

4.3.3. Checkpoint activation and replication speed

Irradiation during the S-phase induces DSBs either directly in the same way as in the G1- or G2-phase or indirectly. In the latter case, the ongoing replication process (fork) collides with a radiation-induced single-strand break (SSB), leading to a one-ended DSB (see model in Figure 34). We therefore asked whether the variable Rad51 kinetics reflect these distinct damage types and whether one-ended DSBs arise more frequently in *AT* cells. This may happen particularly when AT cells fail to induce an intra S-checkpoint.

To address this question, we monitored the phosphorylation/activation of the two major checkpoint kinases Chk1 and Chk2 dependent on the time after irradiation. Both checkpoint kinases are required to some extent for the initiation of the intra S-phase checkpoint. Chk1 is known to be activated by phosphorylation on Ser317 and Ser345, which is executed by ATR (Zou, 2007). Phosphorylated Chk1 in turn targets CDC25A, marks it for proteosomal degradation, and therefore blocks the initiation of replication and the firing of new origins. The phosphorylation of Chk2 on Thr68, on the other hand, is required to induce the G1, intra-S, and G2/M checkpoints in an ATM-dependent manner (Bartek et al., 2001). Concerning the intra S-phase checkpoint, replication in damaged cells is again blocked by the phosphorylation and degradation of CDC25A, in this case via phosphorylated Chk2. We used western blot analysis to monitor the phosphorylation and therefore presumable activation of Chk1 on Ser345 and Chk2 on Thr68. Western blot analysis revealed a rapid phosphorylation of Chk2 on Thr68 in WT cells as early as 15 min after irradiation, as well as the subsequent decline of the signal to an almost mock-treatment level after 1 h (Figure 30A). Chk1 phosphorylation is slower and peaks at 1 and 2 h after IR. *AT* cells, in contrast, displayed a very weak pChk2 signal and a delayed but rather intense pChk1 signal at 4 and 6 h after IR (Figure 30), confirming that ATM is only partially required for checkpoint signaling. The late but intense phosphorylation of Chk1 is presumably due to ATR activity. However, rapid checkpoint induction soon after damage induction requires ATM. In order to functionally address the intra S-phase checkpoint, we quantified the replication speed of irradiated *AT* and WT cells. Cells were labeled with EdU for 30 min directly prior to irradiation with 1 Gy and EdU-positive cells were subsequently followed over a period of 6 h by flow cytometry analysis. Fractions of EdU-positive cells were ascribed to the early or mid/late S-phase (Figure 30B) and quantified. Figure 30C shows the fraction of early compared to all S-phase cells (early + mid/late). This fraction remains constant in WT cells for 2 h after IR and then drops rapidly, indicating that cell progression is stopped immediately following damage for 2 h, after which time DNA synthesis resumes. *AT* cells, in contrast, are not arrested and leave the early S-phase continuously (Figure 30C), compatible with the well-known RDS (Beamish et al., 1994a; Painter et al., 1980). DSBs that are loaded with Rad51 in WT cells during the early 2 h period post-irradiation are unlikely to be associated with replication

progress, but likely rather represent homologous recombination repair of directly induced DSBs. Conversely, the slowly and steadily increasing number of Rad51 foci in *AT* cells is compatible with the accumulation of indirect DSBs due to ongoing replication.
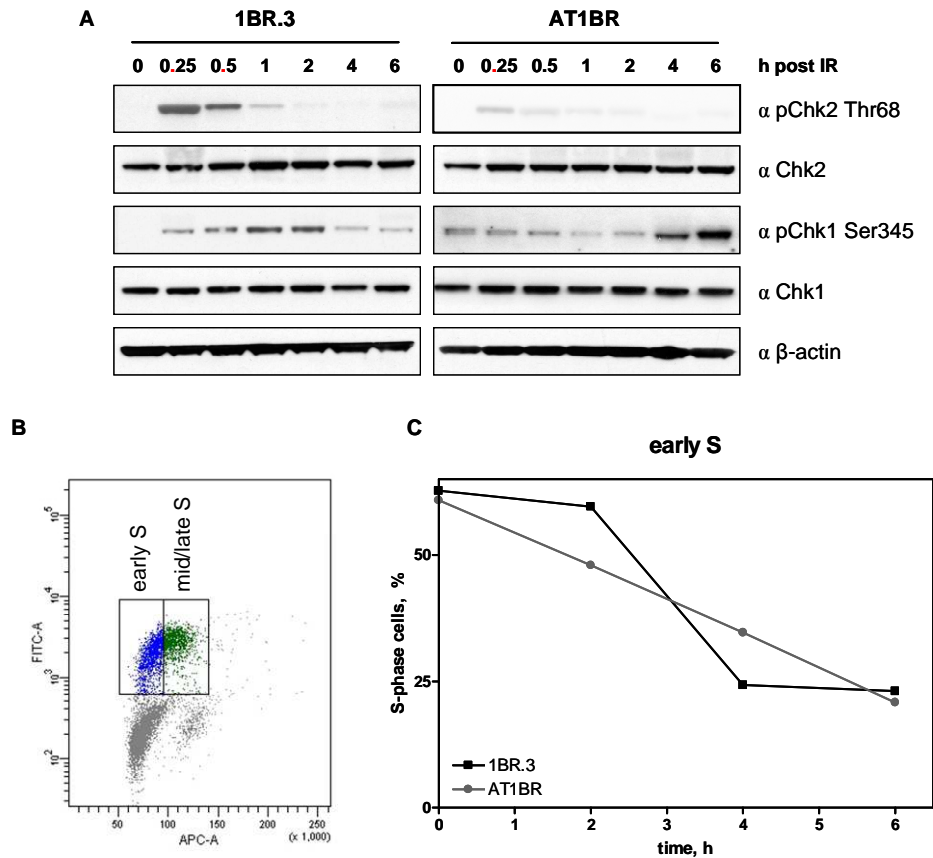
Figure 30. *AT* cells were not efficiently arrested in the S-phase
(A) WT and *AT* cells were irradiated with 10 Gy. Proteins were isolated at the indicated time points and analyzed by Western blot for protein expression of pChk2 Thr68, Chk2, pChk1 Ser345, Chk1, and ß-actin as a loading control. (B,C) Cells were pulse-labelled with EdU and subsequently irradiated (1 Gy) or mock-treated. The fraction of EdU-positive cells was ascribed by flow cytometry to either the early or mid/late S-phase. (C) shows the fraction of cells that remain in early S-phase after IR (1 Gy). WT cells were blocked in early S for about 2 h, while *AT* cells progress continuously into mid- or late S-phase.

4.3.4.   Sensitization of Artemis cells

Having included the S-phase in the repair analysis, we have observed major differences between ATM and Artemis defects for the first time. We thus asked whether the cell survival of Artemis-deficient cells could be further compromised by additional ATM inhibition and whether this occurs preferably in replicating cells.

Colony formation was measured in exponentially growing cells including all cell cycle phases and with all strains being additionally treated with the ATM inhibitor KU55933 for 24 h after irradiation. Strikingly, not only the survival of WT cells but also of *Artemis* cells decreased

significantly upon ATM inhibitor treatment (Figure 31, black open and filled symbols). The inhibitor had no additional effect in *AT* cells.

Next we sought to verify that this additive effect was due to replication-associated damage. To this end, we temporarily blocked replication progress by aphidicolin treatment. We chose a treatment period of 5-6 h post-irradiation, which is exactly the time frame in which most Rad51 foci accumulated in *AT* cells (Figure 27). Even this temporary block of replication significantly reduced the radiosensitization achieved by the ATM inhibitor (Figure 31, compare black and grey filled symbols) in WT and to a different extent in both Artemis strains. Conversely, aphidicolin-treated *AT* cells showed a moderate increase in cell survival (Figure 31) which was less obvious in WT and Artemis cells, validating our previous notion that the abrogation of the intra S-phase checkpoint in *AT* cells is responsible for the accumulation of unrepaired damage during replication.

Together, these results indicate that repair processes in the S-phase strongly rely on ATM but not on Artemis, and that this particular deficiency during replication significantly contributes to the radiosensitive AT-phenotype.
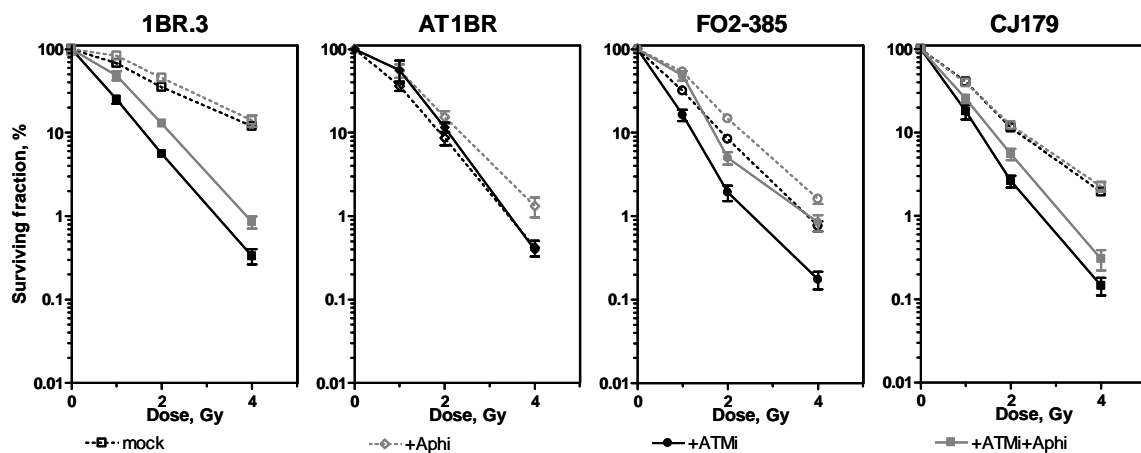
Figure 31. Repair processes in the S-phase are dependent on ATM but not Artemis
1BR.3 (WT), AT1BR (*AT*), FO2-385 and CJ179 (*Artemis*) cells were seeded for colony formation, irradiated and incubated for 24 h in the presence or absence of 10 µM KU55933. Data for cells without ATM inhibitor treatment (black open symbols, dashed lines) are taken from Figure 11. WT and both Artemis lines can be sensitized by the ATM inhibitor KU55933 (black closed symbols). In addition, cells were treated with 5 µM aphidicolin alone for 6 h post-IR (open grey symbols) or in combination with the ATM inhibitor (closed grey symbols), which reversed this sensitization.

## 4.4.   Rad51 focus formation requires functional ATR in the absence of ATM

Irradiation during the S-phase induces DSBs either directly or indirectly upon collision of the replication fork with a SSB, leading to one-ended DSBs. During repair after IR, direct and indirect DSBs co-exist and cannot be systematically distinguished. Our previous results strongly suggest that some the Rad51 foci arising during the S-phase in irradiated *AT* cells are markers of indirect, replication-associated DSBs. However, the repair of these breaks appears to be inhibited in the case of ATM deficiency.

The recruitment of Rad51 to DSBs requires the resection of DNA ends to generate RPA coated 3´-single-stranded overhangs. The resection process and hence Rad51 focus formation have been shown to be ATM-dependent (Adams et al., 2006; Jazayeri et al., 2006; Myers et al., 2006) and may well explain why *AT* cells fail to build Rad51 early after IR. However, the delayed but substantial generation of foci must rely on other factors, which we sought to further elucidate. One of the other PIKKs (DNA-PKcs, ATR) could be a candidate responsible for this process.

4.4.1.   Requirement of DNA-PKcs for Rad51 focus formation in *AT* cells

Though DNA-PKcs has been shown to be not particularly active during the S-phase (Chen et al., 2005b), we had to rule out the possibility of DNA-PKcs being involved in the generation of Rad51 foci in an ATM-deficient background. In order to do so, we employed the inhibitor NU7026 that acts specifically on DNA-PKcs. To confirm that NU7026 sufficiently inhibits DNA-PKcs, we treated WT fibroblasts with 10 µM of the inhibitor and counted γH2AX foci 24 h after irradiation. Enumeration of the residual damage revealed that DSB repair capacity was significantly reduced upon DNA-PKcs inhibition (Figure 32A, right hand chart). In addition, cell survival was drastically decreased upon irradiation with 2 Gy (Figure 32A, left hand chart). We were not able to monitor residual γH2AX foci in *AT* cells after DNA-PK inhibition, since both the absence of ATM and inhibition of DNA-PK result in instable γH2AX signals at the damage sites which can no longer be considered reliable DSB markers.

In contrast to γH2AX, Rad51 foci are not the result of direct in situ phosphorylation by the PIKKs, but rather reflect local recruitment processes of hundreds (or thousands) of molecules. Having established that NU7026 efficiently inhibits DNA-PKcs activity, we wanted to know whether this kinase activity is required for Rad51 focus formation in *AT* cells. Therefore, we applied NU7026 to *AT* cells and monitored Rad51 focus formation 6 h after irradiation with 1 Gy in EdU-positive S-phase cells. We were not able to detect any significance irrespective of DMSO, ATM or DNA-PK inhibitor (Figure 32B). We could therefore exclude the possibility of DNA-PKcs being involved in the generation of Rad51 foci in cells with an ATM-deficient background.
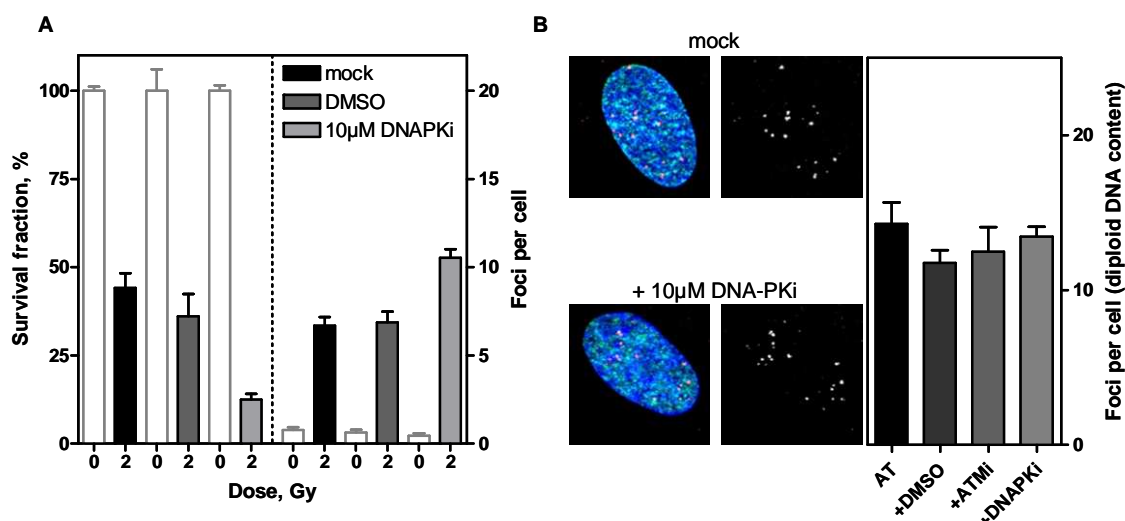
Figure 32. Rad51 focus formation in *AT* is independent of DNA-PKcs
(A) WT fibroblasts were irradiated with 2 Gy and treated with the DNA-PK-specific inhibitor NU7026 (10 μM) for a repair interval of 24 h. Depicted on the left-hand side is the decreased survival (light grey bars) and on the right-hand side the increased number of γH2AX foci (light grey bars) after DNA-PK inhibition. (B) *AT* cells were EdU-labelled, irradiated with 1 Gy, and continuously exposed to the DNA-PK inhibitor NU7026 (10 μM) during repair. Rad51 foci were monitored 6 h later in EdU-positive cells. Cells displayed the same number of Rad51 foci as those without inhibitor treatment. Control DMSO and ATM inhibitor treatment did not influence the number of Rad51 foci after 6 h.

4.4.2. Requirement of the ATR/Chk1 pathway for Rad51 focus formation in *AT* cells

In order to test whether the Rad51 accumulation in the S-phase is ATR dependent, we treated EdU-labeled *AT* cells with 10 mM caffeine, which has been shown to inhibit both ATM and ATR (Sarkaria et al., 1999), and stained for Rad51 6 h after irradiation. In fact, caffeine treatment greatly diminished Rad51 focus formation (Figure 33A). The numerous foci usually observed in *AT* cells could hardly be seen after 5 mM and were completely absent after 10 mM caffeine. Instead, weak and diffuse nuclear staining was eventually seen, the nature of which is not clear. This inhibition of ATR – and ATM – in an ATM-deficient background confirms that ATR is the major kinase with a critical role in the recruitment of Rad51 to DSBs (Adams et al., 2010; Wang et al., 2004). During the completion of this thesis, ATR was knocked down in a collaboration project by Drs. G. Rohaly and I. Dornreiter. They could show in the absence of functional ATM and after ATR siRNA treatment that Rad51 focus formation in S-phase cells was completely abrogated, validating the specificity of our findings.

ATR and its downstream kinase Chk1 have been shown to be essential for Rad51 focus formation after HU (Sorensen et al., 2005). We thus asked whether Rad51 focus formation after irradiation-induced damage in the S-phase depends on ATR alone or also on its effector kinase Chk1. To define the role of Chk1 in Rad51 recruitment after IR-induced damage in S,

we treated the cells with the specific Chk1 inhibitor UCNO1 (0.1 µM) (Sorensen et al., 2005) in the same experimental setting. Inhibition of Chk1 by UCNO1 in EdU-positive *AT* cells reduced Rad51 focus formation to background levels 6 h after irradiation (Figure 33B), confirming that the process of Rad51 focus formation during the S-phase needs not only ATR but also its downstream kinase Chk1.

Although functional ATR/CHK1 is sufficient to form Rad51 foci in the absence of ATM, it appears not to be sufficient to successfully repair IR-induced damage during replication, since we found no evidence of repair by HR during the 6 h observation period, a result confirmed by the increased number of residual Rad51 foci in G2-phase *AT* cells.
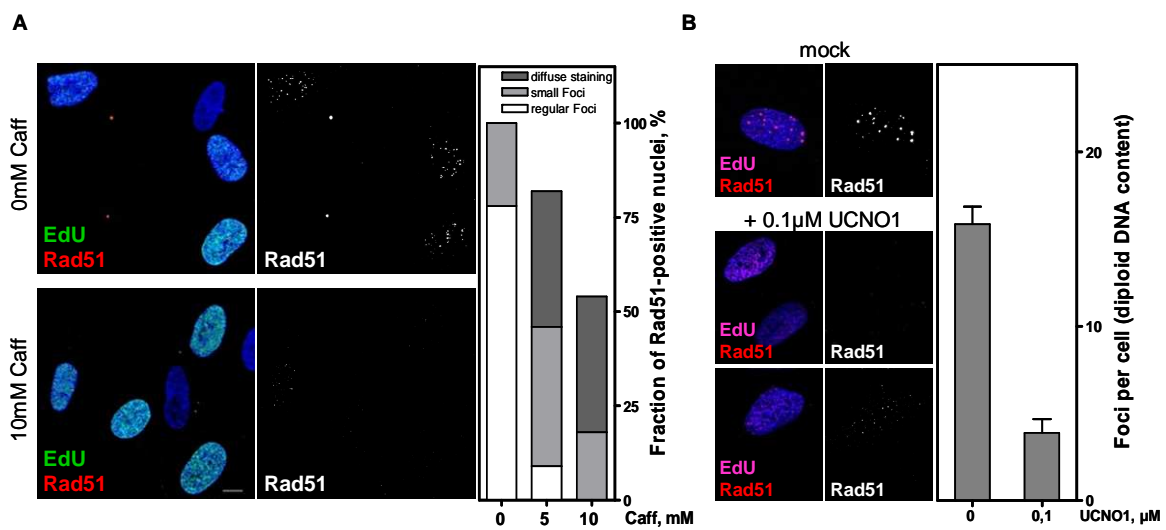
Figure 33. Rad51 focus formation in *AT* cells depends on functional ATR
(A) *AT* cells were pulse-labelled with EdU shortly before 1 Gy and treated with 5 or 10 mM caffeine 1-2 h before IR. Rad51 foci were monitored 6 h later in EdU-positive cells. (B) *AT* cells were EdU-labelled and irradiated as before and continuously exposed to the Chk1 inhibitor UCNO1 (0.1µM) during repair. Cells displayed only background levels but no additional formation of Rad51 foci.

5.   Discussion

Both ATM and Artemis were shown to be equally required for the NHEJ repair of a subset of IR-induced DSBs in both the G1 and G2-phase (Figure 17; Beucher et al., 2009; Deckbar et al., 2007; Riballo et al., 2004).   ATM is also known to be involved in homologous recombination (Meyn, 1993; Bryant et al., 2006; Golding et al., 2004; Morrison et al., 2000). However, its functions are not yet fully understood. Recently, *Artemis* cells were shown to display a HR defect similar to *AT* after IR in the G2-phase (Beucher et al., 2009; this study Figure 26). Interactions with the Artemis nuclease seemed to represent the only direct involvement of ATM in DSB repair so far. Jeggo, Löbrich and coworkers very recently hypothesized that not a particular pathway, but rather the region where the lesion is located is crucial for repair. In this context, ATM was discovered to interact with Kap1. After irradiation, Kap1 is phosphorylated at the DSB site presumably by chromatin-bound ATM, resulting in chromatin relaxation in wider areas around the DSB to facilitate repair particularly in areas of heterochromatin. Goodarzi et al showed that the percentage of DSBs that requires ATM for repair correlates with the amount of heterochromatin. Down-regulation of the heterochromatin building factor Kap1 nullifies the requirement for ATM (Beucher et al., 2009; Goodarzi et al., 2009). Further, a similar defect in DSB repair in *AT* and *Artemis* cells in contrast to the wild type is only observed at later time points (>2 h) after damage induction in the G1 and G2 phase. This fraction of unrepaired breaks has been suggested to account for defects in the repair of DSBs within heterochromatic regions. Epistasis analyses using the ATM inhibitor KU55933 in Artemis- and BRCA2-deficient cells or down-regulations of combinations of targets (ATM/BRCA2, ATM/Rad51, Artemis/BRCA2, Artemis/Rad51) in HeLa cells revealed repair defects similar to those seen when individual factors were affected. Therefore, ATM and Artemis function in the same pathway as BRCA2 and Rad51 in the G2-phase, namely homologous recombination (Beucher et al., 2009). It had been suggested that *AT* and *Artemis* cells are widely epistatic for their repair phenotype, although epistasis analyses were performed separately in the G1- and G2-phase and cell cycle-related effects had not been considered (Beucher et al., 2009; Deckbar et al., 2007; Riballo et al., 2004). However, ATM is known to be a key player in cell cycle checkpoint activation. Here, we report remarkably diverse repair features for each of the genetic defects when considering the entire cell cycle. Particularly during the S-phase, ATM but not Artemis is necessarily required for HR (Figure 27). Critical repair functions appear not to be restricted to activity in heterochromatin.

5.1.   Artemis nuclease in homologous recombination

Artemis – with its nuclease function – is required for efficient DSB repair in the G1- and G2-phase (Beucher et al., 2009; Deckbar et al., 2007; Riballo et al., 2004). Hence, deficient strains show an increase in unrepaired residual DSBs (γH2AX foci in Figure 17) as well as enhanced radiosensitivity (Figure 11). Previously, this sensitivity had been ascribed to a defect in NHEJ, since Artemis exerts its endonuclease activity in complex with DNA-PKcs, a core component of NHEJ. Artemis is believed to be involved in the end-processing steps of NHEJ after IR and prior to ligation. However, *Artemis* and *AT* strains display a similar repair phenotype, not only in G1 but also in the G2 phase of the cell cycle (10-15% of unrepaired DSBs) (Deckbar et al., 2007; Riballo et al., 2004), while Artemis is a phosphorylation target of ATM (Chen et al., 2005b; Riballo et al., 2004). Together, these facts raised the possibility of functions beyond the pure end processing steps of NHEJ. Artemis was therefore proposed to be activated by ATM and involved in the same downstream repair pathway, which also includes HR in the G2-phase (Beucher et al., 2009). Recently it has been hypothesized by Jeggo and coworkers that both the defect in NHEJ in G1 as well as the defect in HR in G2 are related to DSBs within heterochromatic regions. Breaks associated with heterochromatin were proposed to need processing by the Artemis nuclease. Heterochromatin contains a higher number of repetitive and partially palindromic sequences (i.e. LINE and SINE elements). After damage induction, these complementary sequences favor the formation of hairpin structures which might require Artemis nuclease activity for processing prior to ligation.

We now show that the Rad51 focus formation in *Artemis* cells is greatly impaired in the G2-phase (Figure 26). We conclude that *Artemis* cells have defects in HR, possibly in the resection processes necessary for generating 3' single-standed overhangs, the substrate for Rad51 loading. Similar observations have been made by others (Beucher et al., 2009).

Additionally, gene conversion efficiency in the I-SceI reporter assay was reduced when we depleted Artemis (Figure 24), supporting findings that Artemis deficiency leads to a defect in repair by HR. It is not very likely that the construct was stably integrated within the heterochromatin, since the GFP was successfully translated and expressed and thus must have been located in a euchromatic region. Hence, based on our observation that Artemis depletion reduced the gene conversion efficiency in the chromosomal I-SceI reporter assay (Figure 24), we propose that Artemis has a function in HR beyond the repair of only heterochromatic lesions.

5.1.1. Artemis nuclease is dispensable for homologous recombination during the S-phase

Artemis is required for Rad51 focus formation and efficient HR in the G2-phase (Figure 26). Strikingly, we show Rad51 kinetics here similar to those of the WT in S (Figure 27), rendering the Artemis nuclease dispensable for HR during the S-phase.

What makes Artemis nuclease function expendable for HR in the S-phase?

Homologous recombination requires 3' ssDNA overhangs. The end resection process for the generation of these overhangs has been shown to be initiated by the CtiP protein (Huertas et al., 2008; Mimitou et al., 2008; Sartori et al., 2007; Takeda et al., 2007) and in addition requires BRCA1 and MRN (Chen et al., 2008). CtiP contains a highly conserved CDK target motif (Huertas et al., 2008). CDK activity has also been shown to be important for BRCA1-MRN interaction, additional factors of the resection complex (Chen et al., 2008; Huertas et al., 2008). These studies show that end resection is modulated by CDK activity and therefore is highly cell cycle-dependent. The efficiency of end resection peaks in the S-phase (Zierhut et al., 2008). Studies in yeast by Zierhut *et al.* revealed a threefold faster end resection process in the S-phase compared to G2. Therefore, resection in the S-phase might not depend upon the supportive Artemis nuclease, in contrast to the slower and less extensive end degradation in the G2-phase (Zierhut et al., 2008).

Another possibility why Artemis nuclease function could be unnecessary in the S-phase is that structures requiring Artemis processing (i.e. hairpin structures) may not arise in the S-phase. Replication and DNA repair by gene conversion share some proteins such as RPA or polymerases. RPA functions in DNA end protection during normal, unperturbed replication. Therefore, RPA might simply be "handed-off" from replication to repair. Protection of the DNA ends by RPA could prevent the formation of hairpin structures, the substrates for the Artemis nuclease, thus rendering Artemis dispensable for HR in the S-phase

Artemis has been additionally shown to exert its endonuclease activity when complexed with DNA-PKcs rather than through phosphorylation by ATM alone (Goodarzi et al., 2006). DNA-PKcs activity is reduced in the S-phase (Chen et al., 2005a). Therefore, damaged cells in this phase might compensate for processes that would normally require DNA-PKcs activity and use pathways independent of the DNA-PKcs-Artemis complex, which – in conjunction with Artemis - might account not only for NHEJ but for also HR processes.

Alternatively, structures during the replicative S-phase are more relaxed. Since we worked with exponentially growing cells, we included not only early replicating, but also late replicating cells in our studies, in which the heterochromatin is expected to be relaxed (Grewal et al., 2002; Su, 2010). These relaxed DNA structures may favor end-processing independent of Artemis, resulting in Rad51 focus formation that peaks as early as 2 h post-IR

in the S-phase, similar to the WT. Thus, DNA end resection in the S-phase is Artemis independent.

5.2.   A more universal role of ATM in homologous recombination

Although recruitment of the Rad51 recombinase in *AT* cells leads to visible foci, its kinetics are significantly delayed in the S and G2-phase (Figure 26 and 27; Yuan et al., 2003). This may result from both insufficient end resection and H2AX phosphorylation (this study Figure 16, Stiff et al., 2004), a known pre-requisite for timely Rad51 accumulation at sites of DNA damage (Paull et al., 2000; Dodson et al., 2009). Although the kinetics were delayed, *AT* cells displayed numerous residual recombination foci. All un-rejoined DSBs were eventually decorated with Rad51 (Figure 19). We show here that these residual Rad51 foci originated during the S-phase (Figure 27), indicating that replication or replication-associated processes promote Rad51 focus formation in *AT* cells. Despite the eventually successful recruitment of Rad51 to all un-rejoined DSBs (Figure 19), HR appears to be widely inhibited in cells lacking functional ATM, as (i) the number of IR-induced Rad51 foci never declined during the S- or G2-phase (Figure 26, 27) and (ii) the gene conversion efficiency of I-SceI generated DSBs was strongly reduced (Figure 24). In contrast to the I-SceI reporter assay, where we detected on average 30% repair by gene conversion when we inhibited ATM (Figure 24), we did not detect any repair by HR using the Rad51 focus staining technique, as the number of Rad51 foci never declined (Figure 26, 27). On the other hand, the very delayed Rad51 foci kinetics might well include some repair by HR obscured by the simultaneous accumulation of new foci. Hence, the delayed kinetics probably not only reflect a delayed DNA damage response and therefore the recruitment of repair factors in *AT* cells, but also to some extent the repair of DSBs (i.e. 30% by gene conversion).

Recently, Jeggo, Löbrich, and colleagues have shown that the ATM defect in G2 is restricted to the HR of DSBs induced in heterochromatic regions (Beucher et al., 2009), similar to NHEJ in G1 (Goodarzi et al., 2008; Noon et al., 2010). Epistasis analyses revealed that ATM is involved in the HR pathway (Beucher et al., 2009). Additional depletion of the chromatin building factor Kap1 nullified the ATM defect, linking ATM to the DSB repair of heterochromatin breaks. On the other hand, detailed analyses of gene conversion events using the I-SceI reporter system revealed significantly lower HR repair rates after either ATM knock-down using siRNA (Figure 24), inhibition (Figure 24, Beucher et al., 2009) or dominant-negative expression of ATM (Golding et al., 2004). Notably, neither I-SceI cleavage nor the majority of replication-associated DSBs is likely to occur in heterochromatin. DNA-PKcs has also been shown to substitute for ATM regarding Kap-1 phosphorylation (Tomimatsu et al., 2009). Additionally, a study by Chiolo *et al.* very recently showed that ATR

rather then ATM plays a major role in heterochromatin expansion after IR (Chiolo et al., 2011). We therefore suggest that ATM has more universal but still not precisely defined functions in HR. In addition to end resection and the relaxation of heterochromatin, ATM emerges as involved more generally in chromatin remodelling through the activation of RNF20 and 40, which in turn monoubiquitylate histone H2B, a step required for the timely recruitment of central players in DSB repair pathways (Moyal et al., 2011).

ATM also activates the cohesion component SMC1 after DNA damage. SMC1 is a member of the structural maintenance of chromosome family. It was initially identified in yeast as a component of cohesin, a protein complex that is required for the maintenance of sister chromatid cohesion (Michaelis et al., 1997). The cohesin complex also functions in DNA repair (Sjogren et al., 2001). It has been shown that the expression of a SMC1 mutant which cannot be phosphorylated reduces DNA repair efficiency and cell survival after irradiation, similar to the DSB repair phenotype of cells lacking ATM (Kim et al., 2002; Kitagawa et al., 2004; Yazdi et al., 2002). SMC1 is one of the key phosphorylation targets of ATM in response to DNA damage. After damage induction, phosphorylated SMC1 induces sister chromatid cohesion (Yazdi et al., 2002; Bauerschmidt et al., 2010), which facilitates homology search and strand exchange. Hence, cells lacking the ability to phosphorylate SMC1 such as *AT* cells (Yazdi et al., 2002) may fail to find the homologous sequence on the sister chromatid, a mandatory step in homologous recombination downstream of Rad51 filament formation. Thus, *AT* cells would accumulate more DNA damage and chromosomal aberrations after irradiation (George et al., 2009).

Moreover, the accessory factors XRCC2 and 3 are also ATM phosphorylation targets (Matsuoka et al., 2007), of which at least XRCC3 is involved in branch migration and perhaps the resolution of the putative Holliday structure (Brenneman et al., 2002; Liu et al., 2004), another step downstream of Rad51 loading.
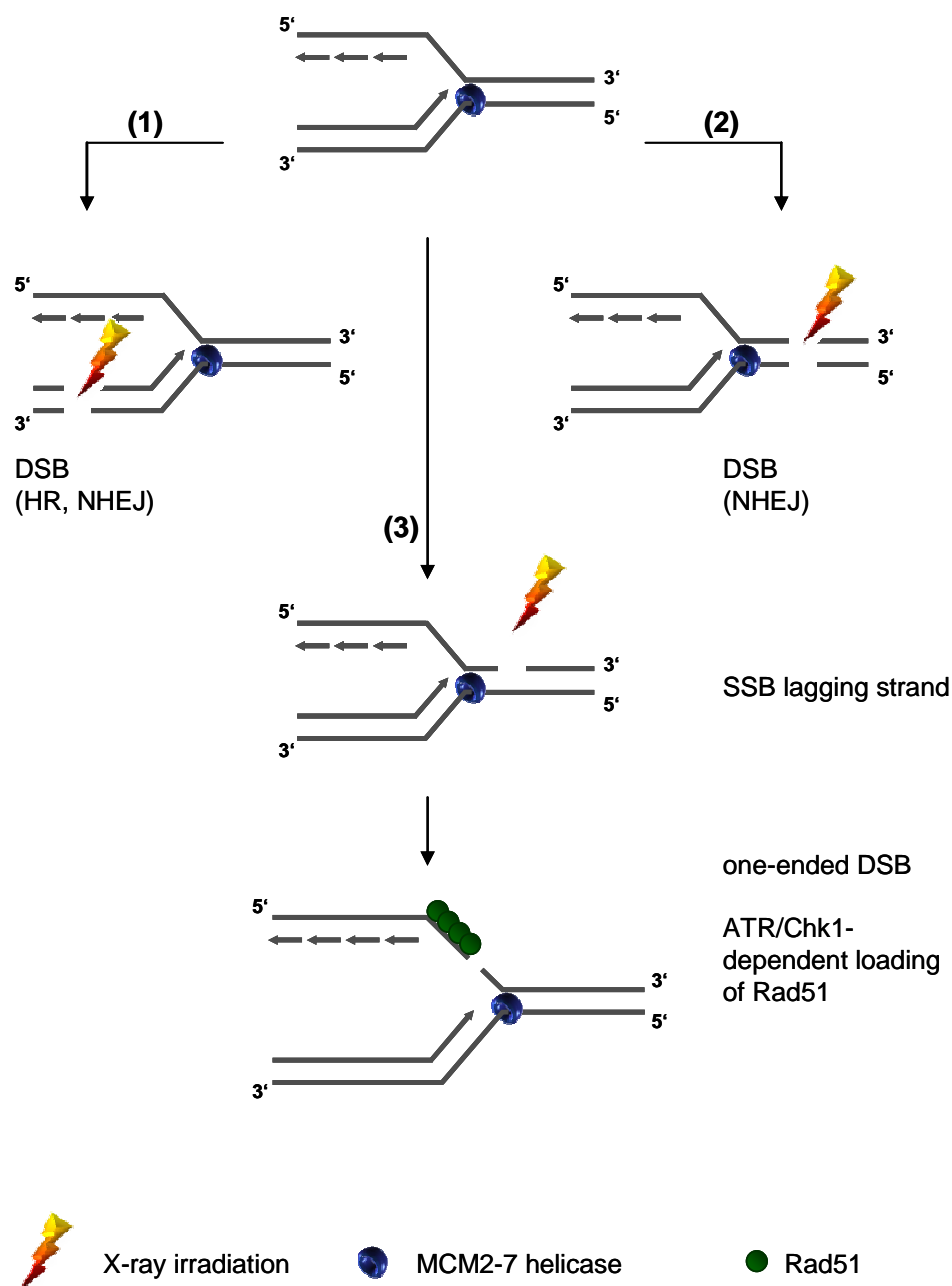
Figure 34. Model for the processing of one- and two-ended DSBs
(1) Post-replicative DSBs repaired by either NHEJ or HR. (2) Pre-replicative DSBs repaired by NHEJ. (3) SSBs on the lagging strand resulting in one-ended DSBs and ATR/Chk1-dependent loading of Rad51.

5.3.   Replication structures allow ATR activation without prior end resection

AT cells irradiated in S build numerous Rad51 foci with time (Figure 27). This focus formation was unexpected, since ATM is known to be required for the resection of 5´ DNA ends (Adams et al., 2006; Jazayeri et al., 2006; Lee et al., 2008; Myers et al., 2006; You et al., 2009). The free 3´ss-tails are rapidly coated by RPA, which is the substrate for the subsequent chromatin loading of Rad51 (Raderschall et al., 1999). ATM presumably

activates several essential components of the resection process through phosphorylation such as the MRN complex, CtIP, BRCA1, WRN, BLM and Exo1 (Buis et al., 2008; Huertas et al., 2009; Matsuoka et al., 2007; Sartori et al., 2007; Beamish et al., 2002; Chen et al., 2008; Bolderson et al., 2010), though its precise role is not yet clear. In the absence of ATM, the related kinase ATR might phosphorylate several of these proteins with delayed kinetics (Bolderson et al., 2010). However, activation of ATR also requires the presence of RPA-coated ssDNA and is thus considered a downstream event of ATM activation (Cuadrado et al., 2006; You et al., 2009; Zou et al., 2003a). Shiotani *et al.* revealed an "ATM-to-ATR-switch" *in vitro*, where ATM was primarily activated by DSBs, in turn facilitating end-resection. Progressive resection of DSB-ends promotes a switch to the ATR kinase. ATR activation during the process of end-resection is coupled with a loss of ATM activation. Taken together, it appears that ATR activation after IR requires initial ATM activity (ATM-induced end resection) (Shiotani et al., 2009). Two explanations may reconcile these apparent contradictions: (i) A yet unknown ATM-independent resection step precedes ATR activation, or (ii) resection is not required because parts of the replication machinery may progress beyond an IR-induced SSB and expose single-stranded DNA sufficient to activate ATR (see model Figure 34 (3)). Such structures may arise on the lagging rather than on the leading strand. The mammalian replicative helicase complex MCM2-7 forms a double-hexameric ring that likely accomodates the leading strand and, in contrast to E.coli DnaB, cleaves interstrand hydrogen bonds by translocation in a 3′-5′direction (Labib et al., 2001; Moyer et al., 2006). Breaks in the leading strand would accordingly block the helicase together with the following polymerase, leading to a blunt-ended DSB. Gaps on the opposite strand, in contrast, may allow limited MCM2-7 progression beyond the break. The ability of the MCM2-7 helicase to progress further, even though the replication complex, is disrupted, as has been shown by Walter, Cimprich and coworkers. They revealed that the inhibition of DNA polymerase α by aphidicolin causes extensive unwinding of the DNA, thus showing that the helicase can become uncoupled from the replication fork (Walter et al., 2000). However, the lagging strand continuity is interrupted, generating a so-called "one-ended DSB", which may preclude synthesis and/or maturation of one or more Okazaki fragments, thus leaving a stretch of ssDNA. Hence, the question arises as to whether this stretch of ssDNA is long enough to activate ATR. MacDougall *et al.* showed that a DNA structure that exposes only 35nt of ssDNA can induce Chk1 phosphorylation mediated by ATR kinase (MacDougall et al., 2007). Thus, a damaged replication fork that lacks the last Okazaki fragment spanning the break site (Figure 34 (3)) freely exposes about 100-200nts of ssDNA and can very likely initiate ATR signalling. In addition, MCM2-7 is a phosphorylation target of ATM (Matsuoka et al., 2007). The kinase activity may inhibit helicase procession after DNA damage. Conversely, cells lacking ATM might expose particularly long ssDNA stretches as an

immediate substrate for ATR-ATRIP and subsequent Rad51 loading (Figure 34 (3)) without prior end resection. The free 3´ end within this stretch could even be used for direct strand invasion and priming of repair synthesis, well in line with the synthesis-dependent strand annealing model for gene conversion, where only one 3' ssDNA-overhang invades the sister chromatid. One potential reason why these one-ended DSBs are not addressed by NHEJ is the fact that long ss-3' overhangs are protected by RPA, which already binds intermediate structures during normal replication. This ssDNA-RPA complex could prevent Ku70/80 binding and therefore NHEJ on one-ended DSBs (Ristic et al., 2003).

These one-ended DSBs on the lagging strand may be an exception, while breaks on the leading strand (not depicted) as well as DSBs induced post-replication (Figure 34. (1)) do not produce ssDNA overhangs and unequivocally require resection in order to be repaired by HR. The possibility that ATR is activated without prior resection does not rule out the possibility that the HR of lagging-strand damage involves delayed secondary resection, i.e. by EXO1. Bolderson *et al.* showed that EXO1 is recruited to laser-induced damage in the absence of ATM, though with slower kinetics (Bolderson et al., 2010), supporting our hypothesis of delayed resection processes triggered by ATR.

Pre- or post-replicative DSBs in G1/early S or in late S/G2, respectively, which are not directed to end resection will be repaired by NHEJ (Figure 34 (2) or (1)).

Beyond that, we gained indirect evidence of the activation of ATR during the S-phase from studies of the cell cycle after irradiation. We showed a pronounced secondary G2-block in *AT* cells, but only when they had previously travelled through the S-phase (Figure 14). An early and transient G2-arrest is dependent on ATM and blocks cells that were in G2 at the time of irradiation (Kim et al., 2002). *AT* cells do not instantly arrest in the G2-phase after IR, but rather rapidly progress into mitosis. Nevertheless, a prolonged G2-arrest in irradiated *AT* cells has been observed at later time points (this study Figure 12; Beamish et al., 1994a; Beamish et al., 1994b), probably due to over-activated ATR/Chk1 in irradiated *AT* cells (Tomimatsu et al., 2009; Wang et al., 2003; Xu et al., 2001).

The secondary ATR-mediated G2-checkpoint is basically the only checkpoint that can be activated in *AT* cells in response to ionizing irradiation. ATM is not only involved in the G1/S checkpoint and G2/M transition, but also in the intra-S-phase checkpoint. The most well-defined branch of the intra-S-phase checkpoint after ionizing irradiation is mediated by ATM-dependent Chk2 phosphorylation and subsequent CDC25A degradation (Goldberg et al., 2003). Another separate branch in the regulation of the intra S-phase checkpoint in response to IR is the interaction of ATM with NBS1, BRCA1 and SMC1. NBS1 and BRCA1 are necessary for ATM to optimally phosphorylate SMC1 on Ser957 and Ser966 (Yazdi et al., 2002). Therefore, the activation of SMC1 is not only required for DNA-DSB repair, but also for the induction of the intra-S-phase checkpoint. Kitagawa *et al.* showed that irradiated cells

in which endogenous SMC1 had been replaced by a non-phosphorylatable mutant continue to synthesize DNA during the S-phase, whereas replication in control cells is inhibited by DNA damage (Kitagawa et al., 2004). In a similar vein, we assessed the replication progress by measuring EdU incorporation in *AT* cells after irradiation (Figure 30B). *AT* cells continued DNA synthesis, whereas WT cells paused replication for 2 h following irradiation (Figure 30C), thus confirming the functional link between ATM and intra-S-phase checkpoint activation. This inability of *AT* cells to reduce the rate of DNA synthesis after exposure to ionizing irradiation had already been shown in the early stages of research on ATM (Houldsworth et al., 1980; Painter et al., 1980) and was termed radioresistant DNA synthesis (RDS). This incapability of *AT* cells to halt replication also supports our theory that the MCM2-7 helicase is able to progress beyond a single-strand break without being stopped by intra-S-phase checkpoint induction, thus generating one-ended DSBs that expose stretches of ssDNA-tails long enough for ATR to be activated.

5.3.1. ATR controls Rad51 focus formation

Numerous Rad51 foci accumulate after IR in an ATM deficient background. This process could be blocked when ATR and its downstream kinase Chk1 are additionally inhibited (Figure 33). Beside its hypothesized function in delayed end resection (Bolderson et al., 2010), ATR is the principal kinase that activates Chk1, which in turn phosphorylates Rad51 at Y309. This phosphorylation step has been shown to be essential for Rad51 focus formation and HR after replication stress induced by HU (Sorensen et al., 2005). We showed here for the first time, the involvement of ATR/Chk1 in Rad51 focus formation after IR (Figure 33). Further, chromatin loading of Rad51 also requires c-Abl-mediated phosphorylation at Y54 and Y315 (Popova et al., 2009; Shimizu et al., 2009). Although the damage-induced activation of c-Abl is known to be ATM-dependent (Matsuoka et al., 2007; Shafman et al., 1997), it is tempting to speculate that ATR can take over in *AT* cells, particularly during the S-phase, which had yet to be demonstrated because previously only asynchronous cell populations had been investigated (Baskaran et al., 1997; Shafman et al., 1997).

As mentioned above, we propose that the slow Rad51 foci kinetics in *AT* cells also represent repair by HR to some extent (30%) and are probably dependent upon ATR. In contrast to ATM, the lack of ATR is more severe and results in lethality in mouse embryos (Brown et al., 2000). Only partial ATR deficiency exists in humans and results in an autosomal recessive disorder, Seckel Syndrome, characterized by severe developmental defects and tumor development (Murga et al., 2009). Together, these observations emphasize the importance

of the ATR kinase and the downstream effector kinase Chk1 in repair processes, especially during HR in the S-phase.

5.4. ATM and Artemis are not epistatic in the S-phase

ATM and Artemis are required for Rad51 focus formation and efficient repair by HR in the G2-phase (Figure 26, Beucher et al., 2009). We now show for the first time remarkable differences in Rad51 focus formation in the S-phase (Figure 27). *AT* cells display delayed but steadily increasing Rad51 foci kinetics. *Artemis* cells behave like the WT, displaying a fast increase and subsequent decline which we confirmed using a second Artemis-deficient line (Figure 27). These results suggest that Artemis is not involved in HR during the S-phase. Strikingly, we showed that ATM inhibition in *Artemis* cells leads to Rad51 foci kinetics similar to those seen in *AT* cells alone, confirming the dependence of HR after IR on ATM. Moreover, we showed an additive effect in gene conversion when using co-depletion of both proteins in the I-SceI reporter assay (Figure 24). Accordingly, the cell survival of Artemis-deficient cells could be further compromised by additional ATM inhibition (Figure 31). Artemis-deficient cells then lost the G1/S checkpoint and additionally failed to execute the HR repair of direct and indirect DSBs during the S-phase. This effect was widely relieved when replication was blocked by aphidicolin treatment (Figure 31), thus demonstrating that the ATM repair defect is linked to active replication.

We therefore propose that ATM and Artemis are not epistatic for HR in the S-phase.

In conclusion, we show that both radiosensitivity syndromes, *AT* and *Artemis*, confer a DSB repair deficiency affecting NHEJ and HR which is similar in both deficient cell lines but not fully epistatic. Only *AT* cells display an additional HR defect in the S-phase that affects the repair of direct and indirect replication-associated DSBs, leading to increased numbers of unresolved recombination foci in G2 and a more prominent G2-arrest 24 h after IR compared to *Artemis* and wild-type cells (Figure 12). We propose that Artemis, similar to ATM, has an HR function beyond the repair of only heterochromatic lesions. However, ATM appears to play a more pivotal role in HR.

Taken together, our results display remarkably diverse repair features of *AT* and *Artemis* cells during the S-phase, emphasizing the dependence of direct and indirect replication-associated DSBs on ATM.

5.5.   Perspectives and clinical relevance

AT cells accumulate in the G2-phase in response to IR, but only after having travelled through the S-phase. These cells display an elevated number of residual DSBs (γH2AX foci), with every DSB being decorated with Rad51, the major recombinase during HR. These Rad51 foci are very likely to represent insufficient HR, since they accumulated during the S-phase but never declined in number (Figure 27). We conclude that ATM has to be involved in HR beyond resection or Rad51 loading processes. Whether it is involved directly by activating additional HR factors (i.e. BLM, WRN, Rad54) or indirectly by phosphorylation of SMC1, a factor that induces sister chromatid cohesion, thereby facilitating strand invasion, HJ formation, homology search, and strand exchange, is still unknown. To address this question it is necessary to explore whether Holliday junctions can be formed in *AT* cells at all or whether Rad51 filaments are able to invade the sister chromatid. To this end, a second marker for HR should be used that is possibly involved in HR beyond the formation of Rad51 foci. One likely candidate is BLM, which has already been shown to co-localize with Rad51 in nuclear foci in response to IR (Wu et al., 2001), though never specifically in irradiated S-phase cells. Formation of these foci would implicate successful formation of Holliday junctions and thus the invasion of the sister chromatid. The persistence of these foci, on the other hand, would indicate a deficient resolution of Holliday junctions.

Another possibility to identify the steps in HR that require ATM would be to monitor the kinetics of Rad51 foci post-irradiation in a non-phosphorylatable SMC1 mutant, especially during the S-phase. Kinetics similar to those of *AT* cells would place ATM and SMC1 in the same pathway concerning directly or indirectly induced DSBs in the S-phase, thus suggesting impaired strand invasion.

Rad51 foci accumulate in *AT* cells during replication. They presumably form at structures that can activate ATR/Chk1 without preceding resection, i.e. one-ended DSBs. During irradiation, a broad spectrum of damage types is induced in addition to DSBs, some of which are SSBs or base damage and which might result in one-ended DSBs upon encountering a replication fork. To confirm that one-ended DSBs are the source of Rad51 focus formation in *AT* cells, we could either (i) increase the numbers of DSBs and – if possible – decrease SSBs, or (ii) increase the number of SSBs. (i) Some radiomimetics such as topoisomerase II inhibitors cause DSBs. Under normal unperturbed conditions, topoisomerase II induces controlled DSBs in order to manage DNA supercoils resulting from torsional stress (Schoeffler et al., 2005). Targeting these topoisomerases by inhibitors (i.e. etoposide) leads to the stabilization of the cleaved DNA intermediates, thereby inducing DSBs. In contrast to IR, the use of topoisomerase II inhibitors would only induce DSBs, reducing the likelihood of one-ended DSBs to occur. Solely DSBs would need ATM-dependent processing in order to generate 3' ssDNA overhangs as a substrate for Rad51 loading and subsequent repair by HR. Therefore

– in the absence of ATM – topoisomerase II inhibitor-induced DSBs would lead to impaired Rad51 focus kinetics in the S-phase. (ii) The number of SSBs, on the other hand, could be increased by the use of poly (ADP-ribose) polymerase (PARP)1-inhibitors. PARP1 is a protein that facilitates SSB repair. PARP1 binds to the DNA at the damage site and synthesizes a poly (ADP-ribose) chain (PAR) as a signal for other DNA repair enzymes (i.e. DNA-ligase III, pol ß, XRCC1) to accumulate. Inhibition of PARP1 is believed to result in persistent SSBs. When the replication fork encounters these SSBs, they are converted into one-ended DSBs which normally are repaired by HR. Thus, increasing the number of one-ended DSBs by PARP1-inhibition either in combination with or without irradiation would increase the number of Rad51 foci generated in S-phase *AT* cells, confirming a dependence on replication processes.

DSBs in the G2-phase are substrates for both HR and NHEJ. DNA lesions produced at replication forks, on the other hand, are solely substrates for HR. NHEJ activity at these lesions could promote mis-joining between a one-ended DSB and another DSB at a different locus. The cells ensure that one-ended DSBs are not accessed by NHEJ by several mechanisms: (i) quicker access of HR factors such as RPA, polymerases etc. to the damage site during replication, (ii) prevention of Ku70/80 binding at ssDNA-RPA structures (Ristic et al., 2003), and (iii) reduced DNA-PKcs activity in the S-phase (Chen et al., 2005a).

Several cancers have mutations in HR genes or these genes are epigenetically silenced. Both may explain the genetic instability that drives cancer development (Helleday, 2010). Thus, either enhancing replication stress specifically in HR-defective cells or enhancing synthetic lethality by the inhibition of a gene in the presence of an additional mutation with a cytotoxic outcome are promising tools for cancer therapies and could therefore be clinically exploited (Evers et al., 2010). Under current investigation (phase III clinical trails) is the usage of the PARP1-inhibitor in BRCA1 and BRCA2-deficient breast cancers, mutations of which are found in 70% of all families with inherited breast or ovarian cancer. PARP1 inhibition increases the number of unrepaired SSBs. During replication, these SSBs are converted into one-ended DSBs requiring repair by HR and thus both BRCA1 and BRCA2. Cells defective in BRCA1 and BRCA2 die after PARP1-inhibition. Very promising results have already been presented from phase II clinical trials showing overall low toxicity and high anti-tumor activity (Helleday, 2010).

In cell culture, it has been shown that cells defective in any HR protein – including ATM - respond to PARP1-inhibition (McCabe et al., 2006). Therefore, it is not only of great importance to identify tumors defective in any of the HR core proteins, but also to identify the involvement and actions of proteins in HR.

It has been discovered that ATM is not only responsible for the genetic disorder *AT* but is also very relevant in tumors; somatic mutations of ATM occur with significant frequency in

lung adenocarcinomas (Ding et al., 2008). Very recently, our lab identified a head and neck tumor cell line (named SKX) that displays extreme radiosensitivity. Protein expression of the NHEJ core proteins was normal, but SKX cells displayed virtually no ATM protein. Sequencing of the ATM gene revealed no mutations; instead, a microRNA that targets ATM mRNA was found to be up-regulated (unpublished data, Mansour *et al.*). Having identified ATM as a core component in the repair of replication-associated DSBs thus introduces new possibilities for cancer therapies in tumors with no or low expression of the ATM protein.

Together, we have shown that ATM and Artemis are involved in HR beyond the repair of heterochromatic lesions. ATM but not Artemis is involved in the homology-directed repair of directly and indirectly-induced DSBs during replication. Rad51 focus formation in S-phase *AT* cells depends fully on ATR/Chk1 signalling. Resolution of the DSB break, on the other hand, requires functional ATM. Therefore, we have identified ATM as a core component of HR downstream of resection and Rad51 filament formation processes.

6. References

Adams, B.R., S.E. Golding, R.R. Rao, and K. Valerie. 2010. Dynamic dependence on ATR and ATM for double-strand break repair in human embryonic stem cells and neural descendants. PLoS One. 5:e10001.

Adams, K.E., A.L. Medhurst, D.A. Dart, and N.D. Lakin. 2006. Recruitment of ATR to sites of ionising radiation-induced DNA damage requires ATM and components of the MRN protein complex. Oncogene. 25:3894-904.

Arnaudeau, C., C. Lundin, and T. Helleday. 2001. DNA double-strand breaks associated with replication forks are predominantly repaired by homologous recombination involving an exchange mechanism in mammalian cells. J Mol Biol. 307:1235-45.

Aylon, Y., B. Liefshitz, and M. Kupiec. 2004. The CDK regulates repair of double-strand breaks by homologous recombination during the cell cycle. Embo J. 23:4868-75.

Bakkenist, C.J., and M.B. Kastan. 2003. DNA damage activates ATM through intermolecular autophosphorylation and dimer dissociation. Nature. 421:499-506.

Bartek, J., and J. Lukas. 2001. Mammalian G1- and S-phase checkpoints in response to DNA damage. Curr Opin Cell Biol. 13:738-47.

Baskaran, R., L.D. Wood, L.L. Whitaker, C.E. Canman, S.E. Morgan, Y. Xu, C. Barlow, D. Baltimore, A. Wynshaw-Boris, M.B. Kastan, et al. 1997. Ataxia telangiectasia mutant protein activates c-Abl tyrosine kinase in response to ionizing radiation. Nature. 387:516-9.

Batty, D.P., and R.D. Wood. 2000. Damage recognition in nucleotide excision repair of DNA. Gene. 241:193-204.

Bauerschmidt, C., C. Arrichiello, S. Burdak-Rothkamm, M. Woodcock, M.A. Hill, D.L. Stevens, and K. Rothkamm. 2010. Cohesin promotes the repair of ionizing radiation-induced DNA double-strand breaks in replicated chromatin. Nucleic Acids Res. 38:477-87.

Beamish, H., P. Kedar, H. Kaneko, P. Chen, T. Fukao, C. Peng, S. Beresten, N. Gueven, D. Purdie, S. Lees-Miller, et al. 2002. Functional link between BLM defective in Bloom's syndrome and the ataxia-telangiectasia-mutated protein, ATM. J Biol Chem. 277:30515-23.

Beamish, H., K.K. Khanna, and M.F. Lavin. 1994a. Ionizing radiation and cell cycle progression in ataxia telangiectasia. Radiat Res. 138:S130-3.

Beamish, H., and M.F. Lavin. 1994b. Radiosensitivity in ataxia-telangiectasia: anomalies in radiation-induced cell cycle delay. Int J Radiat Biol. 65:175-84.

Bekker-Jensen, S., C. Lukas, R. Kitagawa, F. Melander, M.B. Kastan, J. Bartek, and J. Lukas. 2006. Spatial organization of the mammalian genome surveillance machinery in response to DNA strand breaks. J Cell Biol. 173:195-206.

Bentley, J., C.P. Diggle, P. Harnden, M.A. Knowles, and A.E. Kiltie. 2004. DNA double strand break repair in human bladder cancer is error prone and involves microhomology-associated end-joining. Nucleic Acids Res. 32:5249-59.

Beucher, A., J. Birraux, L. Tchouandong, O. Barton, A. Shibata, S. Conrad, A.A. Goodarzi, A. Krempler, P.A. Jeggo, and M. Lobrich. 2009. ATM and Artemis promote homologous recombination of radiation-induced DNA double-strand breaks in G2. Embo J.

Bolderson, E., N. Tomimatsu, D.J. Richard, D. Boucher, R. Kumar, T.K. Pandita, S. Burma, and K.K. Khanna. 2010. Phosphorylation of Exo1 modulates homologous recombination repair of DNA double-strand breaks. Nucleic Acids Res. 38:1821-31.

Bosotti, R., A. Isacchi, and E.L. Sonnhammer. 2000. FAT: a novel domain in PIK-related kinases. Trends Biochem Sci. 25:225-7.

Brenneman, M.A., B.M. Wagener, C.A. Miller, C. Allen, and J.A. Nickoloff. 2002. XRCC3 controls the fidelity of homologous recombination: roles for XRCC3 in late stages of recombination. Mol Cell. 10:387-95.

Brown, E.J., and D. Baltimore. 2000. ATR disruption leads to chromosomal fragmentation and early embryonic lethality. Genes Dev. 14:397-402.

Brugarolas, J., C. Chandrasekaran, J.I. Gordon, D. Beach, T. Jacks, and G.J. Hannon. 1995. Radiation-induced cell cycle arrest compromised by p21 deficiency. Nature. 377:552-7.

Bryant, H.E., and T. Helleday. 2006. Inhibition of poly (ADP-ribose) polymerase activates ATM which is required for subsequent homologous recombination repair. Nucleic Acids Res. 34:1685-91.

Bugreev, D.V., O.M. Mazina, and A.V. Mazin. 2006. Rad54 protein promotes branch migration of Holliday junctions. Nature. 442:590-3.

Buis, J., Y. Wu, Y. Deng, J. Leddon, G. Westfield, M. Eckersdorff, J.M. Sekiguchi, S. Chang, and D.O. Ferguson. 2008. Mre11 nuclease activity has essential roles in DNA repair and genomic stability distinct from ATM activation. Cell. 135:85-96.

Callebaut, I., D. Moshous, J.P. Mornon, and J.P. de Villartay. 2002. Metallo-beta-lactamase fold within nucleic acids processing enzymes: the beta-CASP family. Nucleic Acids Res. 30:3592-601.

Cao, L., E. Alani, and N. Kleckner. 1990. A pathway for generation and processing of double-strand breaks during meiotic recombination in S. cerevisiae. Cell. 61:1089-101.

Carreira, A., J. Hilario, I. Amitani, R.J. Baskin, M.K. Shivji, A.R. Venkitaraman, and S.C. Kowalczykowski. 2009a. The BRC repeats of BRCA2 modulate the DNA-binding selectivity of RAD51. Cell. 136:1032-43.

Carreira, A., and S.C. Kowalczykowski. 2009b. BRCA2: Shining light on the regulation of DNA-binding selectivity by RAD51. Cell Cycle. 8:3445-7.

Chen, B.P., D.W. Chan, J. Kobayashi, S. Burma, A. Asaithamby, K. Morotomi-Yano, E. Botvinick, J. Qin, and D.J. Chen. 2005a. Cell cycle dependence of DNA-dependent protein kinase phosphorylation in response to DNA double strand breaks. J Biol Chem. 280:14709-15.

Chen, L., T. Morio, Y. Minegishi, S. Nakada, M. Nagasawa, K. Komatsu, L. Chessa, A. Villa, D. Lecis, D. Delia, et al. 2005b. Ataxia-telangiectasia-mutated dependent phosphorylation of Artemis in response to DNA damage. Cancer Sci. 96:134-41.

Chen, L., C.J. Nievera, A.Y. Lee, and X. Wu. 2008. Cell cycle-dependent complex formation of BRCA1.CtIP.MRN is important for DNA double-strand break repair. J Biol Chem. 283:7713-20.

Chiolo, I., A. Minoda, S.U. Colmenares, A. Polyzos, S.V. Costes, and G.H. Karpen. 2011. Double-strand breaks in heterochromatin move outside of a dynamic HP1a domain to complete recombinational repair. Cell. 144:732-44.

Chiu, C.Y., R.B. Cary, D.J. Chen, S.R. Peterson, and P.L. Stewart. 1998. Cryo-EM imaging of the catalytic subunit of the DNA-dependent protein kinase. J Mol Biol. 284:1075-81.

Cuadrado, M., B. Martinez-Pastor, M. Murga, L.I. Toledo, P. Gutierrez-Martinez, E. Lopez, and O. Fernandez-Capetillo. 2006. ATM regulates ATR chromatin loading in response to DNA double-strand breaks. J Exp Med. 203:297-303.

Daniel, J.A., M. Pellegrini, J.H. Lee, T.T. Paull, L. Feigenbaum, and A. Nussenzweig. 2008. Multiple autophosphorylation sites are dispensable for murine ATM activation in vivo. J Cell Biol. 183:777-83.

de Villartay, J.P., N. Shimazaki, J.B. Charbonnier, A. Fischer, J.P. Mornon, M.R. Lieber, and I. Callebaut. 2009. A histidine in the beta-CASP domain of Artemis is critical for its full in vitro and in vivo functions. DNA Repair (Amst). 8:202-8.

Deckbar, D., J. Birraux, A. Krempler, L. Tchouandong, A. Beucher, S. Walker, T. Stiff, P. Jeggo, and M. Lobrich. 2007. Chromosome breakage after G2 checkpoint release. J Cell Biol. 176:749-55.

Ding, L., G. Getz, D.A. Wheeler, E.R. Mardis, M.D. McLellan, K. Cibulskis, C. Sougnez, H. Greulich, D.M. Muzny, M.B. Morgan, et al. 2008. Somatic mutations affect key pathways in lung adenocarcinoma. Nature. 455:1069-75.

Dodson, H., and C.G. Morrison. 2009. Increased sister chromatid cohesion and DNA damage response factor localization at an enzyme-induced DNA double-strand break in vertebrate cells. Nucleic Acids Res. 37:6054-63.

Duchaud, E., A. Ridet, D. Stoppa-Lyonnet, N. Janin, E. Moustacchi, and F. Rosselli. 1996. Deregulated apoptosis in ataxia telangiectasia: association with clinical stigmata and radiosensitivity. Cancer Res. 56:1400-4.

Esashi, F., N. Christ, J. Gannon, Y. Liu, T. Hunt, M. Jasin, and S.C. West. 2005. CDK-dependent phosphorylation of BRCA2 as a regulatory mechanism for recombinational repair. Nature. 434:598-604.

Evers, B., T. Helleday, and J. Jonkers. 2010. Targeting homologous recombination repair defects in cancer. Trends Pharmacol Sci. 31:372-80.

Falck, J., J. Coates, and S.P. Jackson. 2005. Conserved modes of recruitment of ATM, ATR and DNA-PKcs to sites of DNA damage. Nature. 434:605-11.

Finnie, N.J., T.M. Gottlieb, T. Blunt, P.A. Jeggo, and S.P. Jackson. 1995. DNA-dependent protein kinase activity is absent in xrs-6 cells: implications for site-specific recombination and DNA double-strand break repair. Proc Natl Acad Sci U S A. 92:320-4.

Geng, L., X. Zhang, S. Zheng, and R.J. Legerski. 2007. Artemis links ATM to G2/M checkpoint recovery via regulation of Cdk1-cyclin B. Mol Cell Biol. 27:2625-35.

George, K.A., M. Hada, L.J. Jackson, T. Elliott, T. Kawata, J.M. Pluth, and F.A. Cucinotta. 2009. Dose response of gamma rays and iron nuclei for induction of chromosomal aberrations in normal and repair-deficient cell lines. Radiat Res. 171:752-63.

Goldberg, M., M. Stucki, J. Falck, D. D'Amours, D. Rahman, D. Pappin, J. Bartek, and S.P. Jackson. 2003. MDC1 is required for the intra-S-phase DNA damage checkpoint. Nature. 421:952-6.

Golding, S.E., E. Rosenberg, A. Khalil, A. McEwen, M. Holmes, S. Neill, L.F. Povirk, and K. Valerie. 2004. Double strand break repair by homologous recombination is regulated by cell cycle-independent signaling via ATM in human glioma cells. J Biol Chem. 279:15402-10.

Goodarzi, A.A., J.C. Jonnalagadda, P. Douglas, D. Young, R. Ye, G.B. Moorhead, S.P. Lees-Miller, and K.K. Khanna. 2004. Autophosphorylation of ataxia-telangiectasia mutated is regulated by protein phosphatase 2A. Embo J. 23:4451-61.

Goodarzi, A.A., A.T. Noon, D. Deckbar, Y. Ziv, Y. Shiloh, M. Lobrich, and P.A. Jeggo. 2008. ATM signaling facilitates repair of DNA double-strand breaks associated with heterochromatin. Mol Cell. 31:167-77.

Goodarzi, A.A., A.T. Noon, and P.A. Jeggo. 2009. The impact of heterochromatin on DSB repair. Biochem Soc Trans. 37:569-76.

Goodarzi, A.A., Y. Yu, E. Riballo, P. Douglas, S.A. Walker, R. Ye, C. Harer, C. Marchetti, N. Morrice, P.A. Jeggo, et al. 2006. DNA-PK autophosphorylation facilitates Artemis endonuclease activity. Embo J. 25:3880-9.

Grewal, S.I., and S.C. Elgin. 2002. Heterochromatin: new possibilities for the inheritance of structure. Curr Opin Genet Dev. 12:178-87.

Haber, J.E. 2000. Recombination: a frank view of exchanges and vice versa. Curr Opin Cell Biol. 12:286-92.

Helleday, T. 2010. Homologous recombination in cancer development, treatment and development of drug resistance. Carcinogenesis. 31:955-60.

Helleday, T., J. Lo, D.C. van Gent, and B.P. Engelward. 2007. DNA double-strand break repair: from mechanistic understanding to cancer treatment. DNA Repair (Amst). 6:923-35.

Hickson, I., Y. Zhao, C.J. Richardson, S.J. Green, N.M. Martin, A.I. Orr, P.M. Reaper, S.P. Jackson, N.J. Curtin, and G.C. Smith. 2004. Identification and characterization of a novel and specific inhibitor of the ataxia-telangiectasia mutated kinase ATM. Cancer Res. 64:9152-9.

Hoeijmakers, J.H. 2001. Genome maintenance mechanisms for preventing cancer. Nature. 411:366-74.

Houldsworth, J., and M.F. Lavin. 1980. Effect of ionizing radiation on DNA synthesis in ataxia telangiectasia cells. Nucleic Acids Res. 8:3709-20.

Huertas, P., F. Cortes-Ledesma, A.A. Sartori, A. Aguilera, and S.P. Jackson. 2008. CDK targets Sae2 to control DNA-end resection and homologous recombination. Nature. 455:689-92.

Huertas, P., and S.P. Jackson. 2009. Human CtIP mediates cell cycle control of DNA end resection and double strand break repair. J Biol Chem. 284:9558-65.

Ira, G., A. Pellicioli, A. Balijja, X. Wang, S. Fiorani, W. Carotenuto, G. Liberi, D. Bressan, L. Wan, N.M. Hollingsworth, et al. 2004. DNA end resection, homologous recombination and DNA damage checkpoint activation require CDK1. Nature. 431:1011-7.

Iwabuchi, K., P.L. Bartel, B. Li, R. Marraccino, and S. Fields. 1994. Two cellular proteins that bind to wild-type but not mutant p53. Proc Natl Acad Sci U S A. 91:6098-102.

Jazayeri, A., A. Balestrini, E. Garner, J.E. Haber, and V. Costanzo. 2008. Mre11-Rad50-Nbs1-dependent processing of DNA breaks generates oligonucleotides that stimulate ATM activity. Embo J. 27:1953-62.

Jazayeri, A., J. Falck, C. Lukas, J. Bartek, G.C. Smith, J. Lukas, and S.P. Jackson. 2006. ATM- and cell cycle-dependent regulation of ATR in response to DNA double-strand breaks. Nat Cell Biol. 8:37-45.

Johnson, R.D., and M. Jasin. 2000. Sister chromatid gene conversion is a prominent double-strand break repair pathway in mammalian cells. Embo J. 19:3398-407.

Kastan, M.B., Q. Zhan, W.S. el-Deiry, F. Carrier, T. Jacks, W.V. Walsh, B.S. Plunkett, B. Vogelstein, and A.J. Fornace, Jr. 1992. A mammalian cell cycle checkpoint pathway utilizing p53 and GADD45 is defective in ataxia-telangiectasia. Cell. 71:587-97.

Kawamoto, T., K. Araki, E. Sonoda, Y.M. Yamashita, K. Harada, K. Kikuchi, C. Masutani, F. Hanaoka, K. Nozaki, N. Hashimoto, et al. 2005. Dual roles for DNA polymerase eta in homologous DNA recombination and translesion DNA synthesis. Mol Cell. 20:793-9.

Kim, S.T., B. Xu, and M.B. Kastan. 2002. Involvement of the cohesin protein, Smc1, in Atm-dependent and independent responses to DNA damage. Genes Dev. 16:560-70.

Kitagawa, R., C.J. Bakkenist, P.J. McKinnon, and M.B. Kastan. 2004. Phosphorylation of SMC1 is a critical downstream event in the ATM-NBS1-BRCA1 pathway. Genes Dev. 18:1423-38.

Knipscheer, P., M. Raschle, A. Smogorzewska, M. Enoiu, T.V. Ho, O.D. Scharer, S.J. Elledge, and J.C. Walter. 2009. The Fanconi anemia pathway promotes replication-dependent DNA interstrand cross-link repair. Science. 326:1698-701.

Kozlov, S.V., M.E. Graham, C. Peng, P. Chen, P.J. Robinson, and M.F. Lavin. 2006. Involvement of novel autophosphorylation sites in ATM activation. Embo J. 25:3504-14.

Kuhne, M., E. Riballo, N. Rief, K. Rothkamm, P.A. Jeggo, and M. Lobrich. 2004. A double-strand break repair defect in ATM-deficient cells contributes to radiosensitivity. Cancer Res. 64:500-8.

Kunkel, T.A., and D.A. Erie. 2005. DNA mismatch repair. Annu Rev Biochem. 74:681-710.

Kurosawa, A., and N. Adachi. 2010. Functions and regulation of Artemis: a goddess in the maintenance of genome integrity. J Radiat Res (Tokyo). 51:503-9.

Labib, K., and J.F. Diffley. 2001. Is the MCM2-7 complex the eukaryotic DNA replication fork helicase? Curr Opin Genet Dev. 11:64-70.

Landberg, G., M. Erlanson, G. Roos, E.M. Tan, and C.A. Casiano. 1996. Nuclear autoantigen p330d/CENP-F: a marker for cell proliferation in human malignancies. Cytometry. 25:90-8.

Lavin, M.F. 2008. Ataxia-telangiectasia: from a rare disorder to a paradigm for cell signalling and cancer. Nat Rev Mol Cell Biol. 9:759-69.

Lavin, M.F., and S. Kozlov. 2007. ATM activation and DNA damage response. Cell Cycle. 6:931-42.

Lee, J.H., and T.T. Paull. 2005. ATM activation by DNA double-strand breaks through the Mre11-Rad50-Nbs1 complex. Science. 308:551-4.

Lee, K., Y. Zhang, and S.E. Lee. 2008. Saccharomyces cerevisiae ATM orthologue suppresses break-induced chromosome translocations. Nature. 454:543-6.

Lengauer, C., K.W. Kinzler, and B. Vogelstein. 1998. Genetic instabilities in human cancers. Nature. 396:643-9.

Li, L., D. Moshous, Y. Zhou, J. Wang, G. Xie, E. Salido, D. Hu, J.P. de Villartay, and M.J. Cowan. 2002. A founder mutation in Artemis, an SNM1-like protein, causes SCID in Athabascan-speaking Native Americans. J Immunol. 168:6323-9.

Li, X., and W.D. Heyer. 2009. RAD54 controls access to the invading 3'-OH end after RAD51-mediated DNA strand invasion in homologous recombination in Saccharomyces cerevisiae. Nucleic Acids Res. 37:638-46.

Lieber, M.R. 2008. The mechanism of human nonhomologous DNA end joining. J Biol Chem. 283:1-5.

Lim, D.S., S.T. Kim, B. Xu, R.S. Maser, J. Lin, J.H. Petrini, and M.B. Kastan. 2000. ATM phosphorylates p95/nbs1 in an S-phase checkpoint pathway. Nature. 404:613-7.

Liu, Y., J.Y. Masson, R. Shah, P. O'Regan, and S.C. West. 2004. RAD51C is required for Holliday junction processing in mammalian cells. Science. 303:243-6.

Lu, H., K. Schwarz, and M.R. Lieber. 2007. Extent to which hairpin opening by the Artemis:DNA-PKcs complex can contribute to junctional diversity in V(D)J recombination. Nucleic Acids Res. 35:6917-23.

Lukas, C., F. Melander, M. Stucki, J. Falck, S. Bekker-Jensen, M. Goldberg, Y. Lerenthal, S.P. Jackson, J. Bartek, and J. Lukas. 2004. Mdc1 couples DNA double-strand break recognition by Nbs1 with its H2AX-dependent chromatin retention. Embo J. 23:2674-83.

Ma, Y., H. Lu, K. Schwarz, and M.R. Lieber. 2005a. Repair of double-strand DNA breaks by the human nonhomologous DNA end joining pathway: the iterative processing model. Cell Cycle. 4:1193-200.

Ma, Y., U. Pannicke, H. Lu, D. Niewolik, K. Schwarz, and M.R. Lieber. 2005b. The DNA-dependent protein kinase catalytic subunit phosphorylation sites in human Artemis. J Biol Chem. 280:33839-46.

Ma, Y., U. Pannicke, K. Schwarz, and M.R. Lieber. 2002. Hairpin opening and overhang processing by an Artemis/DNA-dependent protein kinase complex in nonhomologous end joining and V(D)J recombination. Cell. 108:781-94.

MacDougall, C.A., T.S. Byun, C. Van, M.C. Yee, and K.A. Cimprich. 2007. The structural determinants of checkpoint activation. Genes Dev. 21:898-903.

Mansour, W.Y., S. Schumacher, R. Rosskopf, T. Rhein, F. Schmidt-Petersen, F. Gatzemeier, F. Haag, K. Borgmann, H. Willers, and J. Dahm-Daphi. 2008. Hierarchy of nonhomologous end-joining, single-strand annealing and gene conversion at site-directed DNA double-strand breaks. Nucleic Acids Res. 36:4088-98.

Matsuda, M., K. Miyagawa, M. Takahashi, T. Fukuda, T. Kataoka, T. Asahara, H. Inui, M. Watatani, M. Yasutomi, N. Kamada, et al. 1999. Mutations in the RAD54 recombination gene in primary cancers. Oncogene. 18:3427-30.

Matsuoka, S., B.A. Ballif, A. Smogorzewska, E.R. McDonald, 3rd, K.E. Hurov, J. Luo, C.E. Bakalarski, Z. Zhao, N. Solimini, Y. Lerenthal, et al. 2007. ATM and ATR substrate analysis reveals extensive protein networks responsive to DNA damage. Science. 316:1160-6.

McCabe, N., N.C. Turner, C.J. Lord, K. Kluzek, A. Bialkowska, S. Swift, S. Giavara, M.J. O'Connor, A.N. Tutt, M.Z. Zdzienicka, et al. 2006. Deficiency in the repair of DNA damage by homologous recombination and sensitivity to poly(ADP-ribose) polymerase inhibition. Cancer Res. 66:8109-15.

Meyn, M.S. 1993. High spontaneous intrachromosomal recombination rates in ataxia-telangiectasia. Science. 260:1327-30.

Michaelis, C., R. Ciosk, and K. Nasmyth. 1997. Cohesins: chromosomal proteins that prevent premature separation of sister chromatids. Cell. 91:35-45.

Michel, B., M.J. Flores, E. Viguera, G. Grompone, M. Seigneur, and V. Bidnenko. 2001. Rescue of arrested replication forks by homologous recombination. Proc Natl Acad Sci U S A. 98:8181-8.

Mimitou, E.P., and L.S. Symington. 2008. Sae2, Exo1 and Sgs1 collaborate in DNA double-strand break processing. Nature. 455:770-4.

Mohaghegh, P., J.K. Karow, R.M. Brosh, Jr., V.A. Bohr, and I.D. Hickson. 2001. The Bloom's and Werner's syndrome proteins are DNA structure-specific helicases. Nucleic Acids Res. 29:2843-9.

Morrison, C., E. Sonoda, N. Takao, A. Shinohara, K. Yamamoto, and S. Takeda. 2000. The controlling role of ATM in homologous recombinational repair of DNA damage. Embo J. 19:463-71.

Mortensen, U.H., C. Bendixen, I. Sunjevaric, and R. Rothstein. 1996. DNA strand annealing is promoted by the yeast Rad52 protein. Proc Natl Acad Sci U S A. 93:10729-34.

Moshous, D., I. Callebaut, R. de Chasseval, B. Corneo, M. Cavazzana-Calvo, F. Le Deist, I. Tezcan, O. Sanal, Y. Bertrand, N. Philippe, et al. 2001. Artemis, a novel DNA double-strand break repair/V(D)J recombination protein, is mutated in human severe combined immune deficiency. Cell. 105:177-86.

Moshous, D., L. Li, R. Chasseval, N. Philippe, N. Jabado, M.J. Cowan, A. Fischer, and J.P. de Villartay. 2000. A new gene involved in DNA double-strand break repair and V(D)J recombination is located on human chromosome 10p. Hum Mol Genet. 9:583-8.

Motycka, T.A., T. Bessho, S.M. Post, P. Sung, and A.E. Tomkinson. 2004. Physical and functional interaction between the XPF/ERCC1 endonuclease and hRad52. J Biol Chem. 279:13634-9.

Moyal, L., Y. Lerenthal, M. Gana-Weisz, G. Mass, S. So, S.Y. Wang, B. Eppink, Y.M. Chung, G. Shalev, E. Shema, et al. 2011. Requirement of ATM-dependent monoubiquitylation of histone H2B for timely repair of DNA double-strand breaks. Mol Cell. 41:529-42.

Moyer, S.E., P.W. Lewis, and M.R. Botchan. 2006. Isolation of the Cdc45/Mcm2-7/GINS (CMG) complex, a candidate for the eukaryotic DNA replication fork helicase. Proc Natl Acad Sci U S A. 103:10236-41.

Murga, M., S. Bunting, M.F. Montana, R. Soria, F. Mulero, M. Canamero, Y. Lee, P.J. McKinnon, A. Nussenzweig, and O. Fernandez-Capetillo. 2009. A mouse model of ATR-Seckel shows embryonic replicative stress and accelerated aging. Nat Genet. 41:891-8.

Myers, J.S., and D. Cortez. 2006. Rapid activation of ATR by ionizing radiation requires ATM and Mre11. J Biol Chem. 281:9346-50.

Niewolik, D., U. Pannicke, H. Lu, Y. Ma, L.C. Wang, P. Kulesza, E. Zandi, M.R. Lieber, and K. Schwarz. 2006. DNA-PKcs dependence of Artemis endonucleolytic activity, differences between hairpins and 5' or 3' overhangs. J Biol Chem. 281:33900-9.

Nimonkar, A.V., A.Z. Ozsoy, J. Genschel, P. Modrich, and S.C. Kowalczykowski. 2008. Human exonuclease 1 and BLM helicase interact to resect DNA and initiate DNA repair. Proc Natl Acad Sci U S A. 105:16906-11.

Noon, A.T., A. Shibata, N. Rief, M. Lobrich, G.S. Stewart, P.A. Jeggo, and A.A. Goodarzi. 2010. 53BP1-dependent robust localized KAP-1 phosphorylation is essential for heterochromatic DNA double-strand break repair. Nat Cell Biol. 12:177-84.

Ogawa, T., X. Yu, A. Shinohara, and E.H. Egelman. 1993. Similarity of the yeast RAD51 filament to the bacterial RecA filament. Science. 259:1896-9.

Painter, R.B., and B.R. Young. 1980. Radiosensitivity in ataxia-telangiectasia: a new explanation. Proc Natl Acad Sci U S A. 77:7315-7.

Panier, S., and D. Durocher. 2009. Regulatory ubiquitylation in response to DNA double-strand breaks. DNA Repair (Amst). 8:436-43.

Pannicke, U., Y. Ma, K.P. Hopfner, D. Niewolik, M.R. Lieber, and K. Schwarz. 2004. Functional and biochemical dissection of the structure-specific nuclease ARTEMIS. Embo J. 23:1987-97.

Paull, T.T., and M. Gellert. 1998. The 3' to 5' exonuclease activity of Mre 11 facilitates repair of DNA double-strand breaks. Mol Cell. 1:969-79.

Paull, T.T., E.P. Rogakou, V. Yamazaki, C.U. Kirchgessner, M. Gellert, and W.M. Bonner. 2000. A critical role for histone H2AX in recruitment of repair factors to nuclear foci after DNA damage. Curr Biol. 10:886-95.

Pellegrini, M., A. Celeste, S. Difilippantonio, R. Guo, W. Wang, L. Feigenbaum, and A. Nussenzweig. 2006. Autophosphorylation at serine 1987 is dispensable for murine Atm activation in vivo. Nature. 443:222-5.

Petermann, E., and K.W. Caldecott. 2006. Evidence that the ATR/Chk1 pathway maintains normal replication fork progression during unperturbed S phase. Cell Cycle. 5:2203-9.

Pfeiffer, P., W. Goedecke, and G. Obe. 2000. Mechanisms of DNA double-strand break repair and their potential to induce chromosomal aberrations. Mutagenesis. 15:289-302.

Popova, M., H. Shimizu, K. Yamamoto, M. Lebechec, M. Takahashi, and F. Fleury. 2009. Detection of c-Abl kinase-promoted phosphorylation of Rad51 by specific antibodies reveals that Y54 phosphorylation is dependent on that of Y315. FEBS Lett. 583:1867-72.

Povirk, L.F., T. Zhou, R. Zhou, M.J. Cowan, and S.M. Yannone. 2007. Processing of 3'-phosphoglycolate-terminated DNA double strand breaks by Artemis nuclease. J Biol Chem. 282:3547-58.

Puck, T.T., and P.I. Marcus. 1956. Action of x-rays on mammalian cells. J Exp Med. 103:653-66.

Raderschall, E., E.I. Golub, and T. Haaf. 1999. Nuclear foci of mammalian recombination proteins are located at single-stranded DNA regions formed after DNA damage. Proc Natl Acad Sci U S A. 96:1921-6.

Rattner, J.B., A. Rao, M.J. Fritzler, D.W. Valencia, and T.J. Yen. 1993. CENP-F is a .ca 400 kDa kinetochore protein that exhibits a cell-cycle dependent localization. Cell Motil Cytoskeleton. 26:214-26.

Raynard, S., W. Bussen, and P. Sung. 2006. A double Holliday junction dissolvasome comprising BLM, topoisomerase IIIalpha, and BLAP75. J Biol Chem. 281:13861-4.

Reddy, G., E.I. Golub, and C.M. Radding. 1997. Human Rad52 protein promotes single-strand DNA annealing followed by branch migration. Mutat Res. 377:53-9.

Riballo, E., M. Kuhne, N. Rief, A. Doherty, G.C. Smith, M.J. Recio, C. Reis, K. Dahm, A. Fricke, A. Krempler, et al. 2004. A pathway of double-strand break rejoining dependent upon ATM, Artemis, and proteins locating to gamma-H2AX foci. Mol Cell. 16:715-24.

Richardson, C., and M. Jasin. 2000. Frequent chromosomal translocations induced by DNA double-strand breaks. Nature. 405:697-700.

Richardson, C., J.M. Stark, M. Ommundsen, and M. Jasin. 2004. Rad51 overexpression promotes alternative double-strand break repair pathways and genome instability. Oncogene. 23:546-53.

Ristic, D., M. Modesti, R. Kanaar, and C. Wyman. 2003. Rad52 and Ku bind to different DNA structures produced early in double-strand break repair. Nucleic Acids Res. 31:5229-37.

Rotman, G., and Y. Shiloh. 1999. ATM: a mediator of multiple responses to genotoxic stress. Oncogene. 18:6135-44.

Sargent, R.G., M.A. Brenneman, and J.H. Wilson. 1997a. Repair of site-specific double-strand breaks in a mammalian chromosome by homologous and illegitimate recombination. Mol Cell Biol. 17:267-77.

Sargent, R.G., R.L. Rolig, A.E. Kilburn, G.M. Adair, J.H. Wilson, and R.S. Nairn. 1997b. Recombination-dependent deletion formation in mammalian cells deficient in the nucleotide excision repair gene ERCC1. Proc Natl Acad Sci U S A. 94:13122-7.

Sarkaria, J.N., E.C. Busby, R.S. Tibbetts, P. Roos, Y. Taya, L.M. Karnitz, and R.T. Abraham. 1999. Inhibition of ATM and ATR kinase activities by the radiosensitizing agent, caffeine. Cancer Res. 59:4375-82.

Sartori, A.A., C. Lukas, J. Coates, M. Mistrik, S. Fu, J. Bartek, R. Baer, J. Lukas, and S.P. Jackson. 2007. Human CtIP promotes DNA end resection. Nature. 450:509-14.

Savitsky, K., A. Bar-Shira, S. Gilad, G. Rotman, Y. Ziv, L. Vanagaite, D.A. Tagle, S. Smith, T. Uziel, S. Sfez, et al. 1995. A single ataxia telangiectasia gene with a product similar to PI-3 kinase. Science. 268:1749-53.

Schoeffler, A.J., and J.M. Berger. 2005. Recent advances in understanding structure-function relationships in the type II topoisomerase mechanism. Biochem Soc Trans. 33:1465-70.

Shafman, T., K.K. Khanna, P. Kedar, K. Spring, S. Kozlov, T. Yen, K. Hobson, M. Gatei, N. Zhang, D. Watters, et al. 1997. Interaction between ATM protein and c-Abl in response to DNA damage. Nature. 387:520-3.

Shechter, D., V. Costanzo, and J. Gautier. 2004. ATR and ATM regulate the timing of DNA replication origin firing. Nat Cell Biol. 6:648-55.

Shimizu, H., M. Popova, F. Fleury, M. Kobayashi, N. Hayashi, I. Sakane, H. Kurumizaka, A.R. Venkitaraman, M. Takahashi, and K. Yamamoto. 2009. c-ABL tyrosine kinase stabilizes RAD51 chromatin association. Biochem Biophys Res Commun. 382:286-91.

Shiotani, B., and L. Zou. 2009. Single-stranded DNA orchestrates an ATM-to-ATR switch at DNA breaks. Mol Cell. 33:547-58.

Sigurdsson, S., S. Van Komen, W. Bussen, D. Schild, J.S. Albala, and P. Sung. 2001. Mediator function of the human Rad51B-Rad51C complex in Rad51/RPA-catalyzed DNA strand exchange. Genes Dev. 15:3308-18.

Sjogren, C., and K. Nasmyth. 2001. Sister chromatid cohesion is required for postreplicative double-strand break repair in Saccharomyces cerevisiae. Curr Biol. 11:991-5.

Smith, P.K., R.I. Krohn, G.T. Hermanson, A.K. Mallia, F.H. Gartner, M.D. Provenzano, E.K. Fujimoto, N.M. Goeke, B.J. Olson, and D.C. Klenk. 1985. Measurement of protein using bicinchoninic acid. Anal Biochem. 150:76-85.

Sorensen, C.S., L.T. Hansen, J. Dziegielewski, R.G. Syljuasen, C. Lundin, J. Bartek, and T. Helleday. 2005. The cell-cycle checkpoint kinase Chk1 is required for mammalian homologous recombination repair. Nat Cell Biol. 7:195-201.

Stiff, T., M. O'Driscoll, N. Rief, K. Iwabuchi, M. Lobrich, and P.A. Jeggo. 2004. ATM and DNA-PK function redundantly to phosphorylate H2AX after exposure to ionizing radiation. Cancer Res. 64:2390-6.

Stucki, M., J.A. Clapperton, D. Mohammad, M.B. Yaffe, S.J. Smerdon, and S.P. Jackson. 2005. MDC1 directly binds phosphorylated histone H2AX to regulate cellular responses to DNA double-strand breaks. Cell. 123:1213-26.

Su, T.T. 2010. Heterochromatin replication: better late than ever. Curr Biol. 20:R1018-20.

Subramanian, D., and J.D. Griffith. 2002. Interactions between p53, hMSH2-hMSH6 and HMG I(Y) on Holliday junctions and bulged bases. Nucleic Acids Res. 30:2427-34.

Sun, Y., X. Jiang, S. Chen, N. Fernandes, and B.D. Price. 2005. A role for the Tip60 histone acetyltransferase in the acetylation and activation of ATM. Proc Natl Acad Sci U S A. 102:13182-7.

Symington, L.S. 2002. Role of RAD52 epistasis group genes in homologous recombination and double-strand break repair. Microbiol Mol Biol Rev. 66:630-70, table of contents.

Takagi, M., D. Delia, L. Chessa, S. Iwata, T. Shigeta, Y. Kanke, K. Goi, M. Asada, M. Eguchi, C. Kodama, et al. 1998. Defective control of apoptosis, radiosensitivity, and spindle checkpoint in ataxia telangiectasia. Cancer Res. 58:4923-9.

Takeda, S., K. Nakamura, Y. Taniguchi, and T.T. Paull. 2007. Ctp1/CtIP and the MRN complex collaborate in the initial steps of homologous recombination. Mol Cell. 28:351-2.

Thompson, L.H., and D. Schild. 2002. Recombinational DNA repair and human disease. Mutat Res. 509:49-78.

Tomimatsu, N., B. Mukherjee, and S. Burma. 2009. Distinct roles of ATR and DNA-PKcs in triggering DNA damage responses in ATM-deficient cells. EMBO Rep. 10:629-35.

Ulrich, H.D., and H. Walden. 2010. Ubiquitin signalling in DNA replication and repair. Nat Rev Mol Cell Biol. 11:479-89.

Vanasse, G.J., P. Concannon, and D.M. Willerford. 1999. Regulated genomic instability and neoplasia in the lymphoid lineage. Blood. 94:3997-4010.

Walker, J.R., R.A. Corpina, and J. Goldberg. 2001. Structure of the Ku heterodimer bound to DNA and its implications for double-strand break repair. Nature. 412:607-14.

Walter, J., and J. Newport. 2000. Initiation of eukaryotic DNA replication: origin unwinding and sequential chromatin association of Cdc45, RPA, and DNA polymerase alpha. Mol Cell. 5:617-27.

Wang, H., W. Boecker, H. Wang, X. Wang, J. Guan, L.H. Thompson, J.A. Nickoloff, and G. Iliakis. 2004. Caffeine inhibits homology-directed repair of I-SceI-induced DNA double-strand breaks. Oncogene. 23:824-34.

Wang, H., X. Zhang, L. Geng, L. Teng, and R.J. Legerski. 2009. Artemis regulates cell cycle recovery from the S phase checkpoint by promoting degradation of cyclin E. J Biol Chem. 284:18236-43.

Wang, J., J.M. Pluth, P.K. Cooper, M.J. Cowan, D.J. Chen, and S.M. Yannone. 2005. Artemis deficiency confers a DNA double-strand break repair defect and Artemis phosphorylation status is altered by DNA damage and cell cycle progression. DNA Repair (Amst). 4:556-70.

Wang, X., J. Khadpe, B. Hu, G. Iliakis, and Y. Wang. 2003. An overactivated ATR/CHK1 pathway is responsible for the prolonged G2 accumulation in irradiated AT cells. J Biol Chem. 278:30869-74.

Weinberg, R., A. 2007. The biology of cancer. Garland Science

Weterings, E., and D.C. van Gent. 2004. The mechanism of non-homologous end-joining: a synopsis of synapsis. DNA Repair (Amst). 3:1425-35.

Wong, A.K., R. Pero, P.A. Ormonde, S.V. Tavtigian, and P.L. Bartel. 1997. RAD51 interacts with the evolutionarily conserved BRC motifs in the human breast cancer susceptibility gene brca2. J Biol Chem. 272:31941-4.

Wu, L., S.L. Davies, N.C. Levitt, and I.D. Hickson. 2001. Potential role for the BLM helicase in recombinational repair via a conserved interaction with RAD51. J Biol Chem. 276:19375-81.

Wu, L., and I.D. Hickson. 2003. The Bloom's syndrome helicase suppresses crossing over during homologous recombination. Nature. 426:870-4.

Wyman, C., and R. Kanaar. 2006. DNA double-strand break repair: all's well that ends well. Annu Rev Genet. 40:363-83.

Xu, B., S. Kim, and M.B. Kastan. 2001. Involvement of Brca1 in S-phase and G(2)-phase checkpoints after ionizing irradiation. Mol Cell Biol. 21:3445-50.

Xu, B., S.T. Kim, D.S. Lim, and M.B. Kastan. 2002. Two molecularly distinct G(2)/M checkpoints are induced by ionizing irradiation. Mol Cell Biol. 22:1049-59.

Yang, Q., R. Zhang, X.W. Wang, E.A. Spillare, S.P. Linke, D. Subramanian, J.D. Griffith, J.L. Li, I.D. Hickson, J.C. Shen, et al. 2002. The processing of Holliday junctions by BLM and WRN helicases is regulated by p53. J Biol Chem. 277:31980-7.

Yazdi, P.T., Y. Wang, S. Zhao, N. Patel, E.Y. Lee, and J. Qin. 2002. SMC1 is a downstream effector in the ATM/NBS1 branch of the human S-phase checkpoint. Genes Dev. 16:571-82.

Yoo, S., A. Kimzey, and W.S. Dynan. 1999. Photocross-linking of an oriented DNA repair complex. Ku bound at a single DNA end. J Biol Chem. 274:20034-9.

You, Z., L.Z. Shi, Q. Zhu, P. Wu, Y.W. Zhang, A. Basilio, N. Tonnu, I.M. Verma, M.W. Berns, and T. Hunter. 2009. CtIP links DNA double-strand break sensing to resection. Mol Cell. 36:954-69.

Yuan, S.S., H.L. Chang, and E.Y. Lee. 2003. Ionizing radiation-induced Rad51 nuclear focus formation is cell cycle-regulated and defective in both ATM(-/-) and c-Abl(-/-) cells. Mutat Res. 525:85-92.

Zierhut, C., and J.F. Diffley. 2008. Break dosage, cell cycle stage and DNA replication influence DNA double strand break response. Embo J. 27:1875-85.

Ziv, Y., D. Bielopolski, Y. Galanty, C. Lukas, Y. Taya, D.C. Schultz, J. Lukas, S. Bekker-Jensen, J. Bartek, and Y. Shiloh. 2006. Chromatin relaxation in response to DNA double-strand breaks is modulated by a novel ATM- and KAP-1 dependent pathway. Nat Cell Biol. 8:870-6.

Zou, L. 2007. Single- and double-stranded DNA: building a trigger of ATR-mediated DNA damage response. Genes Dev. 21:879-85.

Zou, L., and S.J. Elledge. 2003a. Sensing DNA damage through ATRIP recognition of RPA-ssDNA complexes. Science. 300:1542-8.

Zou, L., D. Liu, and S.J. Elledge. 2003b. Replication protein A-mediated recruitment and activation of Rad17 complexes. Proc Natl Acad Sci U S A. 100:13827-32.

7.   Appendix

7.1.   Abbreviations

°C	degree Celsius
53BP1	p53 binding protein 1
µ	micro (10^{-6})
A	adenine
APH	aphidicolin
Asp	Asparagine
AT	ataxia telangiectasia
ATLD	ataxia telangiectasia like disorder
ATM	ataxia telangiectasia mutated
ATP	adenosine-5'-triphosphate
ATR	ataxia telangiectasia and Rad3-related
BER	base excision repair
BLM	Bloom syndrome
bp	base pairs
Brca1	breast cancer 1
Brca2	breast cancer 2
BRCT	BRCA1- carboxyl-terminal
BSA	bovine serum albumin
C	cytosine
Caff.	caffeine
CDK	cyclin-dependent kinase
CenpF	centromere protein F
Chk1	checkpoint kinase 1
Chk2	checkpoint kinase 2
CS	Cockaine Syndrome
CSR	class switch recombination
CtIP	C-terminal binding protein interacting protein
DAPI	4',6-Diamidino-2-phenylindole
ddH2O	double distilled water
DDR	DNA damage response
D-loop	displacement loop
DMSO	dimethyl sulfoxide
DNA	deoxyribonucleic acid
DNA LigIV	DNA ligase IV

DNA-PK	DNA-dependent protein kinase
DSB	double-strand break
DSBR	double-strand break repair
dsDNA	double-stranded DNA
DTT	dithiothreitol
ECL	electrochemical luminescence
EDTA	ethylenediaminetetraacetic acid
EdU	5-ethynyl-2'-deoxyuridine
Exo1	exonuclease-like exonuclease 1
FACS	flow cytometry cell sorting
G	guanine
GC	gene conversion
GFP	green fluorescent protein
Gy	Gray
h	hours
HDR	homology-directed repair
His	histidine
HJ	Holliday junction
HR	homologous recombination
HU	hydroxyurea
IgH	Ig heavy chain
IR	ionizing radiation
Kap-1	KRAB-associated protein 1
kDa	kilodaltons
l	liter
LOH	loss of heterozygosity
m	milli (10^{-3})
M	molar (mol/l)
MDC1	mediator of DNA-damage checkpoint protein 1
MDM2	murine double minute gene 2
MEM	minimal essential medium
MGMT	methyl guanine methyltransferase
min	minutes
MMR	mismatch repair
MRN	Mre11/Rad50/Nbs1
mRNA	messenger ribonucleic acid
n	Nano (10^{-9})

NBS1	Nijmegen breakage syndrome 1, Nibrin
NER	nucleotide excision repair
NHEJ	non-homologous end-joining
nt	nucleotides
O6-meG	O6-methyl guanine
ORF	open reading frame
p	pico (10^{-12})
PAGE	polyacrylamide gel electrophoresis
PARP1	poly (ADP-ribose) polymerase 1
PBS	phosphate buffered saline
PCNA	proliferating cell nuclear antigen
PCR	polymerase chain reaction
PI	propidium iodine
PMSF	phenyl methyl sulfonyl fluoride
PP2A	protein phosphatase 2A
PVDF	polyvinylidene difluoride
RNA	ribonucleic acid
Rb	retinoblastoma
RFC	replication factor C
ROS	reactive oxygen species
RPA	replication protein A
rpm	rotations per minute
RT	room temperature
RT-PCR	real time PCR
sec	seconds
SCID	severe combined immune deficiency
SDS	sodium dodecyl sulphate
SDSA	synthesis-dependent strand annealing
Ser	serine
siRNA	small interference RNA
SMC1	structural maintenance of chromosomes protein 1
SSA	single-strand annealing
SSB	single-strand break
SSBR	single-strand break repair
ssDNA	single-stranded DNA
T	thymine
Tcr	T-cell receptor

Thr	threonine
TLS	translesion synthesis
Tween 20	polyoxyethylen-sorbitanmonolaurate 20
Tyr	tyrosine
UV	ultraviolet
V	volts
V(D)J	variable (V), diversity (D) and joining (J)
v/v	volume per volume
w/v	weight per volume
WRN	Werner syndrome
XLF	XRCC4-like factor
XRCC	X-ray cross complementation gene

7.2. List of publication

05/2011   **Köcher S.**, Rieckmann T., Rohaly G., Dikomey E., Mansour W.Y., Dornreiter I., Dahm-Daphi J.
"Dissecting the requirement of ATM and Artemis for homologous recombination in S and G2 phase"
submitted

05/2011   Mansour W.Y., Dörk T., Kasten-Pisula U., Rieckmann T., **Köcher S.**, Borgmann K., Baumann M., Krause M., Petersen C., Dikomey E., and Dahm-Daphi J.
"miR421-mediated ATM-depletion leads to a pronounced DNA repair defect: A novel mechanism for clinical tumor radiosensitivity"
submitted

04/2011   **Köcher S.**, Rieckmann T., Rohaly G., Dikomey E., Mansour W.Y., Dornreiter I., Dahm-Daphi J.
"Dissecting the requirement of ATM and Artemis for homologous recombination in S and G2 phase", Responses to DNA damage conference, Egmond aan Zee, Netherlands (poster)

09/2010   **Köcher S.**, Rieckmann T., Rohaly G., Dikomey E., Mansour W.Y., Dornreiter I., Dahm-Daphi J.
"Homologous recombination is differentially affected by ATM and Artemis", ESTRO 29, Barcelona, Spain (selected speaker)

09/2010:   **Köcher S.**, Dahm-Daphi J.
"Homologous recombination is differentially affected by ATM and Artemis", 11th Biannual DGDR Meeting, Jena (selected speaker)

09/2010:   **Köcher S.**, Dahm-Daphi J.
"Homologous recombination is differentially affected by ATM and Artemis", GBS, Hamburg (poster)

09/2009:   **Köcher S.**, Dahm-Daphi J.
"Different pattern of Cell Cylce Checkpoint activation but similar DSB repair defects in ATM- and Artemis- deficient cells", GBS, Essen (poster)

09/2009:   **Köcher S.**, Dahm-Daphi J.
"Different pattern of Cell Cylce Checkpoint activation but similar DSB repair defects in ATM- and Artemis- deficient cells", 2nd German-French DNA Repair Meeting, Konstanz (poster)

GRANTS and AWARDS

04/2011:   **Travel grant** Responses to DNA damage conference, Egmond aan Zee, Netherlands

09/2010:   **Travel grant** 11th Biannual DGDR Meeting

09/2009:   **Poster award** 2nd German-French DNA Repair Meeting

7.3. Danksagung

Audrey MacDougall   *Lutterothstr. 9, 20255 Hamburg*

An den Fachbereich Biologie

der Universität Hamburg,

zur Weiterleitung

an den Promotionsausschuss

Hamburg, den 9. Mai 2011

Hiermit bestätige ich die Korrektheit der englischen Sprache der Dissertation "Role of ATM (ataxia telangiectasia mutated) and Artemis proteins for the repair of DNA double-strand breaks by homologous recombination in mammalian cells" von Frau Sabrina Köcher.

Audrey MacDougall (native speaker)